THE PLASTIC DEFORMATION OF HIGH PURITY IRON

by

Dhanraj Maheshwari

A thesis submitted to the
Faculty of Science and Engineering
of the University of Ottawa
in partial fulfilment of the requirements for
the degree of
MASTER OF APPLIED SCIENCE
in Mechanical Engineering

December 1972

ABSTRACT

In this thesis, an attempt has been made to explain the probable mechanism of plastic deformation in high purity iron. The stress dependence of plastic strain rate has been investigated using the technique of stress relaxation in tension at room temperature.

The rate theory was applied to analyze the experimental results. It was discovered that the early stage of relaxation process can be explained by a one term rate equation, whereas the later stage can be attributed to a system of two obstacles operating in series. It was observed that the backward movement of the dislocations is insignificant throught the relaxation process. There is strong evidence to suggest that the nucleation of double kink to surmount the Peierls-Nabarro stress hill is the probable mechanism of plastic deformation in high purity iron.

The internal stresses were measured at different stress levels and were found to be increasing with increasing strain.

ACKNOWLEDGEMENT

The author is deeply indebted to his supervisor, Dr. A.S. Krausz, for the advice, guidance, encouragement and critical suggestions throughout the course of this research.

The author wishes to thank Dr. E. Smith, Dr. C.M. Mitchel and Mr. E. Cousineau of the Department of Energy, Mines and Resources, Ottawa, for their assistance in the determination of grain orientation.

Thanks are also extended to Mr. G. Toth and Mr. P. Inderbitzin for their technical assistance and Mr. D. Seaman for his assistance.

The author also wishes to express his appreciation for financial support from National Research Council of Canada, Ontario Government and the Department of Mechanical Engineering, University of Ottawa.

Finally, the author is thankful to his friends for their encouragement and help and wife, Shakuntala, for her patience and understanding throughout the course of this work.

CONTENTS

LIST OF FIGURES

LIST OF TABLES

NOMENCLATURE

A	Pre-exponential factor in the rate equation
b	Burgers vector
C	Rate constant in chemical process
c	Proportionality constant for changing tensile strain into shear strain
d	Distance covered by the dislocation in overcoming the energy barrier
E	Elastic modulus of material
E'	Combined elastic modulus of material and testing machine
ΔE_i	Energy of the system in ith state
ΔE_t	Total energy of the ensemble
ΔE_w	Energy supplied by the external applied stress
$\Delta E\ (\tau_{eff})$	Apparent activation energy
F_w	Force exerted by the external applied stress
$G_{(g)}$	Number of possible states of the ensemble
g_i	Number of systems in ith energy state
h	Planck's constant
k	Boltzmann constant
k	Rate constant
k_i	Rate constant for ith barrier
$(k_i)_1$	Rate constant for ith barrier considering the activation energy from ground level of state 1 to saddle point of state i.
l^*	Length of the dislocation loop involved in activation
$\bar{l}$	Distance between two obstacles

M	Number of systems in an ensemble
m	Slope of $\log \sigma_a$ vs $\log(-\Delta\sigma)$ relation
m*	Slope of $\log \sigma_{eff}$ vs $\log(-\Delta\sigma)$ relation
m_a	Mass of atom
N	Number of atoms in a system
n	$V^*/2kT$
P	Probability
R	Universal gas constant
Str	Structure
T	Absolute temperature
t	Time
q	Partition function
V^*	Activation volume
V_e	Volume of an ensemble
v	Average dislocation velocity
v_o	Constant in the equation $v = v_o \left(\frac{\tau_a}{\tau_o}\right)^m$

Greek Letter Symbols

α	Geometrical factor in Orowan's equation
δ	Width of the activated state
ε	Tensile strain
$\dot{\varepsilon}$	Tensile strain rate
ε_a	Elastic strain of the specimen due to deformation of the load cell and machine parts
ε_e	Elastic tensile strain
ε_p	Plastic tensile strain

ε_t	Total tensile strain of the specimen during stress relaxation
γ	Shear strain
$\dot{\gamma}$	Shear strain rate
γ_e	Elastic shear strain
γ_p	Plastic shear strain
ν	Frequency factor
ρ	Number of dislocations
ρ_m	Mobile dislocation density
σ	Tensile stress
$\Delta\sigma$	Tensile stress relaxed
σ_a	Applied tensile stress
σ_{eff}	Effective tensile stress
σ_i	Internal tensile stress
σ_o	Tensile stress at the start of relaxation process
κ	Transmission coefficient
τ	Shear stress
τ_a	Applied shear stress
τ_{eff}	Effective shear stress
τ_i	Internal shear stress
τ_o	Constant in the equation $v = v_o(\frac{\tau_a}{\tau_o})^m$

Superscripts

Denotes the activated state

Denotes the constant for movement in backward direction

Subscripts

Denotes the backward movement of the dislocations

Denotes the forward movement of the dislocations

CHAPTER 1

INTRODUCTION

Numerous investigations, utilizing various methods have been carried out to identify the mechanism of plastic deformation in high purity iron. Basinski and Christian (1) were the first to propose the overcoming of Peierls-Nabarro force field as the probable rate controlling mechanism of thermally activated plastic deformation in pure iron. Contrary to this Feltham (2) suggested that the probable mechanism could be conservative migration of jogs. The mechanism proposed by Basinski and Christian was supported by Conrad (3). Conrad and Fredrick (4), Conrad (5), Christian and Masters (6), Arsenault (7), Smidt (8), and Wray and Horne (9). Wilson and Garofalo (10) concluded that there are two types of deformation processes occurring simultaneously at room temperature. The conclusion of the investigators (1, 3-9) was further supported by Smidt (11).

The analysis in the majority of these investigations is based on the empirical relation of Becker (12) and lack a true physical understanding of the plastic deformation processes. Recently Krausz and Eyring (13) have shown that the study of plastic deformation processes is part of chemical kinetics and can be described by the rate theory. Therefore, investigation for establishment of the mechanism of plastic deformation in pure iron was to be carried out in the light of chemical kinetics.

It was the purpose of this work to obtain further information on the mechanism of plastic deformation of high purity iron using the theory of thermally activated processes.

1.1 Plastic Deformation in Crystalline Materials

There are four major variables which control the plastic deformation of crystalline materials: the shear stress τ, the shear strain rate $\dot{\gamma}$, the temperature T and the structure. Therefore it is the purpose of the study of plastic deformation processes to establish a relationship between these parameters.

In an ideal crystal, the atoms are arranged in a perfect geometrical order. In reality crystals rarely exist in the ideal form and the lattice is disturbed in some part of the crystal. The type of imperfection in which an array of atoms is mismatched is a dislocation. The plastic deformation process is a consequence of the dislocation movement which causes the gliding of one atomic plane over the other in a definite crystallographic direction.

1.2 Dislocation Theory

Depending upon the type of mismatch, the dislocations are classified as:

(a) Edge dislocation,

(b) Screw dislocation and

(c) Mixed dislocation.

These are described below.

(a) Edge dislocation: If the crystal lattice is subjected to a shear stress as shown in Fig 1.1, the upper part of the crystal lattice is pushed ahead by one atomic distance in the direction of stress. The line of mismatch between the slipped and unslipped region is the edge dislocation. This is usually represented by the symbol ($\perp$). As shown

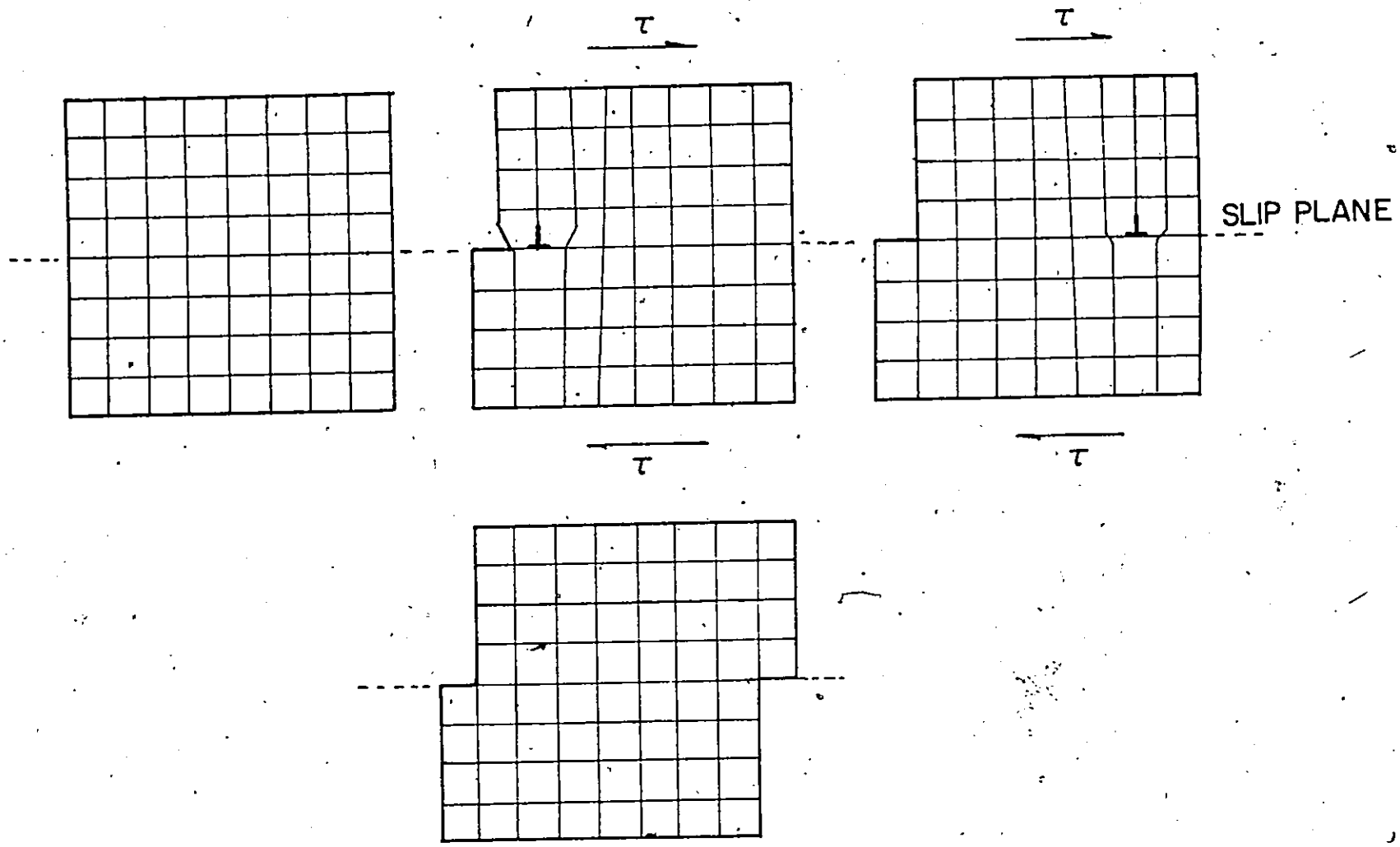

Figure 1.1 The diagram illustrates the generation and motion of dislocation under the effect of an applied stress τ causing slip.

in Fig. 1.2, the displacement of the atoms is perpendicular to the edge dislocation line.

(b) Screw dislocation: Burgers suggested a second type of dislocation, screw dislocation, represented by the symbol (⟲). In this type, the line of atoms defining the dislocation has the proper number of coordinating atoms but the lattice is distorted. The displaced atoms follow a screwlike sequence which continues and extends along the dislocation line. The displacement of atoms is parallel to the dislocation line (Fig. 1.3).

(c) Mixed dislocation: If the shift of atoms over the slip plane is such that the dislocation line separating the slipped and unslipped regions is neither parallel nor perpendicular to the displacement, the dislocation is mixed (Fig. 1.4).

1.2.1 Origin of dislocations:

The first dislocation can be considered to be generated in the perfect crystal by one of the following ways.

(i) Heterogeneous nucleation,

(ii) Homogeneous nucleation, and

(iii) Regenerative multiplication.

These are discussed below.

(i) Heterogeneous nucleation: It has been observed that the first dislocation is generated at:

(a) the surface which has been touched accidentally by a hard object,

(b) the stress field around inclusions or precipitates, and

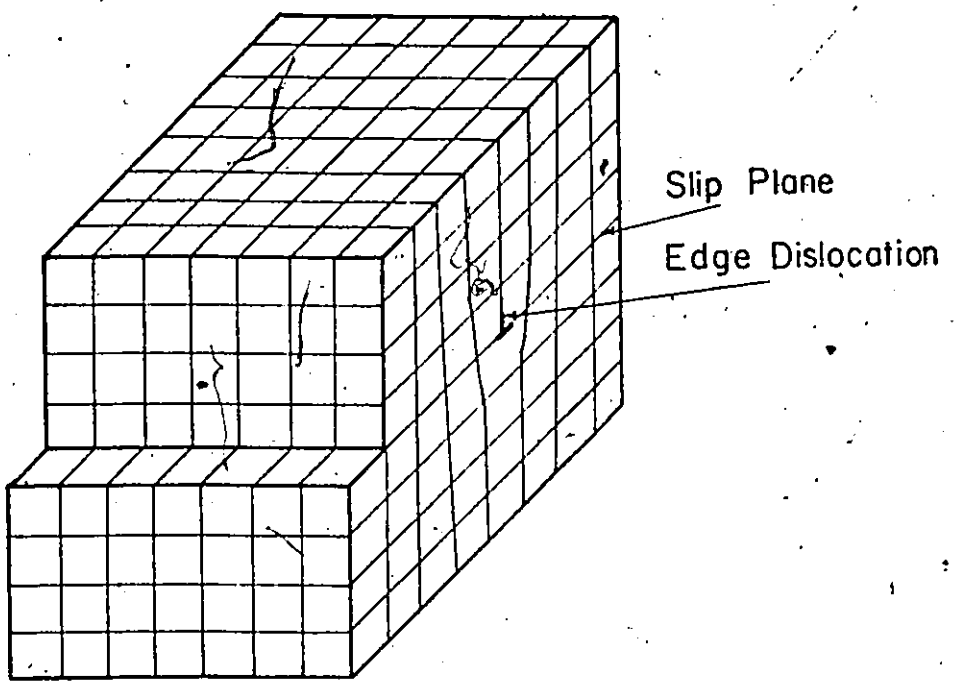

Figure 1.2 The figure illustrates an edge dislocation

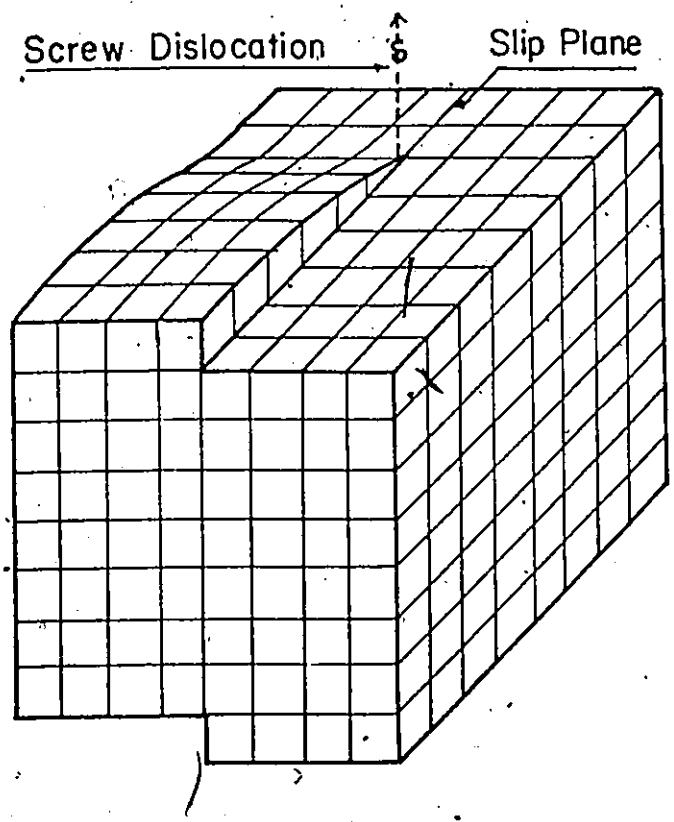

Figure 1.3 The figure illustrates a screw dislocation

(c) thermal gradients.

(ii) Homogeneous nucleation: In the absence of heterogeneous nucleation, the dislocation can be generated only through homogeneous nucleation. This is due to high applied stress of magnitude of the order of $G/4\pi$. In practice it is rarely possible to achieve this stress. Thus, the possibility of dislocation generation by homogeneous nucleation is remote.

(iii) Regenerative multiplication: It has been observed that dislocations multiply under the influence of an external applied stress. The rate of multiplication increases with increasing stress. In 1950 F.C. Frank and W.T. Read proposed a mechanism for edge dislocation multiplication. A variant of Frank-Read source, multiple cross slip, was proposed later by Koehler.

The dislocations generated by any of the above sources move under the influence of the external applied stress causing slip.

1.3 Slip by dislocation Movement

In a crystal lattice the restoring force acting on an atom is zero at an equilibrium position. The distance between two neighbouring atoms corresponding to this position is an equilibrium distance. If a crystal is subjected to external stress and the energy, ΔE_w, supplied by the applied stress is higher than the inherent resistance of the crystal lattice, the dislocation starts gliding over the slip plane from one equilibrium position to the next in succession. During the movement of the dislocation, old bonds are broken and new bonds are established.

This process of breaking and establishing of bonds is a discontinuous process. When the dislocation reaches the end of the crystal, a step is formed resulting in a permanent shape change (Fig. 1.1). This is the fundamental process of plastic deformation. As only a few atoms are displaced at a time, the energy required to cause the dislocation movement is only a fraction of the total energy required to move one plane of atoms over the other.

The dislocation glides over the slip plane at high speed until stopped by a high energy barrier (Fig. 1.5). The energy barrier may be Peierls-Nabarro stress field, solute atoms, other dislocations or grain boundaries. The dislocation is held up at the barrier till the total energy of the atomic configuration is equal to the energy, $\Delta E^{\ddagger}$, corresponding to activated state $\ddagger$. Becker (13) proposed in 1925 that the energy difference $\Delta E^{\ddagger} - \Delta E_w$, is supplied by the thermal energy of the crystal. Thus the overcoming of the barrier and consequently the plastic deformation process is a thermally activated process. He described the rate of plastic deformation process by an empirical equation of Arrhenius type

$$\dot{\epsilon} = \nu \exp\left[-\frac{\Delta E(\tau_{eff})}{kT}\right] \qquad (1.1)$$

where ν is the frequency factor, τ_{eff} is the resultant of applied and internal shear stress, $\Delta E_p(\tau_{eff})$ is the apparent activation energy which decreases with increasing τ_{eff}, k is the Boltzmann constant and T is the absolute temperature.

The dislocation is free to move at a high speed till it is stopped by an obstacle. The time needed to move the dislocation from one energy

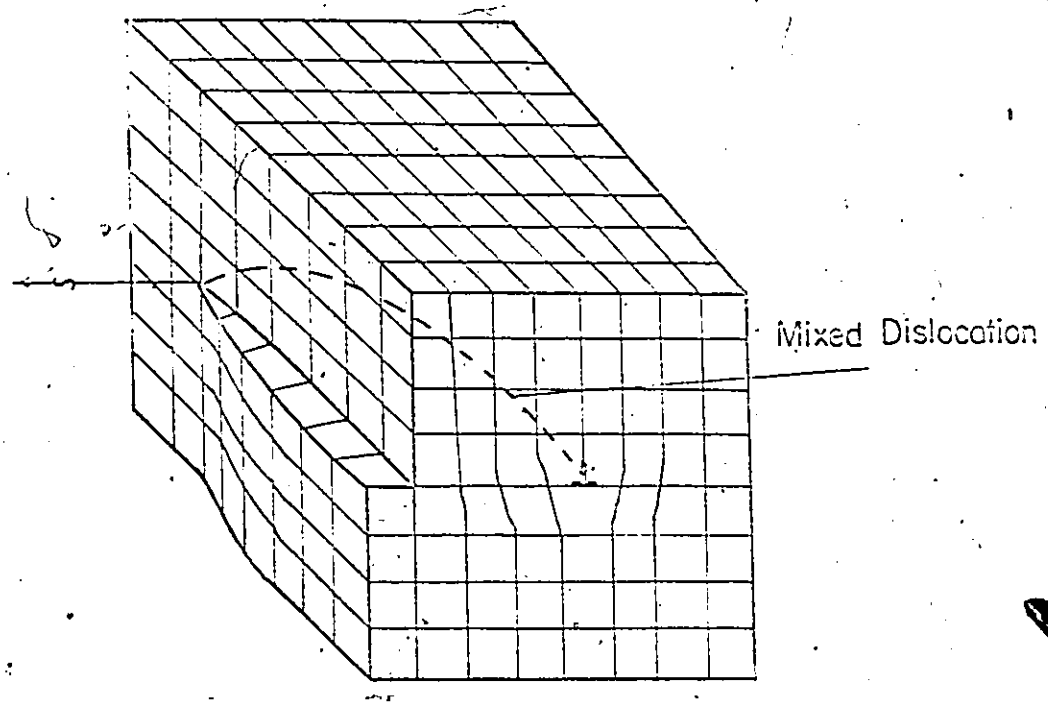

Figure 1.4 The figure illustrates a edge dislocation

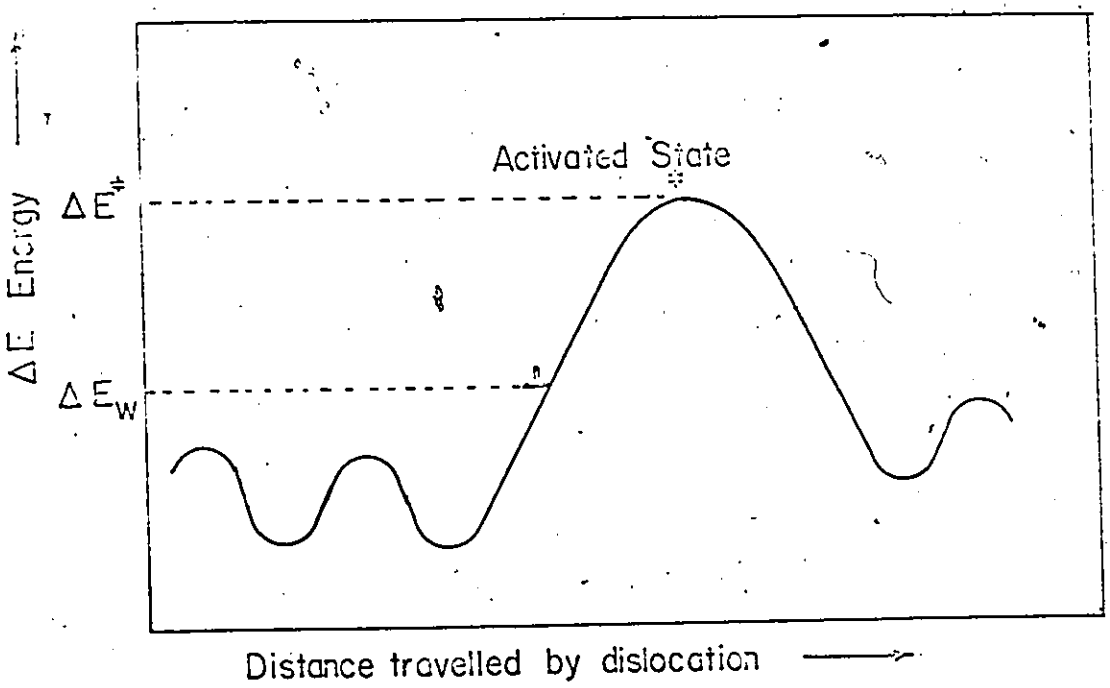

Figure 1.5 The diagram illustrates the energy field encountered by the dislocation.

barrier to the other is thus equal to the waiting time in front of the obstacle plus the time required to travel the distance between two obstacles. Because the dislocation moves at very high speed, the time required to travel the distance between two obstacles is negligible compared to the waiting time. Therefore, the total time required to move the dislocation from one energy barrier to the other is approximately equal to the waiting time in front of the barrier and the average dislocation velocity v is

$$v \alpha \nu \bar{l} \exp\left(-\frac{\Delta E(\tau_{eff})}{kT}\right) \qquad (1.2)$$

where $\bar{l}$ is the average distance travelled by the dislocation.

The plastic strain rate $\dot{\gamma}_p$ is related to the dislocation velocity according to Orowan's equation

$$\dot{\gamma}_p = \alpha b \rho_m v(\tau, T, \text{structure}) \qquad (1.3)$$

where α = a geometric factor,

b = the Burgers vector and

ρ_m = the mobile dislocation density

The above equation completely describes the plastic deformation process. In this equation all the parameters, except the dislocation velocity, are constant when it is assumed that ρ_m remains constant for a particular testing condition (14). Therefore, the study of plastic deformation process reduces to the study of dislocation velocity.

The rate of the process given by equation (1.2) is analogous to the chemical reaction in which the rate of reacion is given by

$$\text{Rate} = C \exp\left(-\frac{(\Delta E)}{RT}\right)$$

where C = the rate constant

ΔE = the activation energy and

R = the Universal gas constant.

Consequently, plastic deformation process can be described by the rate theory.

CHAPTER 2

THE THEORY OF THERMALLY ACTIVATED PLASTIC DEFORMATION OF CRYSTALLINE MATERIALS

2.1 The Probability of Activation

It has been discussed in Chapter 1 that the plastic deformation process is analogous to a chemical reaction. To determine the rate of deformation process it is essential to know the probability of activation in a crystal subjected to externally applied stress. This crystal can be considered to be composed of several systems. Every atom in these systems is vibrating with a different amplitude and in different direction. When the configuration of atoms forming a dislocation acquires sufficient energy, vibrating in the direction of stress, activation takes place. The dislocation can be considered as one of the systems and the probability of the system acquiring the activation energy $\Delta E^{\dagger}$ is given by (15).

$$P = \frac{\exp(-\Delta E^{\dagger}/kT)}{\sum_i \exp(-\Delta E_i/kT)} \qquad (2.1)$$

where ΔE_i is the total energy of the i^{th} system.

(The derivation of equation 2.1 appears in Appendix I).

In the above equation $\sum_i \exp(-\Delta E_i/kT)$ is the partition function, defined as the sum of $\exp(-\Delta E_i/kT)$ terms of all forms of energy possessed by the system and is denoted by q.

According to this probability the atoms forming a dislocation acquire the necessary energy and cross the barrier. The state of atoms corresponding to the top of the barrier is the activated state (Fig. 2.2).

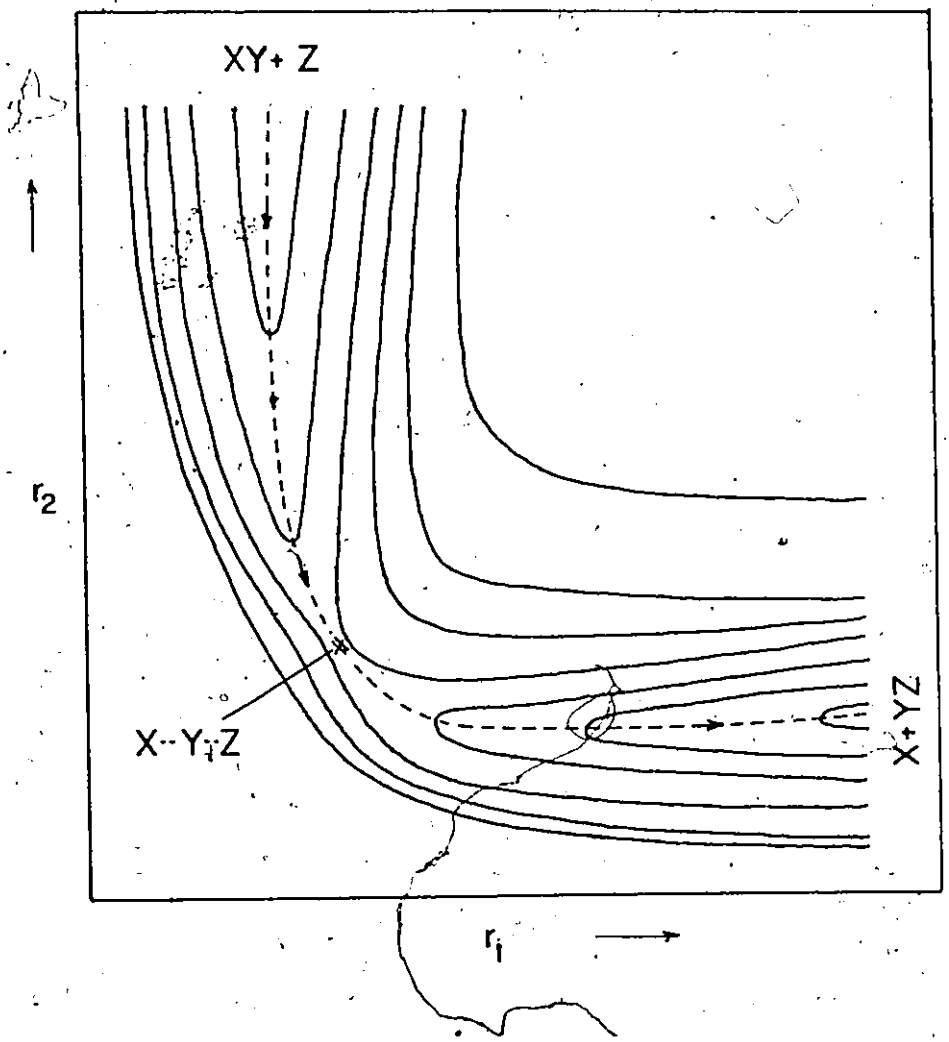

Figure 2.1 Energy field for the reaction XY + Z = X + YZ.

The rate theory analysis of plastic deformation process is given in the following section.

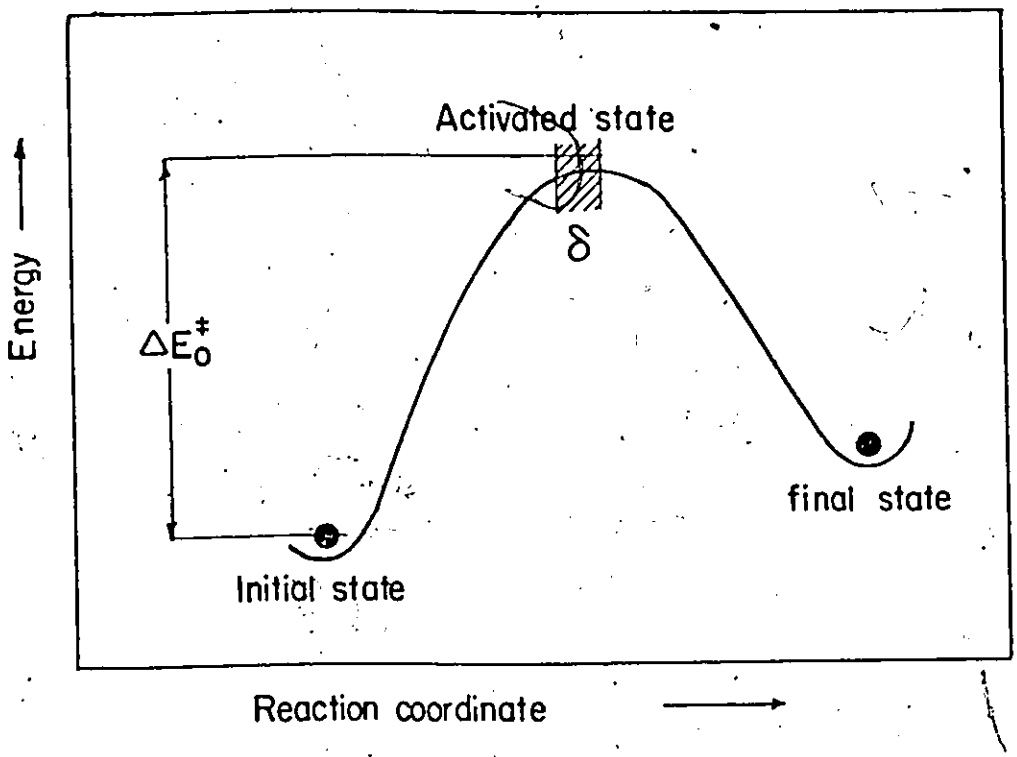

Fig. 2.2 Energy curve showing the variation of energy during reaction.

2.2 Absolute Rate Theory

The absolute rate theory (16) is based on the assumption that the activated complexes are in equilibrium with the reactants. This is equivalent to assuming that the flow in one direction is independent of the flow in the other direction. This assumption makes the analysis of the rate theory simple.

For the understanding of the absolute rate theory, consider a reaction

$$XY + Z \rightleftharpoons X + YZ$$

where X, Y and Z are the atoms, XY and YZ are the molecules. The po-

tential energy corresponding to the interatomic distance r_1 and r_2 between the atoms X-Y and Y-Z respectively can be calculated. The energy contour lines drawn against the interatomic distance r_1 and r_2 are shown in Fig. 2.1. For the above reaction to occur, the reactant will follow the path of minimum energy which is shown by dotted line on the contour diagram. This is the reaction coordinate. The variation of energy along reaction coordinate is given in Fig. 2.2. The saddle point corresponds to a maximum point along reaction coordinate and minimum along other coordinates. This is indicated by $\ddagger$ in Fig. 2.2. The rate at which the complexes pass over the saddle point is given by the absolute rate theory and the rate of the activation for the complexes is

$$k = \frac{kT}{h} \frac{q^{\ddagger}}{q_i} \exp\left(\frac{-\Delta E^{\ddagger}}{kT}\right) \qquad (2.2)$$

where h = the Planck's constant

$q^{\ddagger}$ = the partition function of the activated complexes excluding the translational partition function in reaction coordinate

q_i = the partition function of the reactants.

(For detailed derivation of this equation, see Appendix II).

Applying this theory to the plastic deformation process the rate of activation for the dislocations will be given by equation 2.2. In this derivation, it is assumed that all the dislocations reaching the top of the barrier cross it. However, some of the dislocations may glide back to the initial position. Also, some of the dislocations may cross the barrier due to tunnelling effect. This can be explained by

quantum mechanics. According to this theory, there is a probability that the particles having smaller energy than the activated state may reach the final state without surmounting the barrier. To account for these effects, the rate equation is modified as follows:

$$R = \kappa \frac{kT}{h} \frac{q^*}{q_i} \exp\left(-\frac{\Delta E^\ddagger}{kT}\right)$$

In the above expression κ is the transmission coefficient. If $\bar{l}$ is the distance between two obstacles, then the dislocation velocity will be given by

$$v = \bar{l}\, \kappa \frac{kT}{h} \frac{q^*}{q_i} \exp\left(-\frac{\Delta E^\ddagger}{kT}\right)$$

There is a probability that the dislocations may move in the backward direction. Denoting the forward movement by the subscript f and the backward movement by subscript b, the net velocity can be written as

$$\begin{aligned} v &= v_f - v_b \\ &= \bar{l}_f\, \kappa_f \frac{kT}{h} \frac{q^*}{q_f} \exp\left(-\frac{\Delta E_f^\ddagger}{kT}\right) \\ &\quad - \bar{l}_b\, \kappa_b \frac{kT}{h} \frac{q^*}{q_b} \exp\left(-\frac{\Delta E_b^\ddagger}{k\bar{l}}\right) \end{aligned} \qquad (2.3)$$

If the lattice is subjected to applied stress τ_a, the effective stress causing the dislocation movement will be

$$\tau_{eff} = \tau_a - \tau_i$$

where τ_i is the internal stress. This effective stress exerts a force of magnitude $\tau_{eff}\, bl^*$, where l^* is the length of the dislocation loop involved in activation. The energy-distance curve for such system is

modified as shown in Figure 2.3. The corresponding force distance curve is shown in Figure 2.4. The energy required to overcome the barrier will be (8), $\Delta E\ (\tau_{eff}) = \Delta E^{\ddagger}$ - work done by applied stress or

$$\Delta E\ (\tau_{eff}) = \int_{x_1}^{x_2} [f(x) - \tau_{eff}\ b\ l^*]\ dx$$

$$= \Delta E^{\ddagger} - \tau_{eff}\ b\ l^*\ (x_2 - x_1)$$

$$= \Delta E^{\ddagger} - \tau_{eff}\ b\ d\ l^* = \Delta E - \tau_{eff}\ V^*$$

where $\int_{x_1}^{x_2} f(x)\ dx = \Delta E^{\ddagger}$, the total energy required to overcome the barrier.

$d = x_2 - x_1$, the width of the barrier, and

V^* = the activation volume.

Therefore, after application of the stress, τ_{eff}, the net dislocation velocity in the forward direction will be

$$v = \frac{kT}{h}\left[\bar{l}_f\ \kappa_f\ \frac{q^{\ddagger}}{q_f}\ \exp\left(-\frac{\Delta E_f^{\ddagger} - V_f^*\ \tau_{eff}}{kT}\right)\right.$$

$$\left. -\bar{l}_b\ \kappa_b\ \frac{q^{\ddagger}}{q_b}\ \exp\left(-\frac{\Delta E_b^{\ddagger} + V_b^*\ \tau_{eff}}{kT}\right)\right] \qquad (2.4)$$

This equation describes the dislocation velocity in explicit form for a quantum statistical system in terms of the absolute rate theory.

In the above analysis the movement of dislocations over one obstacle

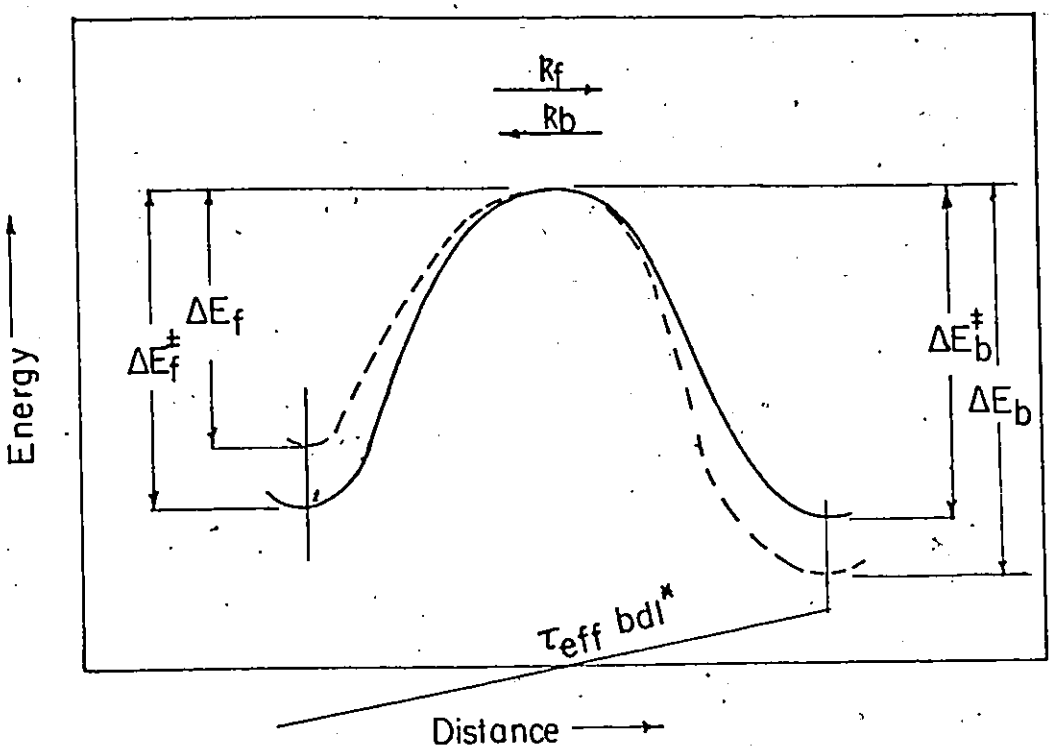

Figure 2.3 Energy-distance curve for shear process

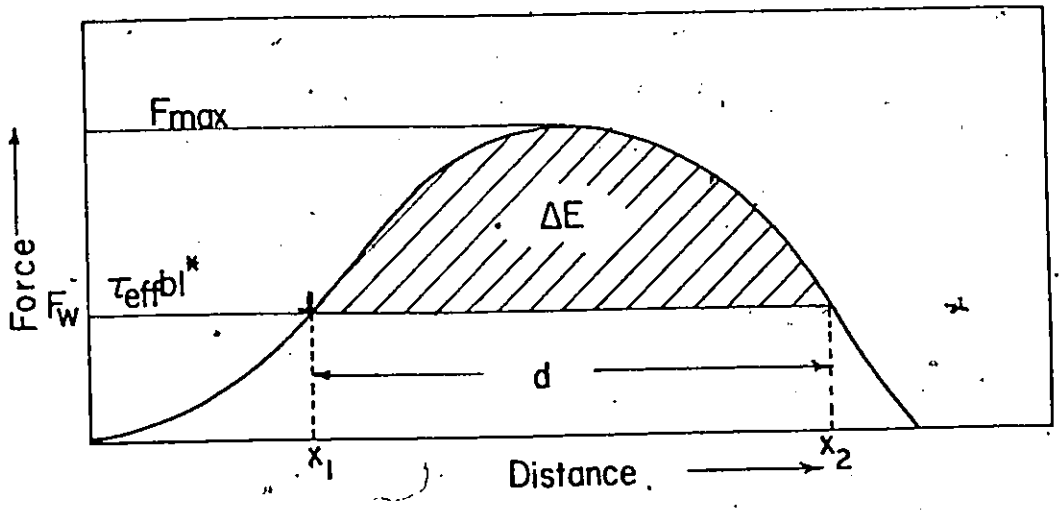

Figure 2.4 Force-distance curve for shear process

has been considered. These obstacles may be in series, in parallel or in series-parallel. The general form of dislocation velocity for any of the above systems having n obstacles can be written as

$$v_n = \left(\frac{d\rho_n}{dt}\right) l_n \tag{2.5}$$

where $\frac{d\rho_n}{dt}$ = the rate at which the dislocations cross the n^{th} barrier,

l_n = the distance between 1st and nth barrier

Krausz and Eyring (13) have analyzed these systems, which are summarized below.

System of obstacles in series: Consider a system of n obstacles as shown in Fig. 2.5, where ρ_1 is the initial mobile dislocations held up at first barrier in forward direction. For steady state in front of the second barrier $\frac{d\rho_2}{dt} = 0$. These dislocations are moving at a rate k_2 in forward direction and k_1 in backward direction. If the mobile dislocations ρ_{n+1} are in the final state, moving at a rate k_n' in backward direction, the rate at which the dislocations will cross the n^{th} barrier will be

$$\frac{d\rho_n}{dt} = \frac{\rho_1 - \rho_{n+1} \exp\left(\frac{(\Delta E)_1}{kT}\right)}{\sum_{i=1}^{n} (k_i)_1^{-1}} \tag{2.6}$$

where $(\Delta E)_1 = \Delta E_1 - \Delta E_1' + \Delta E_2 - \Delta E_2' \ldots + \Delta E_n - \Delta E_n'$

$(k_i)_1$ = the rate of crossing the ith type of barrier considering the activation energy from ground level of stage 1 to the saddle point level of stage i.

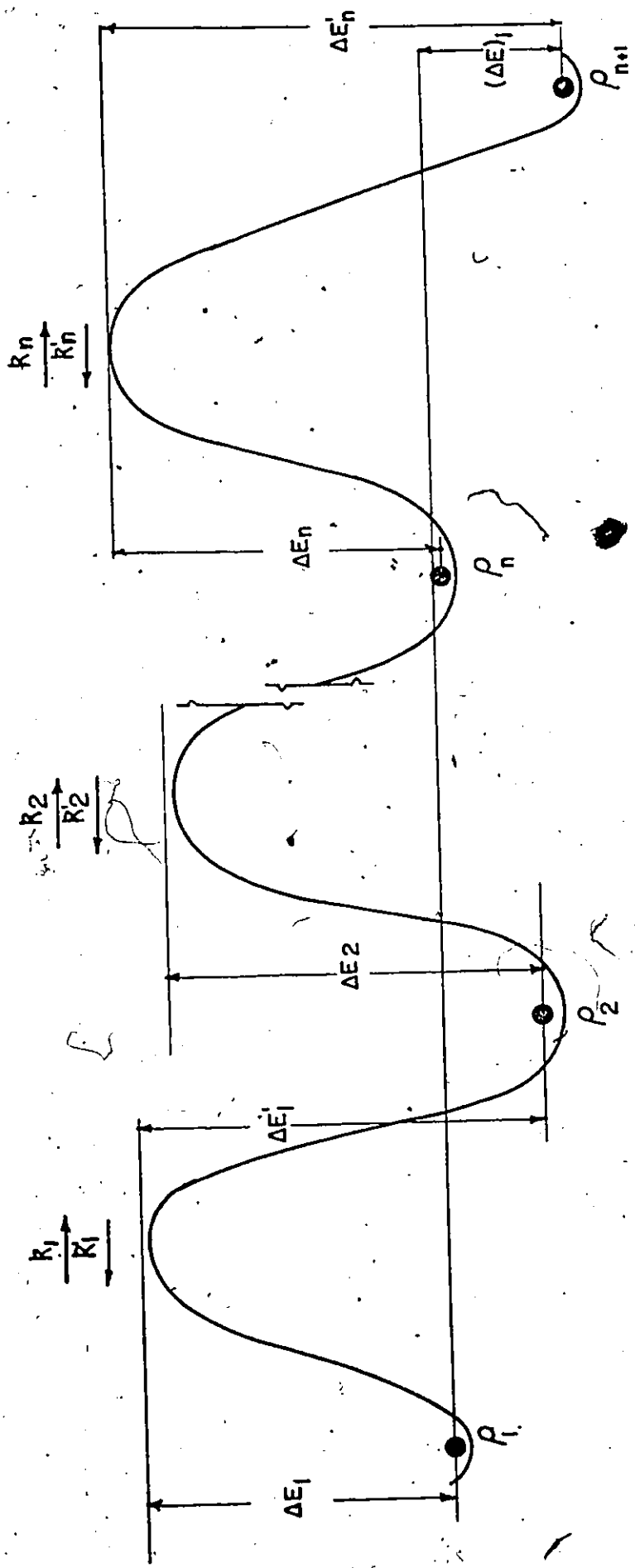

Figure 2.5 Schematic diagram showing n obstacles in series.

(For detailed derivation of equation 2.6, see Appendix III)

System of obstacles in parallel: For only one obstacle, the rate of crossing the barrier is given by

$$\frac{d\rho_1}{dt} = (k_1 \rho_{initial} - k'_1 \rho_{final})$$

If m processes of this type are in parallel, then the rate of crossing the obstacle will be

$$\frac{d\rho_m}{dt} = \sum_{J=1}^{m} (k_j \rho_j \text{ initial} - k'_j \rho_j \text{ final})$$

System of obstacles in series - parallel: If m systems are in parallel and each system has n obstacles in series, the rate of crossing this type of system will be

$$\frac{d\rho_n}{dt} = \sum_{j=1}^{m} \left[\frac{\rho_1 - \rho_{n+1} \exp\left(\frac{(\Delta E)_1}{KT}\right)}{\sum_{i=1}^{n} (k_i)_1^{-1}} \right]$$

where n depends on the branch considered. Thus $n = n(j)$ and $\rho_1 = \rho_1(j)$.

The strain rate for any of the systems considered, can be obtained by substituting equation 2.5 in equation 1.3. Thus, the strain rate will be

$$\dot{\gamma}_p = ab\rho_m \left(\frac{d\rho_n}{dt}\right) \bar{l} \qquad (2.7)$$

Equation 2.7 describes the plastic deformation process for all possible systems of obstacles.

2.3 Various Methods for the Determination of the Stress Dependence of Dislocation Velocity:

The etch pit technique is the most reliable method of determining the stress dependence of the dislocation velocity by direct observation. As this method is tedious, time consuming and cannot be applied to various metals, the indirect methods of dislocation velocity measurement have been developed using Orowan's equation.

Three most common methods are:

(i) The strain rate change

(ii) The discrete stress change and

(iii) The stress relaxation. These are described below.

(i) Strain rate change method: If the specimen is pulled at a constant strain rate $\dot{\gamma}_1$ and at some stage the strain rate is changed to $\dot{\gamma}_2$, an instantaneous stress change $\Delta\tau$ is observed as shown in Fig. 2.6. The stress is related to the strain by the relation (17).

$$\Delta\tau = \frac{kT}{V^*} \ln \frac{\dot{\gamma}_2}{\dot{\gamma}_1}$$

From this equation the activation volume can be calculated. This relation can be obtained by the rate theory neglecting the backward movement of dislocations.

(ii) Discrete stress change method: In this method, the material is allowed to creep under constant stress σ_1 for some time and then the stress is instantaneously increased to stress level σ_{II}. Creep is continued at this new stress level (Fig. 2.7). Wyatt (18) analyzed these experiments and found that at low temperatures, the creep curve II can be matched with curve I by a suitable time shift Δt and a linear relationship exists between stress change and the logarithm of time shift ($\Delta \log t$).

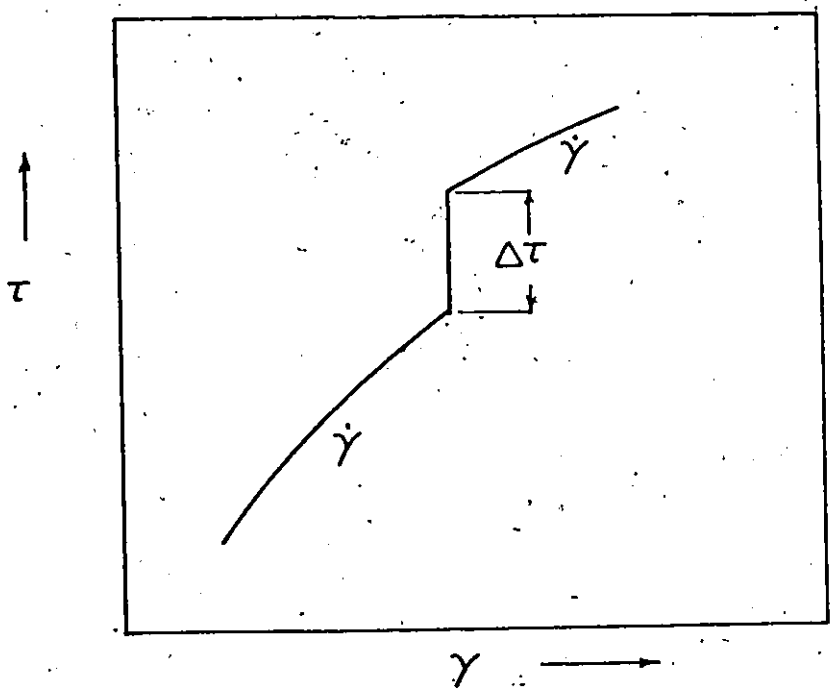

Figure 2.6 The figure illustrates the variables associated with strain rate change experiments.

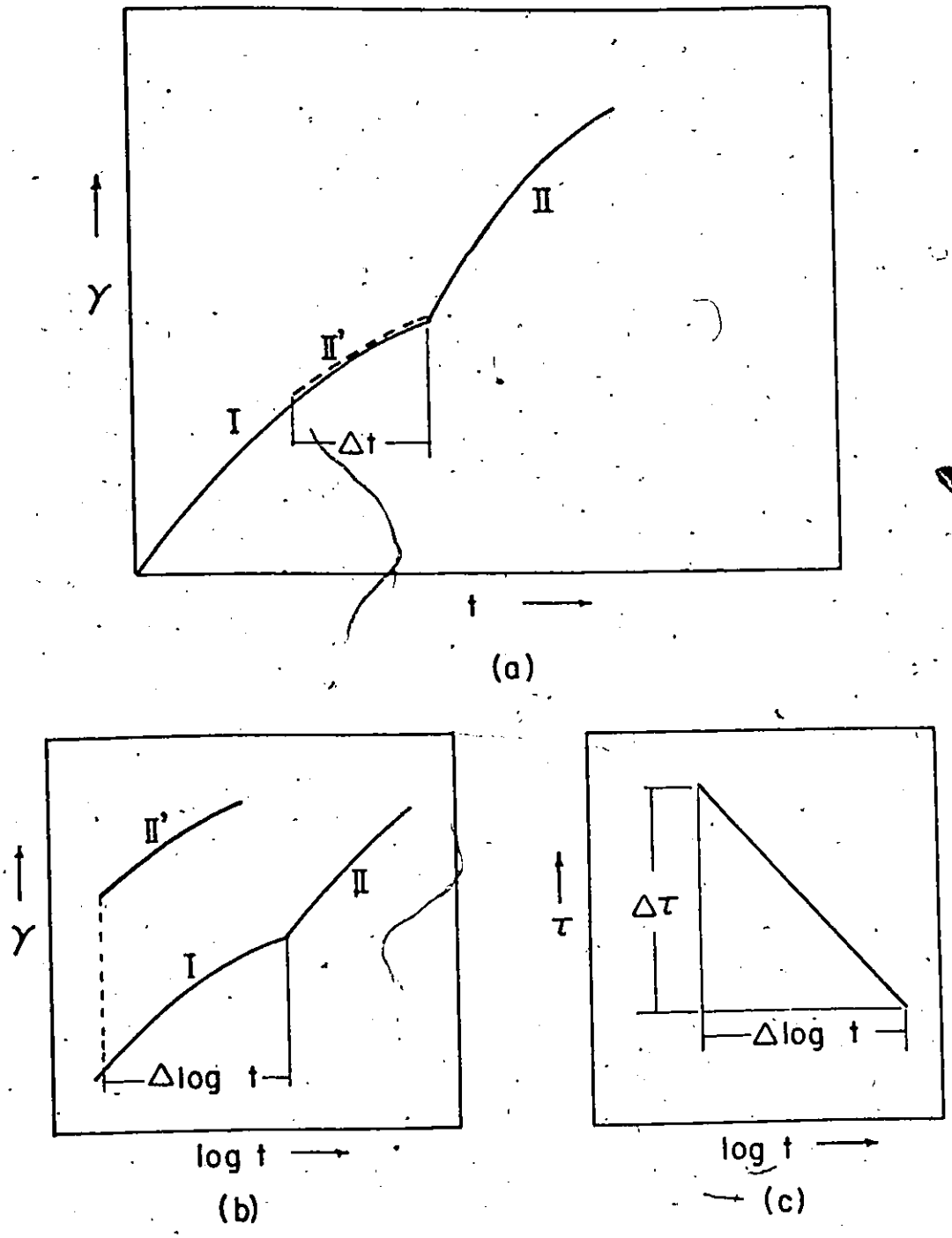

Figure 2.7 (a) to 2.7 (c) The figures illustrate the variables associated with the discrete stress change method.

Activation volume can be obtained by using the relation derived by Cotrell (19).

$$\frac{d \ln t}{d \tau} = -\frac{V^*}{kT}$$

This is in agreement with the rate theory when the backward movement of dislocations is negligible.

(iii) Stress relaxation method: When a material is deformed to a particular strain in a testing machine and the cross head is arrested, thus keeping the total length of the specimen constant, a continuous decrease in load is observed. This phenomenon is "the stress relaxation." The decrease in load is a consequence of plastic deformation of material. As this method is used in the present investigations, it is described in detail.

2.4 Theory of Stress Relaxation

Since the total length of the specimen remains constant during stress relaxation, the plastic deformation of specimen is equal in magnitude but opposite in sign to the elastic strain, ε_e (Fig. 2.8). Therefore,

$$\varepsilon_t = 0 = \varepsilon_e + \varepsilon_p$$

or

$$\varepsilon_e = -\varepsilon_p$$

Further, if $\Delta\sigma$ represents the stress relaxed and E is the elastic modulus of material, then for uniaxial conditions

$$\varepsilon_e = -\varepsilon_p = \frac{\Delta\sigma}{E}$$

The ideal conditions cannot be achieved in the process of stress relaxation as the length of the specimen changes continuously due to elastic deformation of load cell and machine parts as shown in Fig. 2.9. Hence the total strain is given by

$$\varepsilon_t = \varepsilon_a = -[\varepsilon_e + \varepsilon_p]$$

where ε_a is the strain due to deformation of machine parts and load cell, and the plastic strain is

$$-\varepsilon_p = \varepsilon_a + \varepsilon_e$$

Therefore the stress relaxed (20) will be

$$\Delta\sigma = E'(\varepsilon_a + \varepsilon_e)$$

$$= -E'\varepsilon_p \qquad (2.8)$$

where E' is the combined elastic modulus of the testing machine and the specimen.

2.5 Review of Stress Relaxation Test

There are two types of experimental methods used for stress relaxation tests.

(i) Stress decrementation and

(ii) Rigid machine "fixed end."

The detailed description of these methods follows.

(i) Stress decrementation: In this method the length of the specimen is kept constant within limits by removing appropriate weights hanging on the specimen. Trouton and Rankine (21) were the first to perform the stress relaxation test on lead in 1904 by this technique. Boyd (22) per-

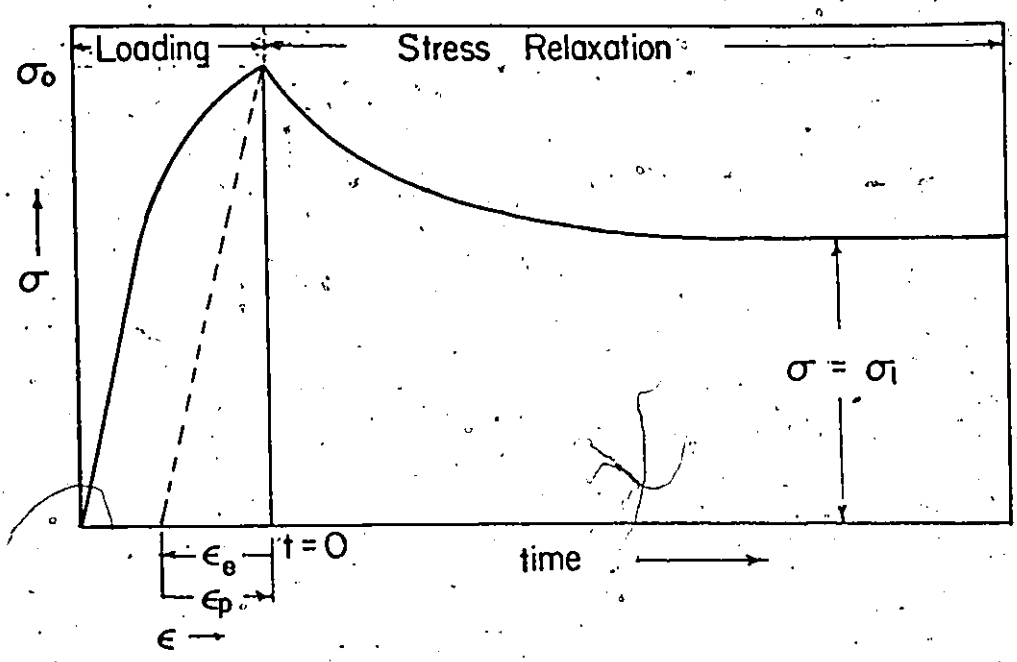

Figure 2.8 The figure illustrates the ideal stress relaxation process.

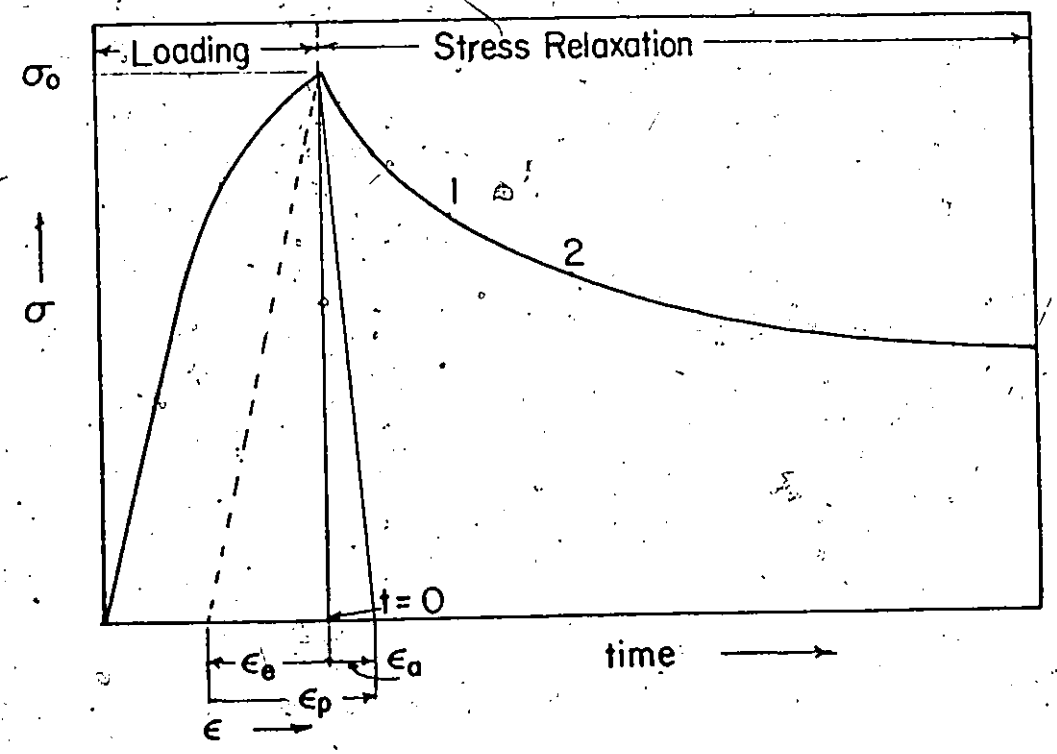

Figure 2.9 The figure illustrates the actual stress relaxation process.

formed tests on lead by maintaining the length of the specimen within specific limits over a gage length of 20" by an automatic relay controlled system.

(ii) Rigid machine "fixed end": In this type of test the specimen is stressed to a desired level and both ends of the specimen are kept fixed. As the ideal conditions cannot be achieved, a change in length equal to the deformation of load cell and machine parts is allowed in the experiments. For the minimum stress change during the test, very rigid machines of Instron type are preferred.

Due to simplicity in experimentation, the fixed end method is widely used. Feltham (1, 23-25) performed stress relaxation tests on α-Iron, α-Brass, Cu and α-Brass and Mg on a Hounsfield Tensometer. Stress relaxation experiments were carried out on Instron by Gibbs (26) on Mg, Sargent (27) on Nb, Wilson and Garofalo (10) on high purity iron, Cu, Al, Pb, and Al alloy 1100, Sargent and Shaw (28) on Mo, Krausz and Craig (29) on Cu, Wray and Horne (9), Li (30) and Ohr (31) on Fe, Rohde and Pitt (14) and Feltham and co-workers (32) on Ni, Krausz (33) on ice, Kelly and Round (34) on Fe, Gupta and Li (35) on some B.C.C. metals, Sargent and Conrad (36,37) on unalloyed titanium and titanium - 4 wt% aluminum alloy, and Krishna (38) on sintered iron.

2.6 Rate Theory of Stress Relaxation:

The stress relaxation process can be analyzed by the rate theory if the dependence of stress change rate on stress change is known. To obtain this relationship consider equation 2.8.

Differentiating with respect to time one obtains

$$\Delta\dot{\sigma} = -E' \dot{\epsilon}_p$$

$$\Delta\dot{\sigma} = -E' c\dot{\gamma}_p \qquad (2.9)$$

For polycrystalline materials (39)

$$\dot{\gamma}_p = \frac{1}{2} \dot{\epsilon}_p$$

Therefore $$\Delta\dot{\sigma} = -E' \frac{1}{2} \dot{\gamma}_p.$$

From Orowan's equation

$$\dot{\gamma}_p = \alpha b \rho_m v$$

Substituting for $\dot{\gamma}_p$ in equation 2.9, the rate of stress change

$$\Delta\dot{\sigma} = -E' \frac{1}{2} \alpha b \rho_m v$$

Now substituting for dislocation velocity from equation 2.4, the rate of stress change can be written as

$$\Delta\dot{\sigma} = -E' \frac{1}{2} \alpha b \frac{kT}{h} \left[\rho_{mf} \kappa_f \bar{l}_f \frac{q^{\ddagger}}{q_f} \exp\left(-\frac{\Delta E_f^{\ddagger} - V_f^{*} \tau_{eff}}{kT}\right) \right.$$

$$\left. -\rho_{mb} \kappa_b \bar{l}_b \frac{q^{\ddagger}}{q_b} \exp\left(-\frac{\Delta E_b^{\ddagger} + V_b^{*} \tau_{eff}}{kT}\right) \right] \qquad (2.10)$$

During stress relaxation

$$\sigma_{eff} = \sigma_t - \sigma_i$$

where σ_t is the applied stress at time t. If $\Delta\sigma$ represents the stress relaxed in time t then the applied stress will be

$$\sigma_t = \sigma_o + \Delta\sigma$$

where σ_o = the tensile stress at the start of relaxation process.

Thus the effective stress acting on the dislocations will be

$$\sigma_{eff} = \sigma_o + \Delta\sigma - \sigma_i$$

Therefore

$$\tau_{eff} = \frac{\sigma_{eff}}{2} = \frac{\sigma_o + \Delta\sigma - \sigma_i}{2}$$

Now substituting for τ_{eff} in equation 2.10, one obtains

$$\dot{\Delta\sigma} = -A_f \exp(n_f \Delta\sigma) + A_b \exp(-n_b \Delta\sigma) \qquad (2.11)$$

$$A_f = E' \frac{1}{2} \alpha b \rho_{mf} \frac{kT}{h} \kappa_f \bar{l}_f \frac{q^{\ddagger}}{q_f} \exp\left(-\frac{\Delta E_f^{\ddagger} - V_f^* \left(\frac{\sigma_o - \sigma_i}{2}\right)}{kT}\right)$$

$$A_b = E' \frac{1}{2} \alpha b \rho_{mb} \frac{kT}{h} \kappa_b \bar{l}_b \frac{q^{\ddagger}}{q_b} \exp\left(-\frac{\Delta E_b^{\ddagger} + V_b^* \left(\frac{\sigma_o - \sigma_i}{2}\right)}{kT}\right)$$

$$n_f = \frac{V_f^*}{2kT}$$

$$n_b = \frac{V_b^*}{2kT}$$

Equation (2.11) describes the rate of stress change for one obstacle considering backward movement of dislocations.

2.7 Internal Stress

The movement of dislocation occurs due to effective stress which is resultant of applied stress τ_a and the internal stress τ_i. The internal stress τ_i is the consequence of inherent resistance and imperfections in the material.

Thus

$$\tau_{eff} = \tau_a - \tau_i$$

When $\tau_a = \tau_i$, no dislocation movement takes place and $\dot{\gamma}_p = 0$ at $\tau_{eff} = 0$. Contrary to this argument Krausz (40) has pointed out that the dislocations stop at finite effective stress τ_{effo}. This is justified by the rate theory. Using the rate equation with two terms, the stress at which the strain rate becomes zero will be

$$\tau_{effo} = \frac{kT}{V_f^* + V_b^*} \ln \frac{A'_b}{A'_f}$$

where $$A'_f = \alpha b \rho_{mf} \bar{l}_f \kappa_f \frac{q^{\ddagger}}{\bar{q}_f} \exp\left(-\frac{\Delta E_f^{\ddagger}}{kT}\right)$$

$$A'_b = \alpha b \rho_{mb} \bar{l}_b \kappa_b \frac{q^{\ddagger}}{q_b} \exp\left(-\frac{\Delta E_b^{\ddagger}}{kT}\right)$$

Majority of the methods for the measurement of internal stresses are based on the concept $\dot{\gamma}_p = 0$ at $\tau_a = \tau_i$. These are discussed below.

2.7.1 Internal stress measurement

Using the above concept, various methods have been developed for the measurement of internal stresses. All these methods are based on the basic assumption that the internal stress and the mobile dislocation density remains constant during the test. These can be classified as:

(i) Direct methods

(ii) Indirect methods.

(i) Direct Methods:

1. Stress Relaxation: In stress relaxation, the effective stress τ_{eff} acting on dislocations decreases with time. The relaxation curve levels off at $\tau_{eff} = 0$ (Fig. 2.8). The corresponding stress is the internal stress. It is quite difficult to obtain this levelling off region due to the time and experimental limitations.

2. Stress reduction: When the stress is reduced below the internal stress level, a net backward movement of dislocations is observed. Gibbs (26) performed experiments by decreasing the stress below internal stress level and obtained the contraction in length of specimen in creep tests. Using this concept various methods have been developed for the determination of the internal stresses. These are discussed below.

(i) Stress transient dip test: (41, 42). In this test the specimen is strained to a particular level and allowed to relax at constant strain. The stress level is decreased in stages and the relaxation curve is observed. The level, at which $(\frac{\partial \tau}{\partial t})_{\varepsilon} = 0$, is the internal stress level. If the stress is decreased below this level, negative relaxation is observed as shown in Fig. 2.10.

(ii) Strain transient dip test: (43) This method is essentially a creep test in which the strain rate is measured after reducing the stress in stages from initial stress level τ_o. When the strain rate is zero, $(\frac{\partial \varepsilon}{\partial t})_{\tau} = 0$, the corresponding stress level is equal to the average internal stress. If stress is dropped below this level, contraction is observed as shown in Fig. 2.11.

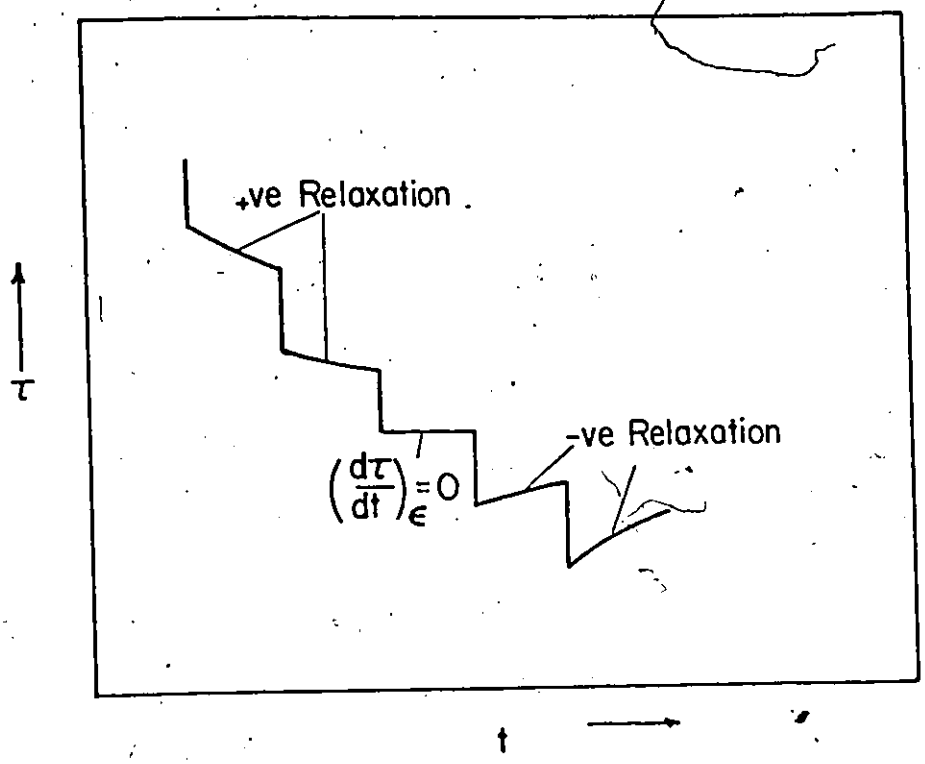

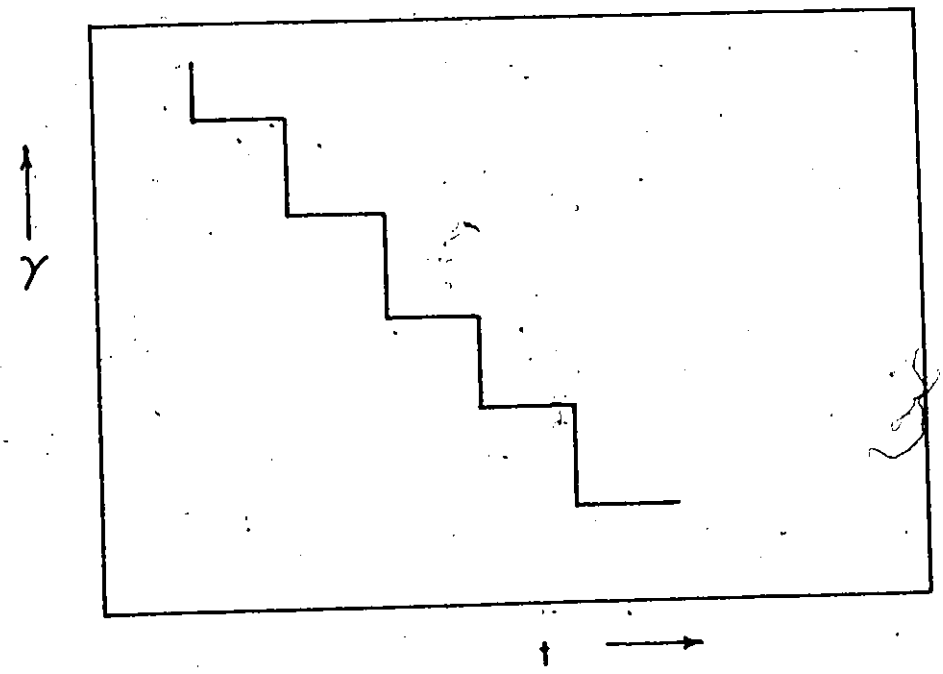

Figure 2.10 Schematic diagram of a stress transient dip test.

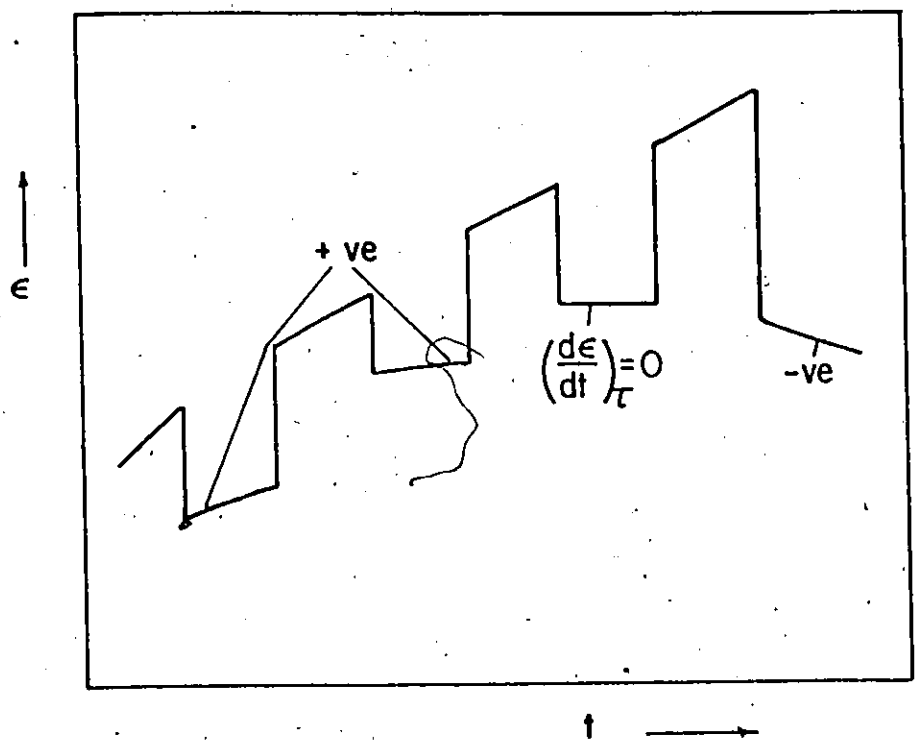

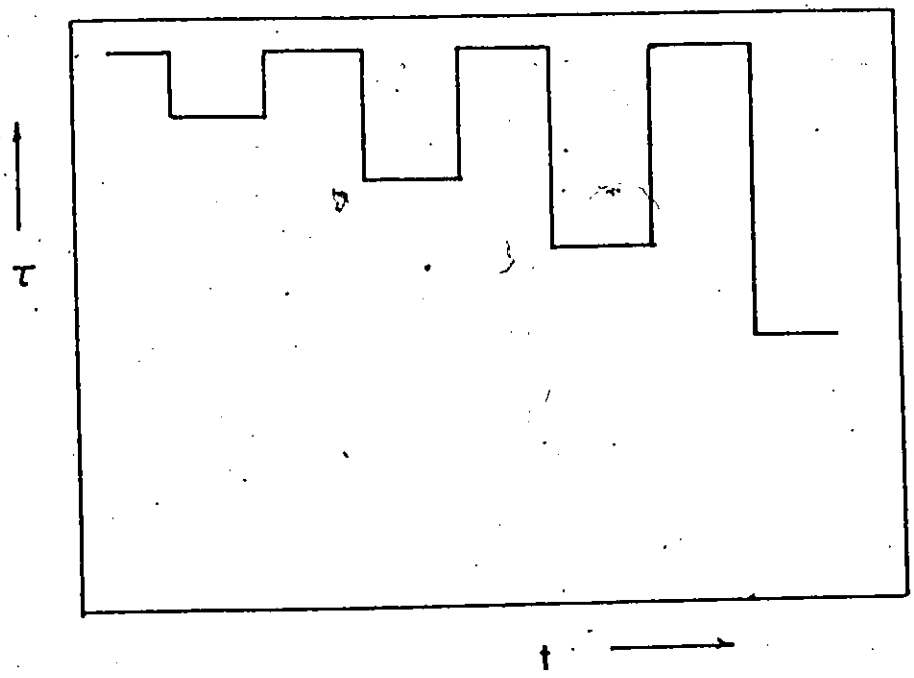

Figure 2.11 Schematic diagram of a strain transient dip test

(ii) Indirect Methods:

1. Stress relaxation: Gilman and Johnston (44) used an empirical expression

$$v = v_o \left(\frac{\tau_{eff}}{\tau_o}\right)^{m^*} \qquad (2.11)$$

relating dislocation velocity v to the effective stress τ_{eff}. In the above equation v_o, τ_o and effective stress exponent m* are constants for particular test. Gupta and Li (45) have used stress relaxation test for the determination of effective stress exponent m* and then for the average internal stress using the relation

$$\frac{\tau_2 - \tau_i}{\tau_1 - \tau_i} = \left[\frac{t_1 + a}{t_2 + a}\right]^{\frac{1}{1-m^*}}$$

In this expression a is a constant, τ_1 and τ_2 are the stresses at any time t_1 and t_2 during the test (Fig. 219). Internal stress τ_i can be calculated as other quantities are known in the above expression.

2. Strain rate change method:

Menezes and Nix (46) proposed this technique for the determination of the average internal stress of the material whose effective stress exponent is known. The specimen is allowed to creep at constant stress τ_1 and then at any point the stress level is changed to τ_2 as shown in Fig. 2.12. Using expression 2.12, relationship between the strain rate before and just after the stress change is given by

$$\frac{\dot{\epsilon}_1}{\dot{\epsilon}_2} = \left[\frac{\tau_1 - \tau_i}{\tau_2 - \tau_i}\right]^{m^*}$$

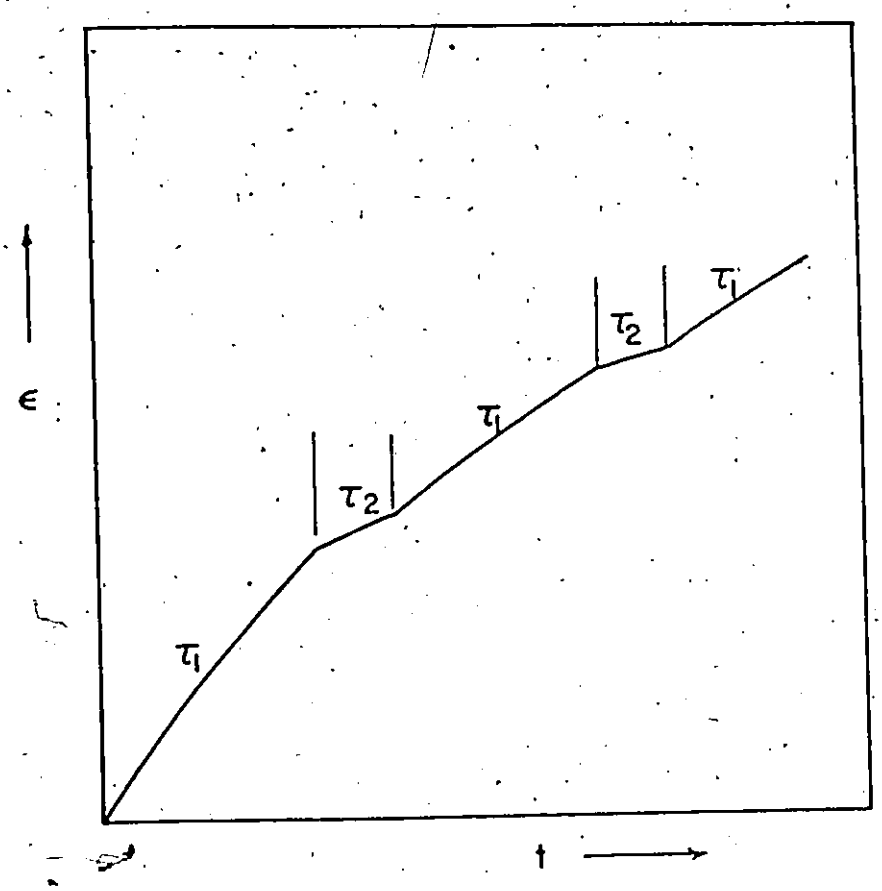

Figure 2.12 Schematic diagram of a strain rate cycling during a creep test.

where subscripts 1 and 2 refer to the stress levels before and after the stress change.

Ahlquist (47) has compared some of the experimental techniques for measuring the average internal stresses and shown that the internal stress level is approximately the same by all the methods. Conrad (48) concluded that the results obtained by the various methods for measuring internal stresses are in good agreement.

CHAPTER 3

EXPERIMENTAL PROCEDURE AND RESULTS

3.1 Material, Preparation of Specimen, and Grain Size and Grain Orientation Determination

3.1.1 Specification of material:

High Purity Iron Grade I - 10 ppm impurities (mainly Si and Mn)

General Properties - Lattice constant = 2.866 A^{o}

Crystal Structure - B.C. C.

3.1.2 Grain Size and Grain Orientation Determination

Grain Size Determination

The grain size was determined by the plannimetric method according to ASTM Standard 112-63. Slabs of the specimen were cut perpendicular and parallel to the longitudinal axis and were embedded in resin. The embedded material was polished and then was etched in Nital for about 10 to 30 seconds. The etched part was magnified 100 times on a microscope screen and the number of grains were counted. The results of grain size measured are given in Table 3.1. Representative photographs of the grain structure are shown in Fig. 3.1.

Grain Orientation Determination

The orientation of grains was determined in the metallurgical laboratory of the Department of Energy, Mines and Resources, Ottawa. The specimen was mounted on a table and an x-ray beam was directed at an angle θ at the etched flat surface of the specimen. The intensity of the

TABLE 3.1

GRAIN SIZE DETERMINATION

Specimen No.	Average Grains / Sq. mm.	Average Grain Size 10^{-3} mm
I	120	95
II	203	70
III	183	74
IV	171	76

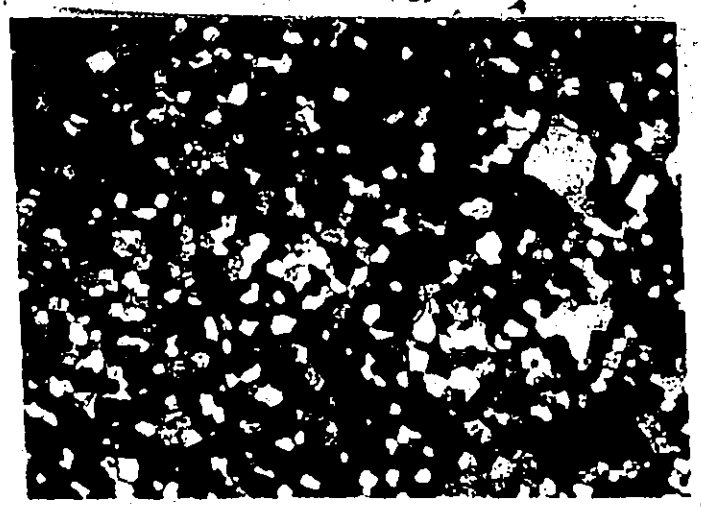

Large and Small Grains

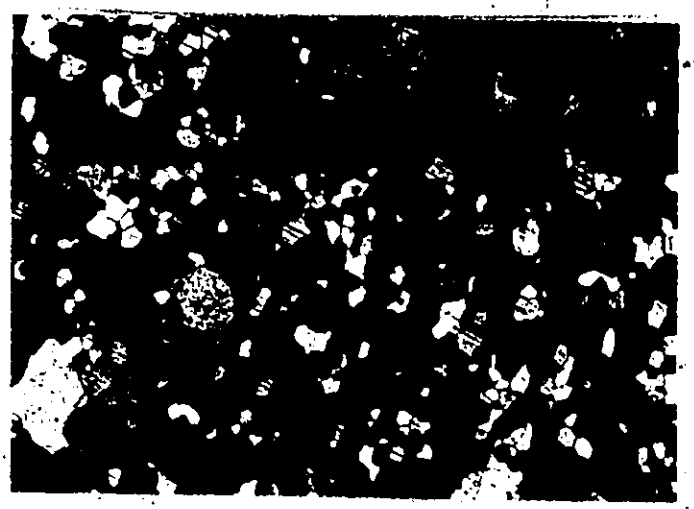

Large and Medium Grains

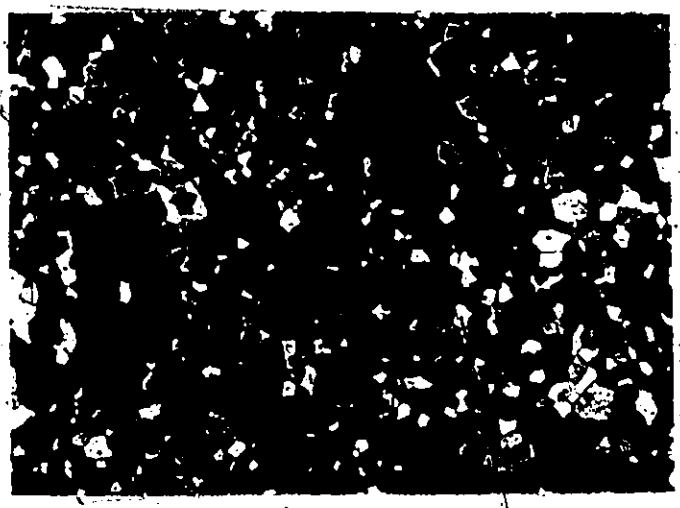

Medium with few Large Grains 25 μ

Figure 3.1 The figures show the representative photographs of the structure.

diffracted beam was measured. This intensity is the measure of the preferred orientation.

3.1.3 Machining:

The specimens were machined from rods of 5 mm. diameter. The diameter of machined specimen was 3.00 ± 0.015 mm. and the gage length was 42.00 ± 0.1 mm. (Fig. 3.2).

3.2 Testing Procedure

3.2.1 Internal Stress Measurement

In the present investigation, the stress reduction technique (41,42) was used for the measurement of average internal stresses. The specimen was strained to a predetermined level and then allowed to relax. The load on the specimen was instantaneously decreased and the nature of the relaxation curve was observed. The stress at which last positive and first negative relaxation occurred, was taken as the upper and lower limit of the internal stress respectively. The results of internal stress measurement are given in Table 3.2.

3.2.2 Stress Relaxation Tests

The stress relaxation tests were carried on Instron machine of T.T.C. model equipped with zero suppression and ten step load suppression unit. A strain gage type electronically calibrated load cell of 500 Kg. capacity was used to measure the load. Stress changes of the order of 0.014 Kg./mm^2 could be detected by this load cell. A set of grips shown in Figure 3.3 was used to hold the specimen in self aligning universal joint.

The specimen was stressed at a constant strain rate of 1.984×10^{-4} sec^{-1} until a predetermined load level P_o was reached. The cross head

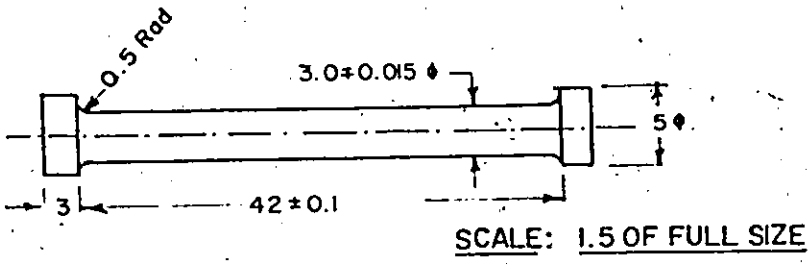

Figure 3.2 The diagram shows the specimen tested in present study.

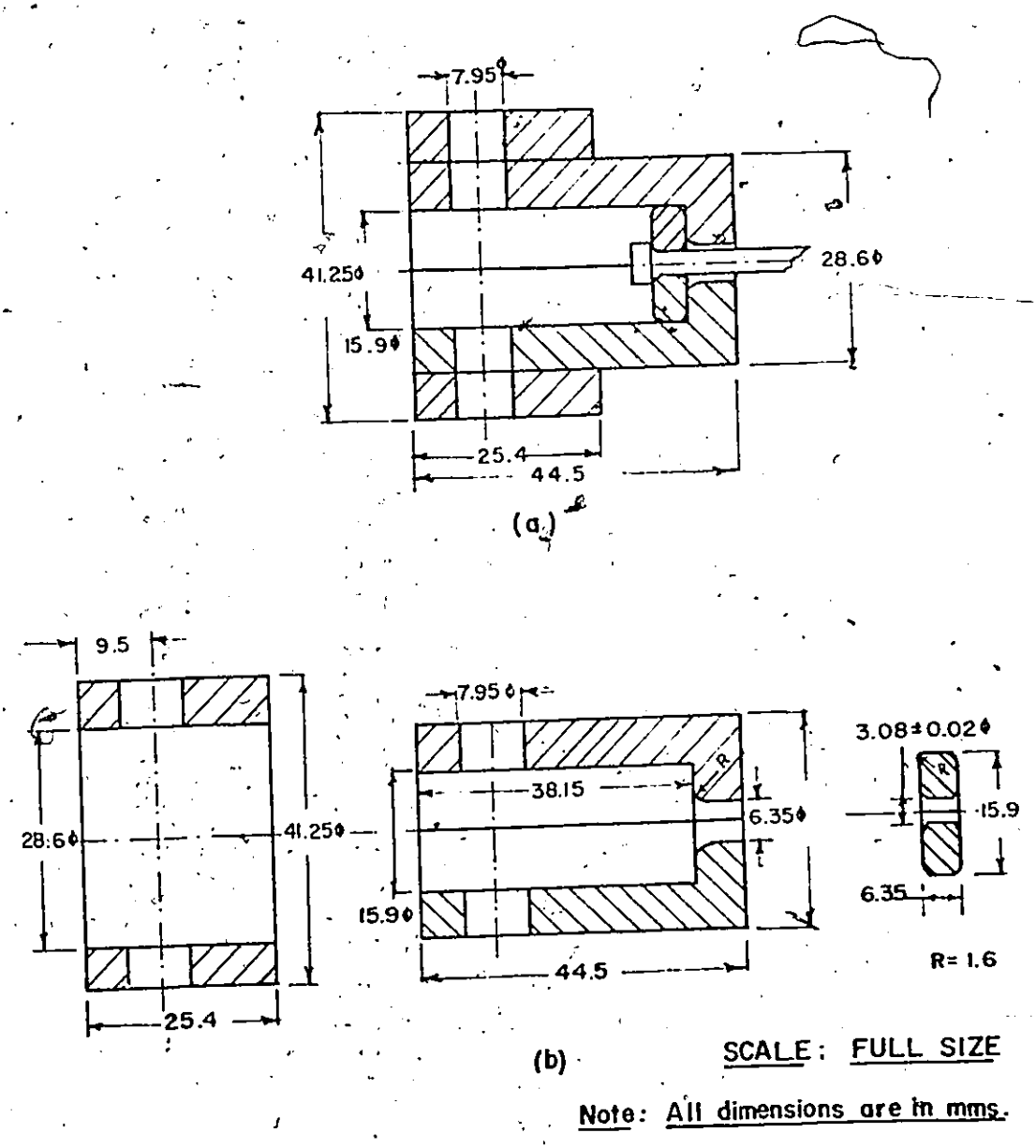

Figure 3.3 The diagrams illustrate the grips used to hold the specimen (a) assembly. (b) details of parts.

TABLE 3.2

INTERNAL STRESS MEASUREMENT

Group No.	Test No.	Stress Level τ kg/mm^2	% Strain γ	Internal Stress kg/mm^2	Internal Stress as % of applied stress kg/mm^2
00	16	2.50	0.09	2.30 $\pm$ 0.13	92.00 $\pm$ 5.00
	17	2.80	0.14	2.51 $\pm$ 0.13	90.00 $\pm$ 4.75
	18	2.59	0.22	2.47 $\pm$ 0.04	95.50 $\pm$ 1.60
0	15	9.54	0.24	6.36 $\pm$ 0.74	66.80 $\pm$ 0.77
	16	7.54	0.24	6.71 $\pm$ 0.08	89.00 $\pm$ 1.06
	17	7.54	0.24	6.74 $\pm$ 0.06	89.50 $\pm$ 0.79
	18	7.45	0.29	6.75 $\pm$ 0.08	90.60 $\pm$ 1.07
1	15	12.16	0.37	9.40 $\pm$ 0.18	77.30 $\pm$ 1.48
	16	12.25	0.38	11.20 $\pm$ 0.22	91.50 $\pm$ 1.83
	17	12.18	0.36	9.51 $\pm$ 0.08	78.00 $\pm$ 0.65
1.1	17	11.80	0.70	9.45 $\pm$ 0.16	80.00 $\pm$ 1.31
1.2	17	12.11	1.59	10.88 $\pm$ 0.13	90.00 $\pm$ 1.07
1.3	17	13.32	3.15	12.10 $\pm$ 0.12	90.80 $\pm$ 0.90
3	15	13.75	3.48	11.50 $\pm$ 0.25	83.50 $\pm$ 1.60
	16	13.75	4.75	12.20 $\pm$ 0.13	88.75 $\pm$ 0.98
	17	13.95	3.62	12.28 $\pm$ 0.12	88.00 $\pm$ 0.96
3.1	16	14.90	5.30	12.82 $\pm$ 0.05	86.00 $\pm$ 0.34
3.2	16	15.42	6.40	13.47 $\pm$ 0.14	87.50 $\pm$ 0.11

was then arrested and the load was allowed to relax. All tests were carried out at a constant temperature of $27 \pm 0.12^{\circ}$ C. The stress change due to temperature variation of 0.12° C was found to be 0.7×10^{-2} Kg/mm^2. Two or three tests were carried out on the same specimen at different stress levels. These stress levels are given in Table 3.3.

Deformation of load cell and machine parts during experiment was measured by linear voltage differential transducer. The schematic arrangement for the measurement of strain change is shown in Figure 3.4. The combined elastic modulus of machine was found to be 5×10^3 Kg/mm^2.

TABLE 3.3

GROUPING OF STRESS RELAXATION TESTS

Group No.	Stress Level Kg./mm^2
00	5.30 ± 0.15
0	15.50 ± 0.10
1	24.50 ± 0.20
2	26.13 ± 0.12
3	27.60 ± 0.30

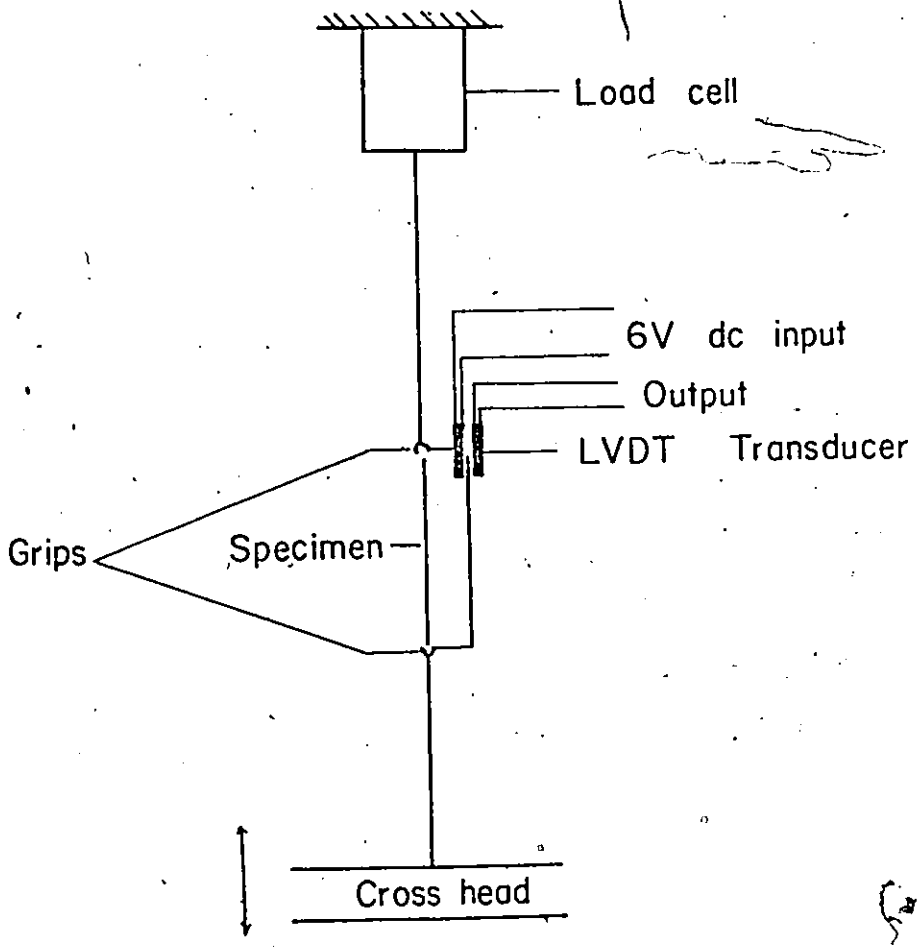

Figure 3.4 Schematic diagram illustrating experimental set up of the Instron.

CHAPTER 4

DISCUSSION

4.1 Tensile Properties of Pure Iron

To obtain tensile properties of pure iron, engineering stress - strain and true stress - strain diagrams were drawn for different specimens. Typical engineering and true stress - strain curves are given in Figures 4.1 and 4.2 respectively. In all the cases sharp yield point was observed. Yield properties of pure iron are given in Table 4.1.

4.2 Internal Stress Measurement

Effective stress causes the movement of dislocations. Therefore, to determine the dependence of dislocation velocity on effective stress, it is of interest to measure the internal stress. Figure 4.3 represents the dependence of applied stress, internal stress and effective stress on strain for test #17. It has been found that the internal stress increases with increasing strain. The effective stress increases up to yield point and then starts decreasing with strain. This type of behaviour is well supported by theory. With increasing strain, the mobile dislocation density increases, consequently the dislocation velocity decreases resulting in a decrease in the effective stress.

4.3 Stress Relaxation Tests

The change in stress as a function of log time is plotted in Figures 4.4 to 4.6. During initial period of relaxation, the process is rapid. The process slows down after about 1000 seconds. Figures 4.7 to 4.10 represent the rate of stress change as a function of stress change. More scatter in experimental points is observed at lower stress

TABLE 4.1

TENSILE PROPERTIES OF PURE IRON

Specimen	Upper Yield Point		Yield Drop
	Stress σ kg/mm^2	% Strain	kg/mm^2
2	25.55	1.59	0.03
4	26.35	1.34	1.07
6	25.20	1.15	1.03
7	26.75	1.10	1.40
9	25.70	1.61	3.00
10	25.25	1.16	2.04
11	25.20	2.77	0.44
13	25.05	1.49	0.50

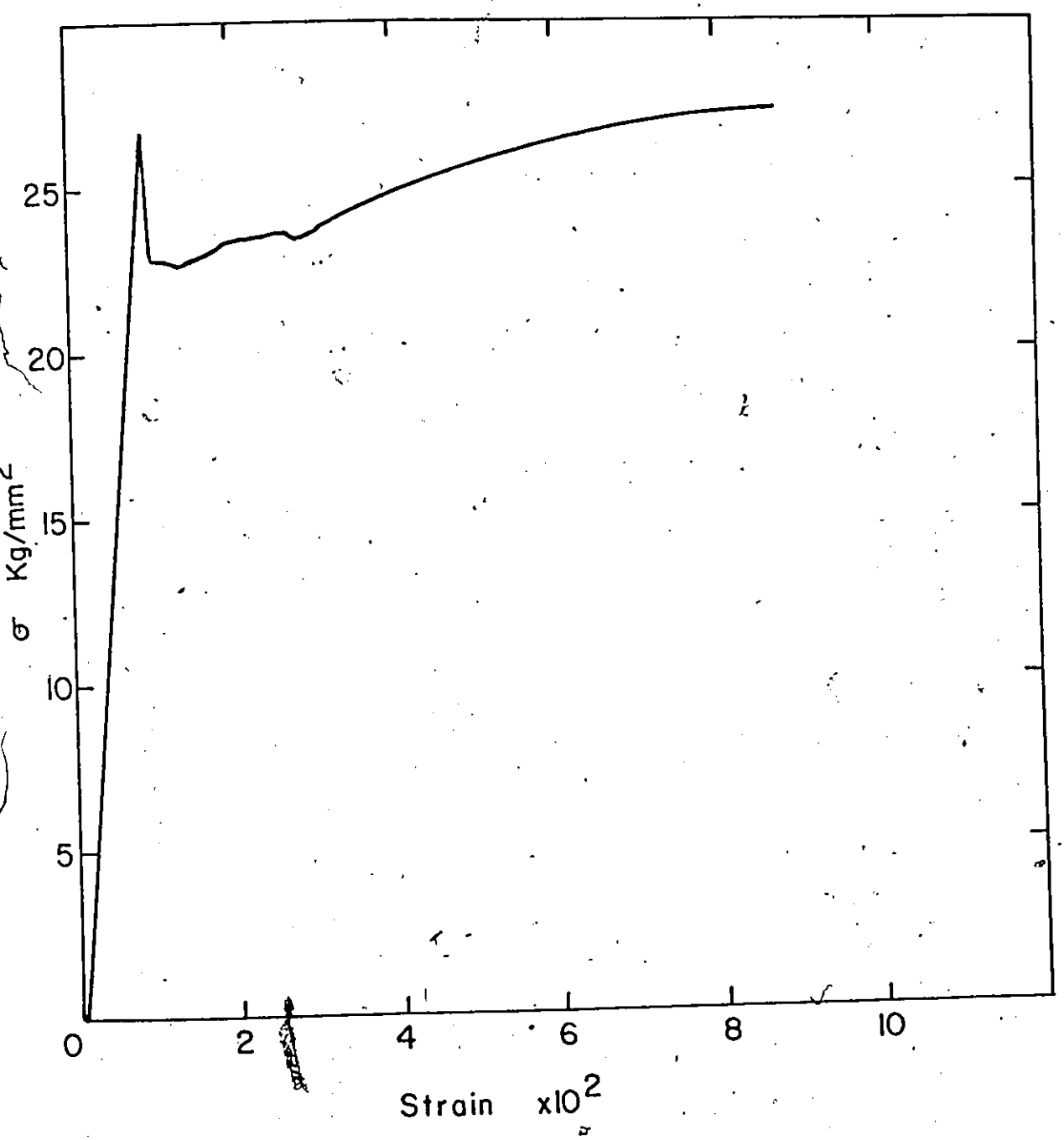

Figure 4.1 The figure illustrates a typical engineering stress-strain curve.

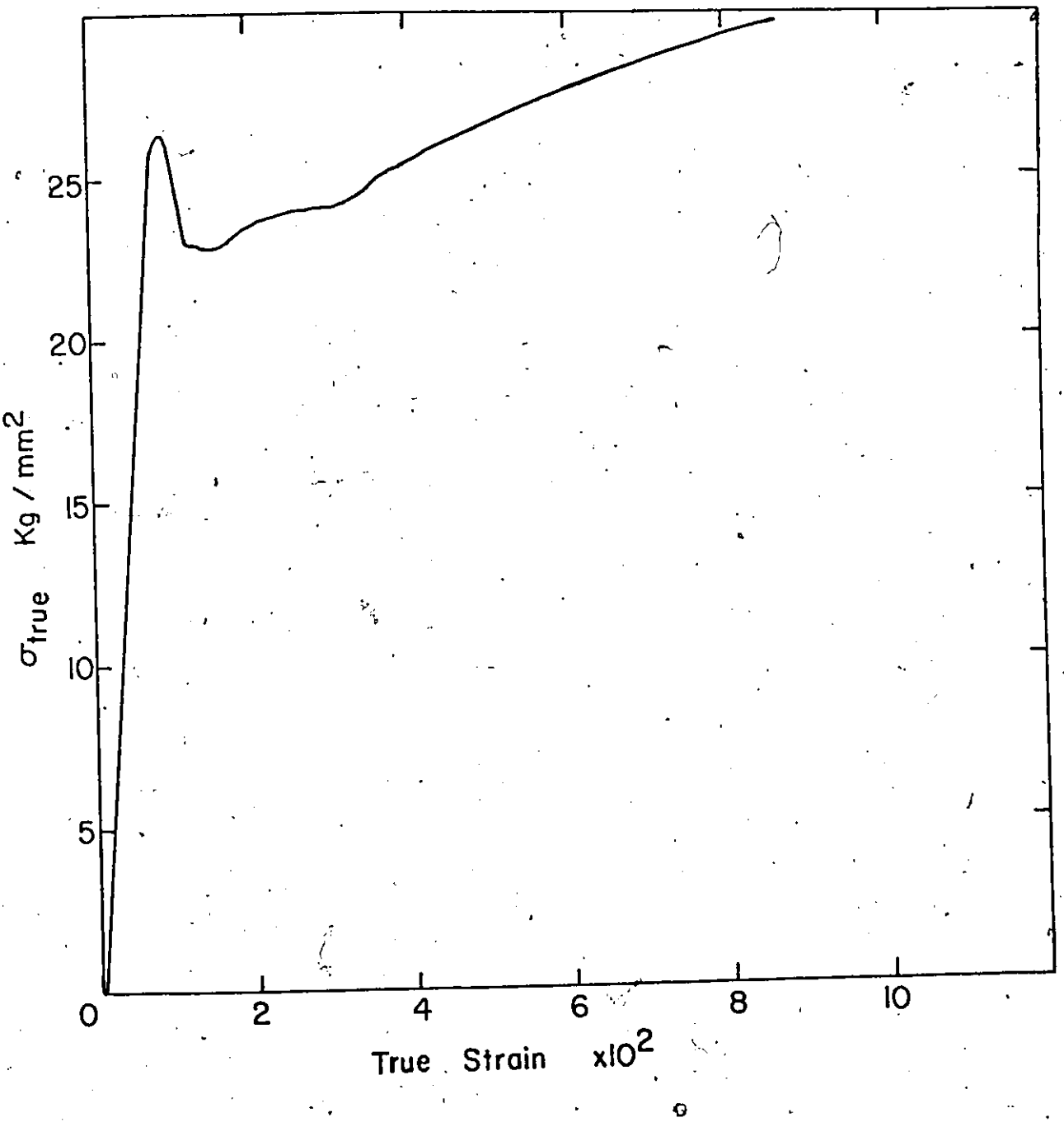

Figure 4.2 The figure illustrates a typical true stress-strain curve.

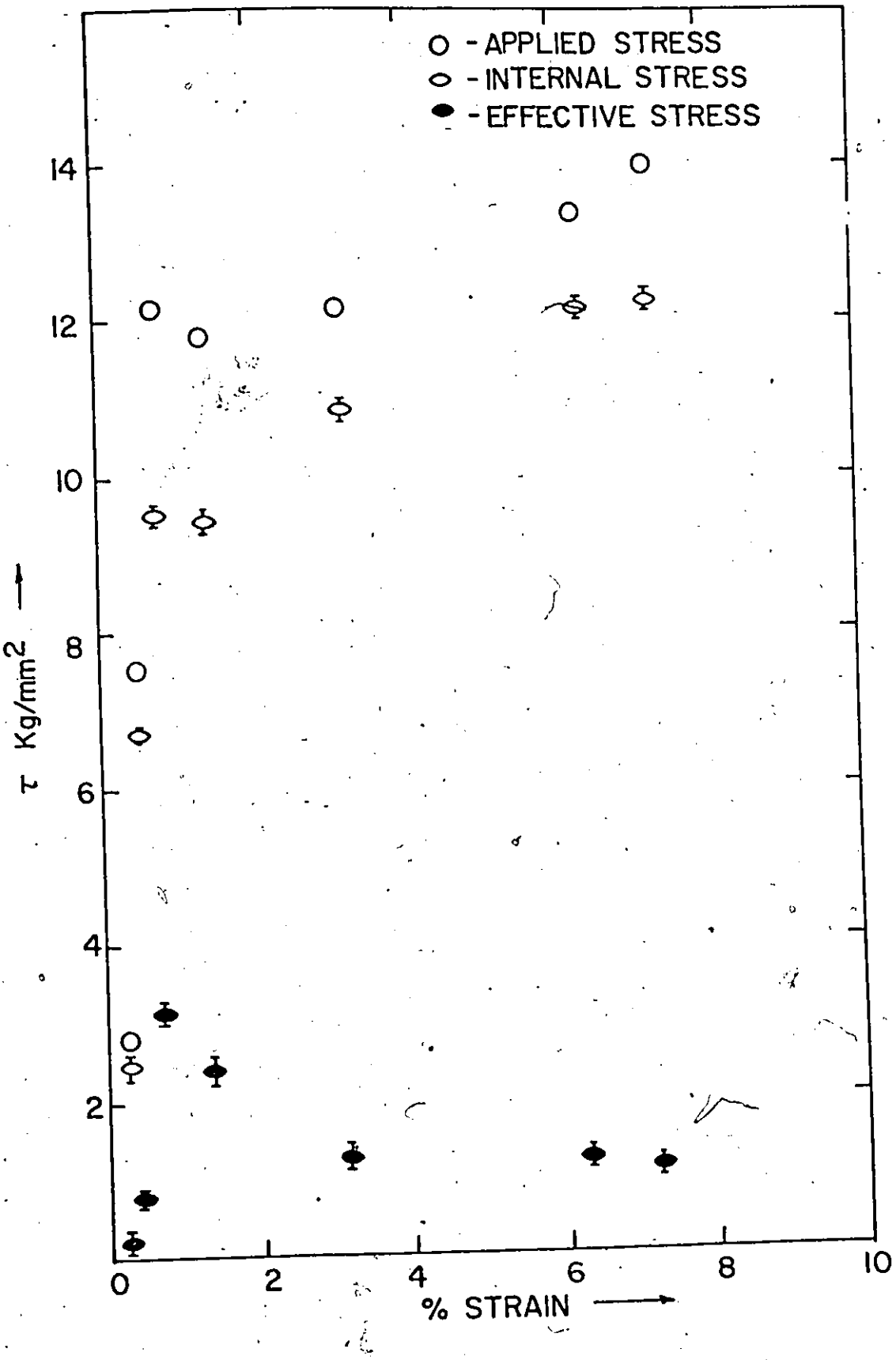

Figure 4.3 The diagram shows the dependence of applied stress, internal stress and effective stress on strain.

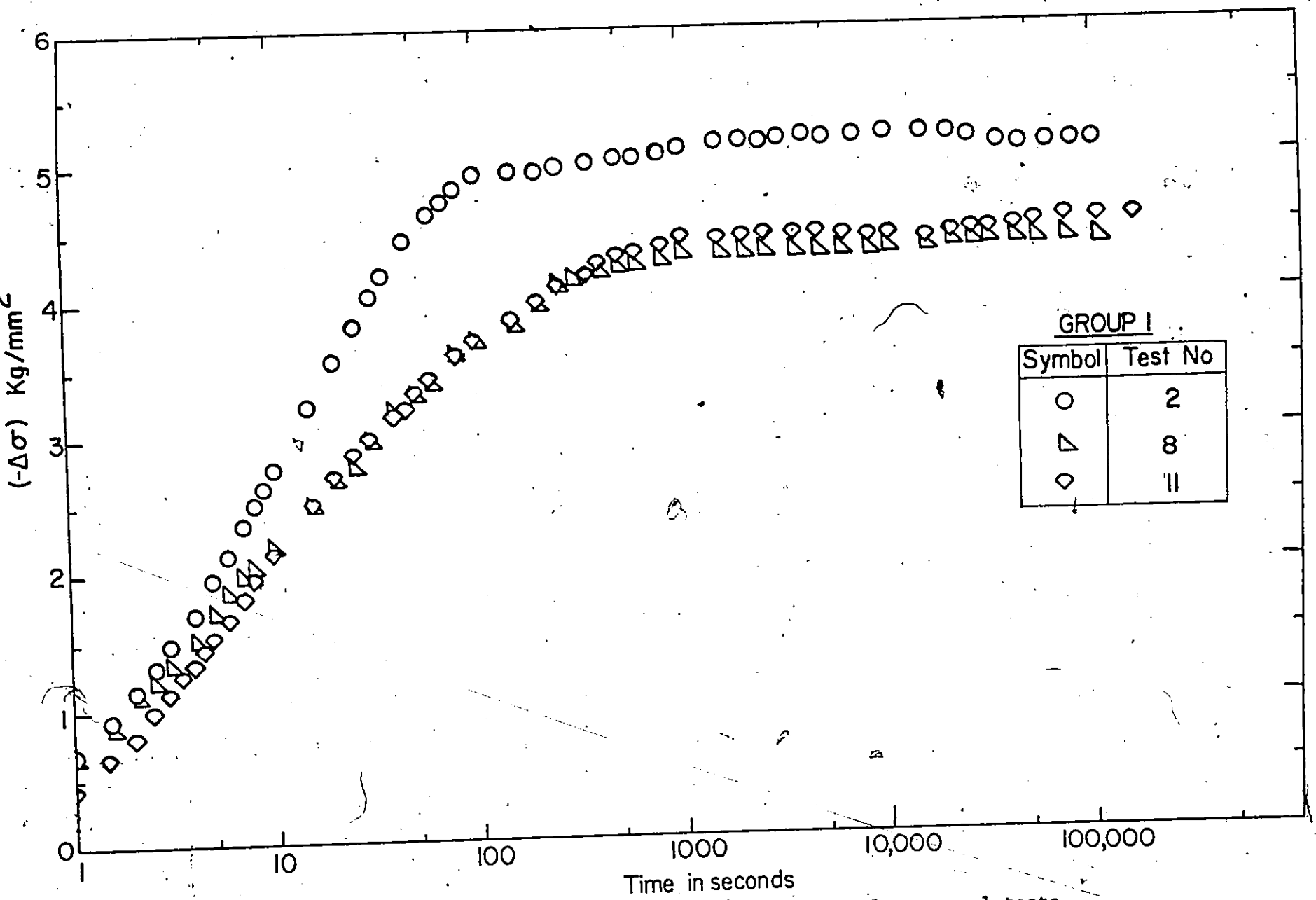

Figure 4.4 A The figure illustrates the dependence of $(-\Delta\sigma)$ on log t for group 1 tests.

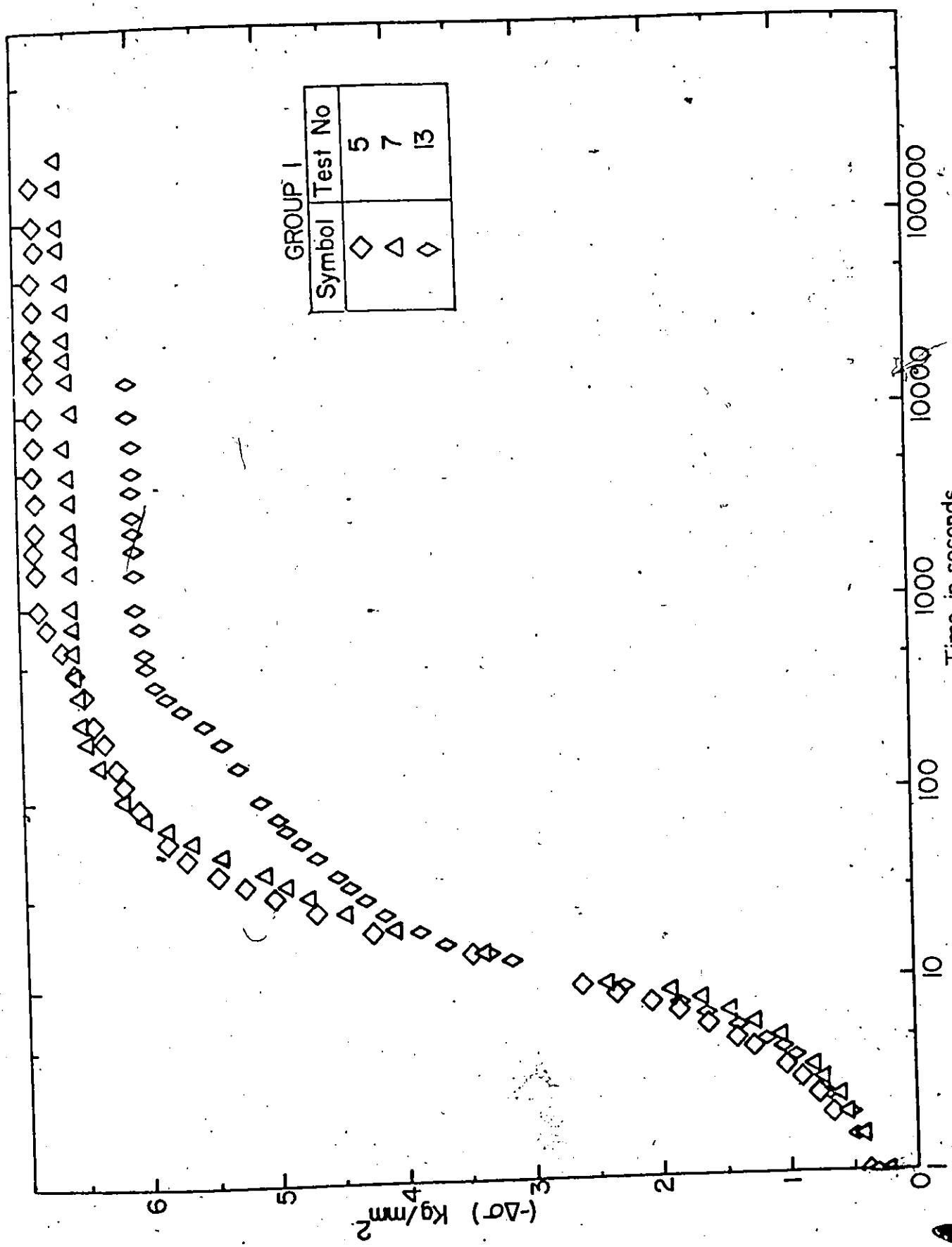

Figure 4.4 B The figure illustrates the dependence of $(-\Delta\sigma)$ on log t for group 1 tests.

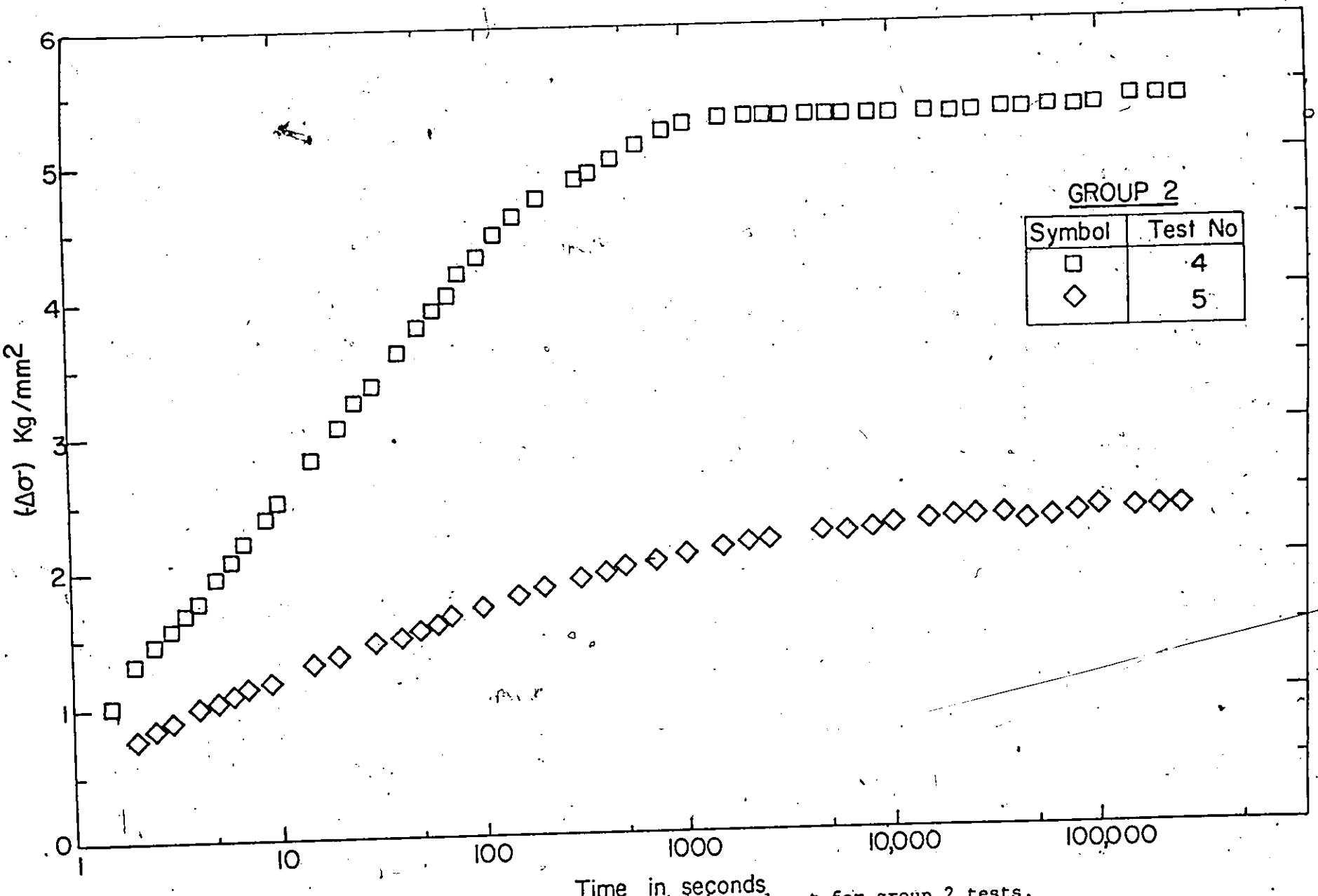

Figure 4.5 The figure illustrates the dependence of $(-\Delta\sigma)$ on log t for group 2 tests.

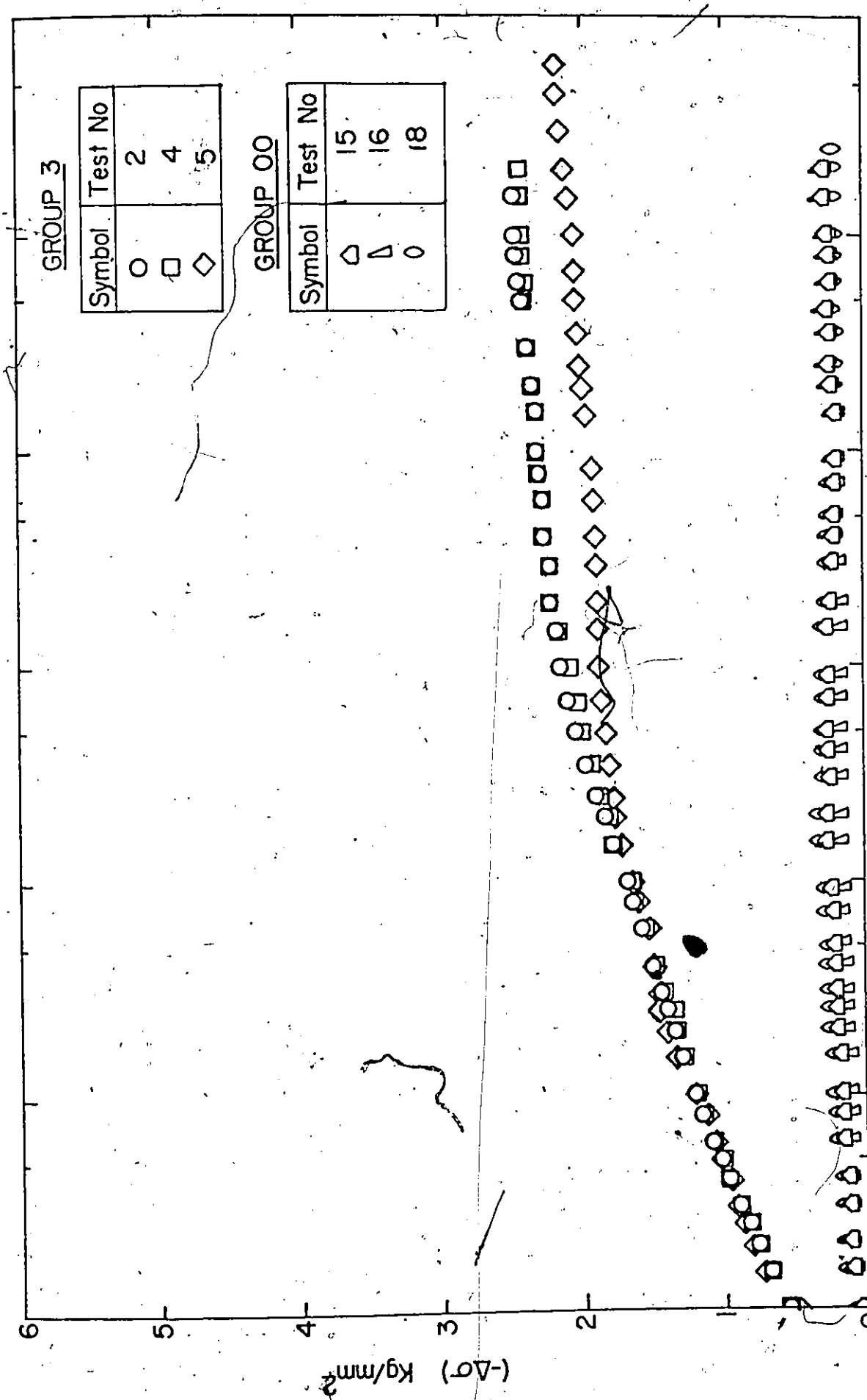

Figure 4.6 A The figure illustrates the dependence of ($-\Delta\sigma$) on log t for groups 00 and 3 tests.

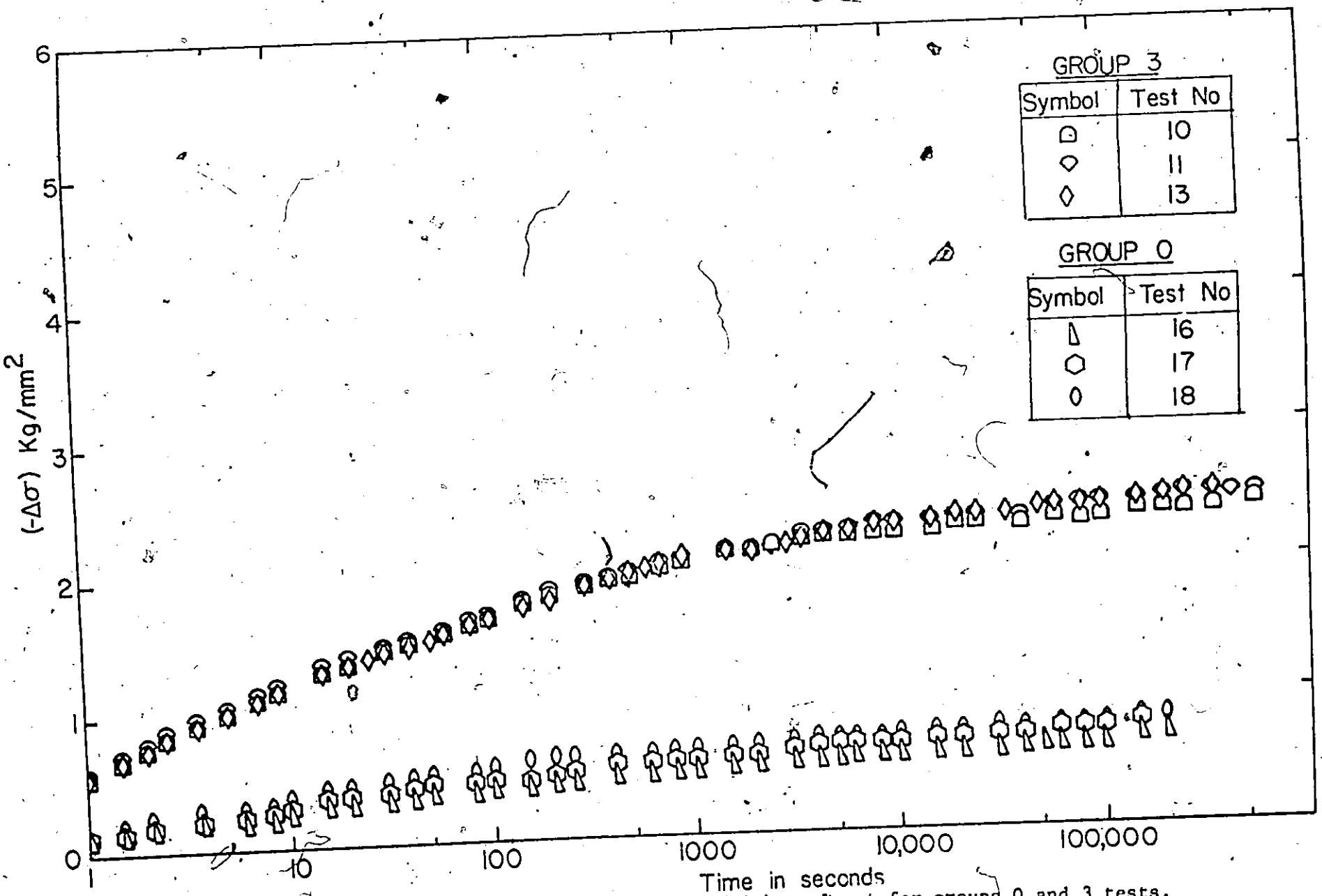

Figure 4.6 B The figure illustrates the dependence of $(-\Delta\sigma)$ on log t for groups 0 and 3 tests.

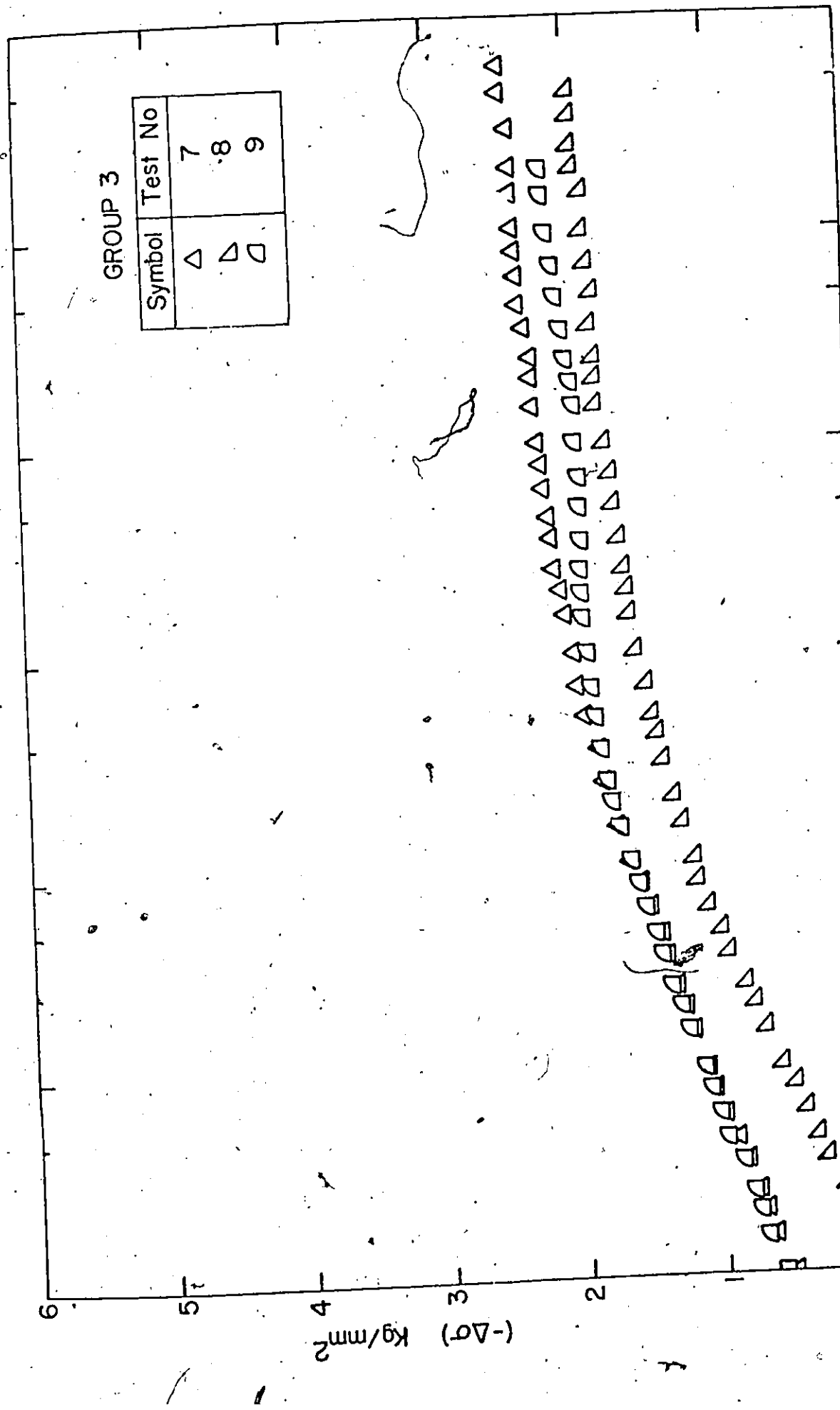

Figure 4.6 C The figure illustrates the dependence of $(-\Delta\sigma)$ on log t for group 3 tests.

levels than those at high stress levels. The probable cause of this type of behaviour is as follows.

Krausz (49) has explained that the plastic behaviour of material is influenced by the structure which is sensitive to the method of production, heat treatment and previous history. At low strains the effect of previous history is pronounced. As the structure of one specimen differs from the other, the pretesting history causes the scatter at low strains. At high strains, the new structure dominates the previous history resulting in less scatter. The results of stress relaxation process were analyzed by the rate theory.

Rate Theory Analysis of the Stress Relaxation

The analysis of stress relaxation test was carried out by considering the simplest but physically admissible system of one obstacle with movement of dislocations in forward direction only. When one term expression of rate equation cannot describe the process, the backward movement incorporating the second term of rate equation was considered. In case the two term rate equation fails to describe the process, the possibility of two barriers working in parallel, or in series was considered. The detailed analysis of stress relaxation is given below.

The initial portion of log of stress change rate vs stress change plot is linear. This can be analyzed by taking one term expression of rate theory. Therefore, in initial region of the relaxation process the rate of stress change will be

$$\Delta\dot{\sigma} = -A_f \exp(n_f \Delta\sigma) \qquad (4.1)$$

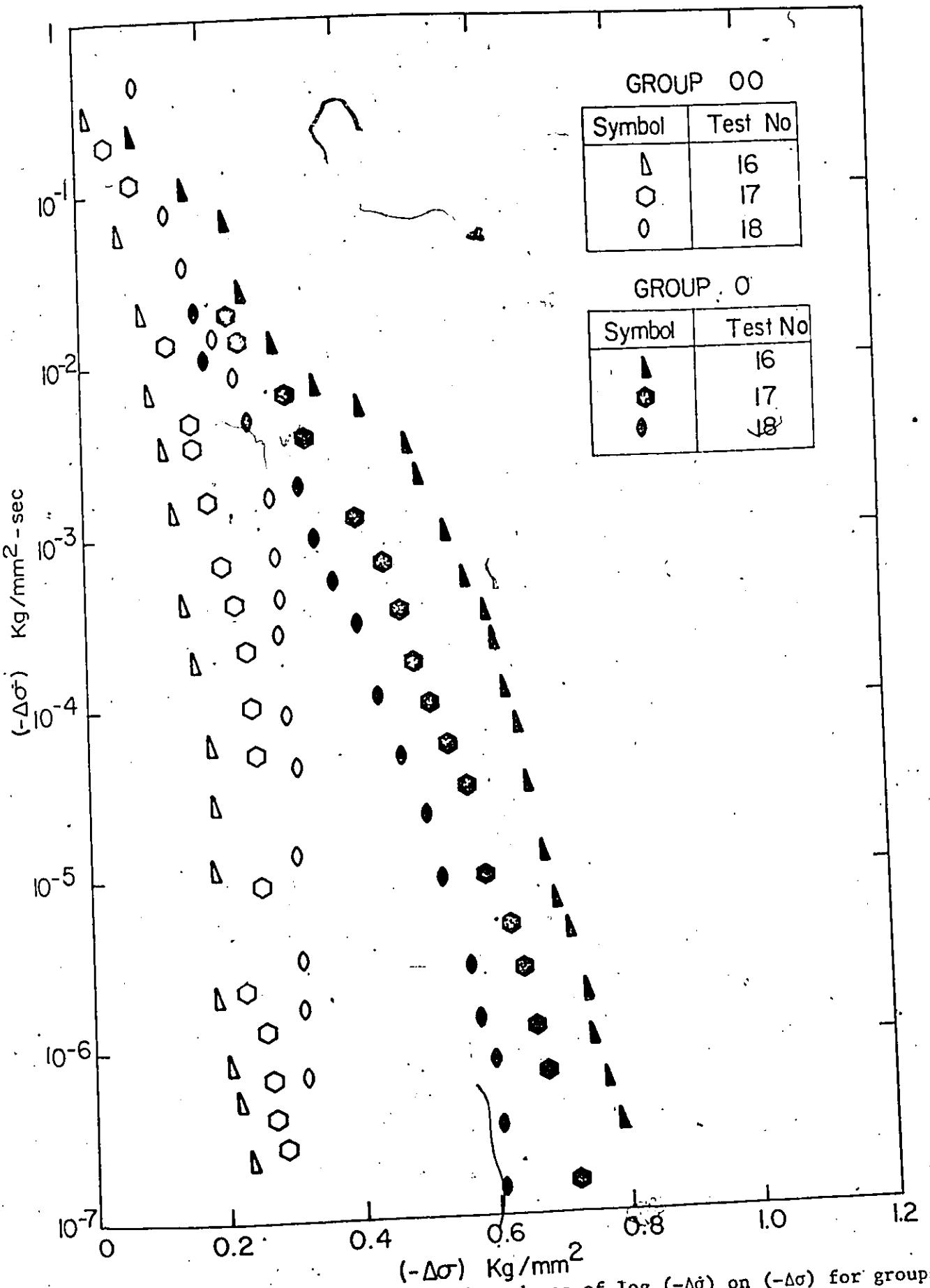

Figure 4.7. The figure illustrates the dependence of log $(-\Delta\dot{\sigma})$ on $(-\Delta\sigma)$ for groups 00 and 0 tests.

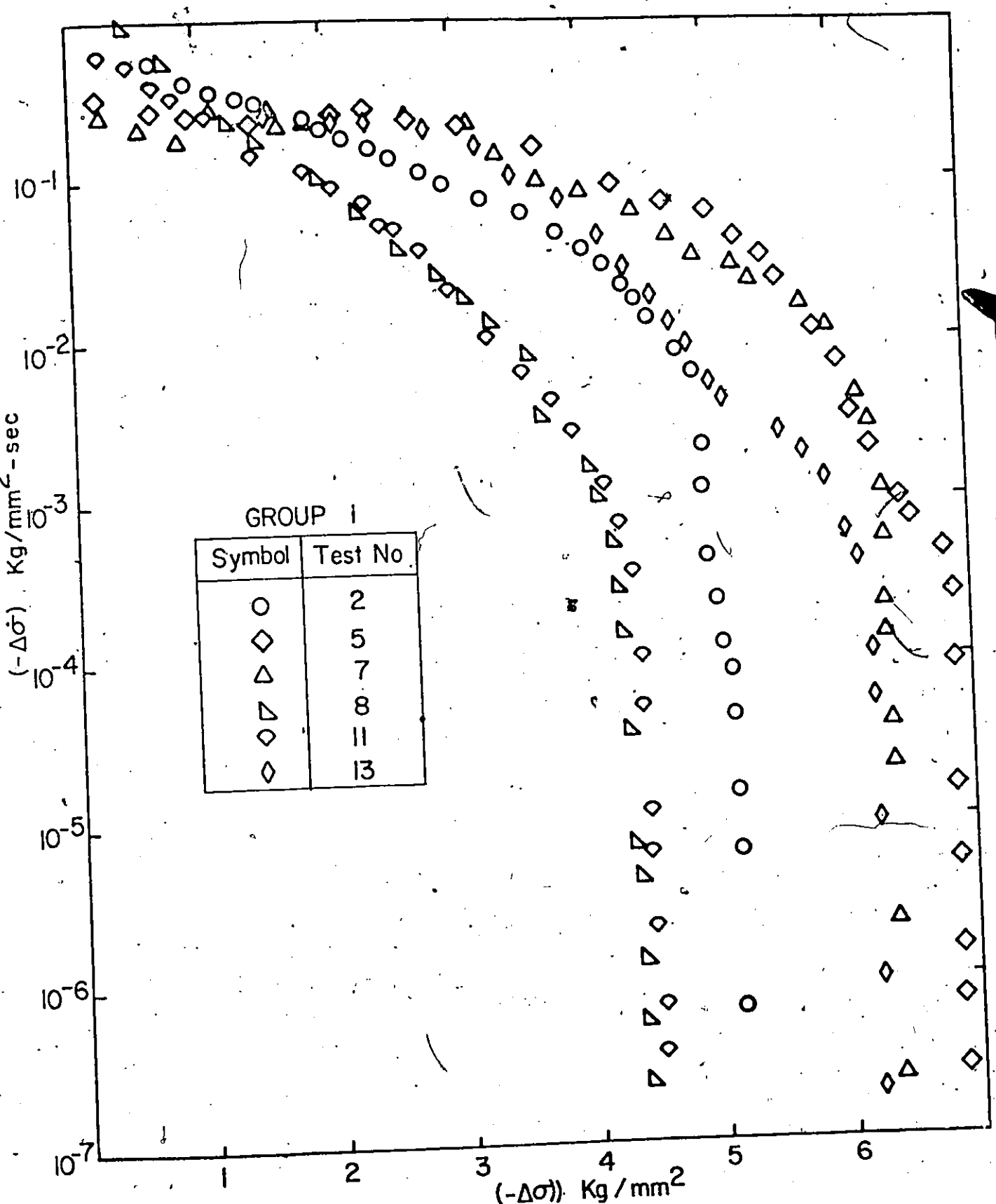

Figure 4.8 The figure illustrates the dependence of log $(-\Delta\dot{\sigma})$ on $(-\Delta\sigma)$ for group 1 tests.

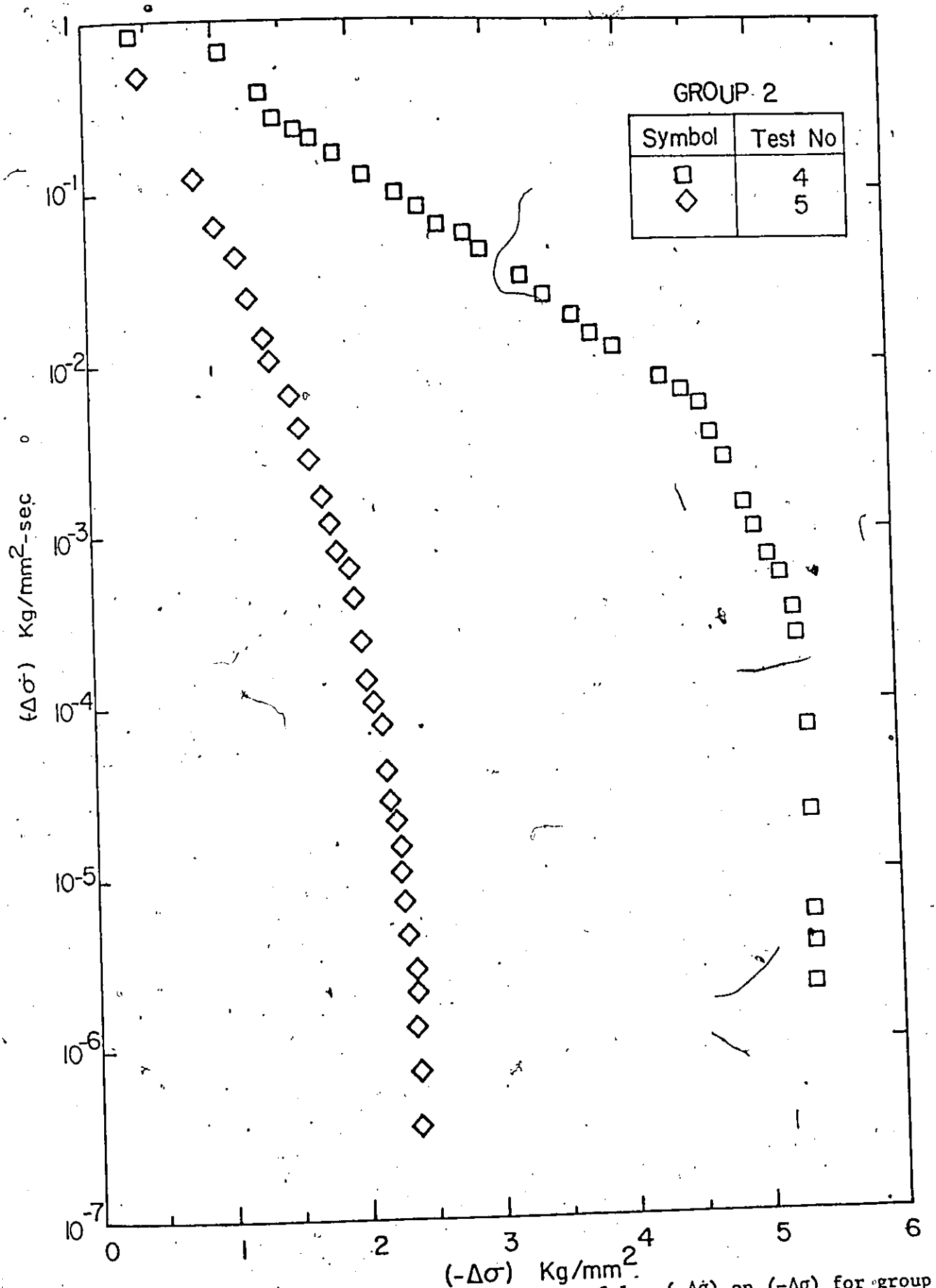

Figure 4.9 The figure illustrates the dependence of log $(-\Delta\dot{\sigma})$ on $(-\Delta\sigma)$ for group 2 tests.

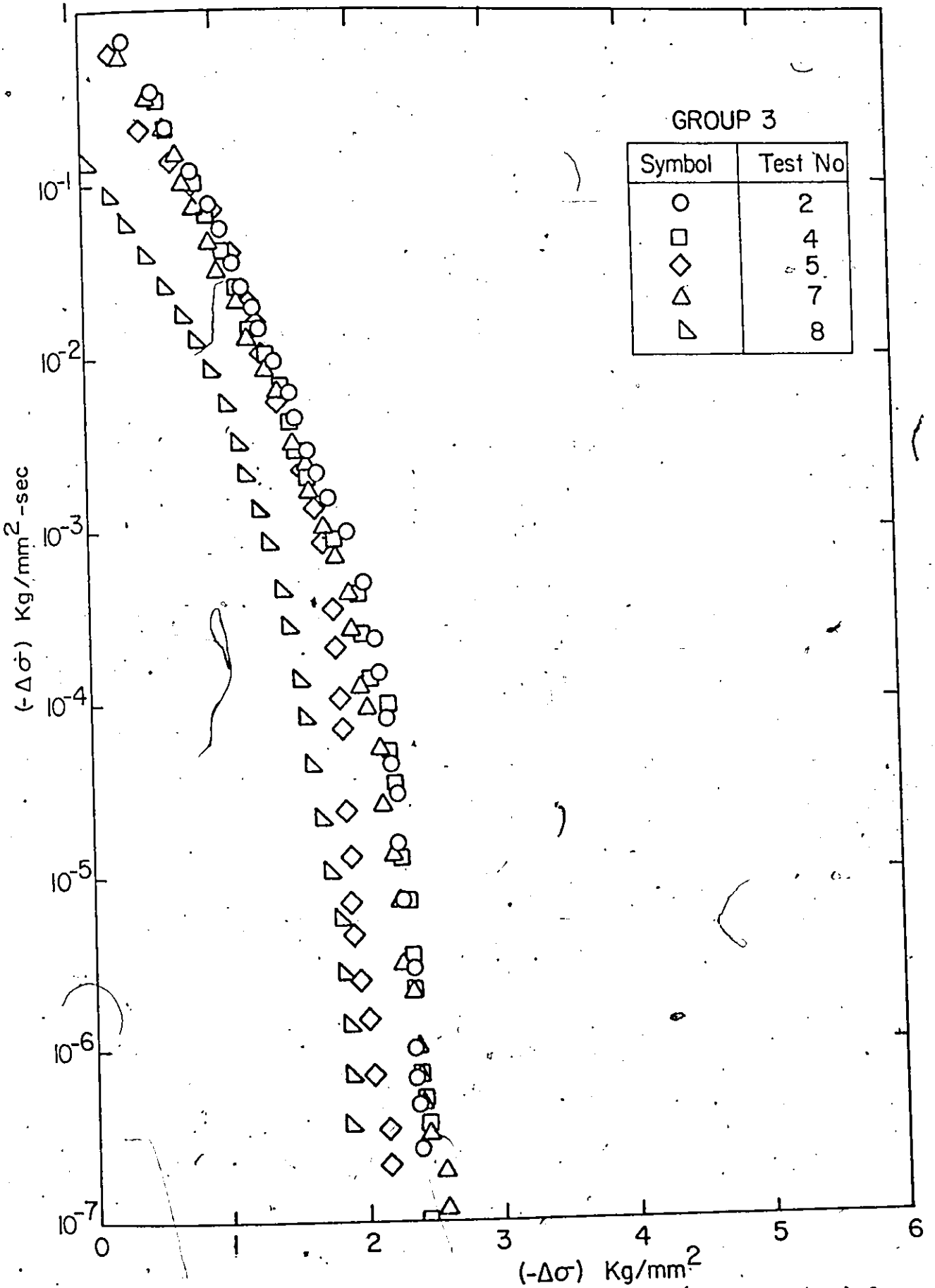

Figure 4.10 A The figure illustrates the dependence of log $(-\Delta\dot{\sigma})$ on $(-\Delta\sigma)$ for group 3 tests.

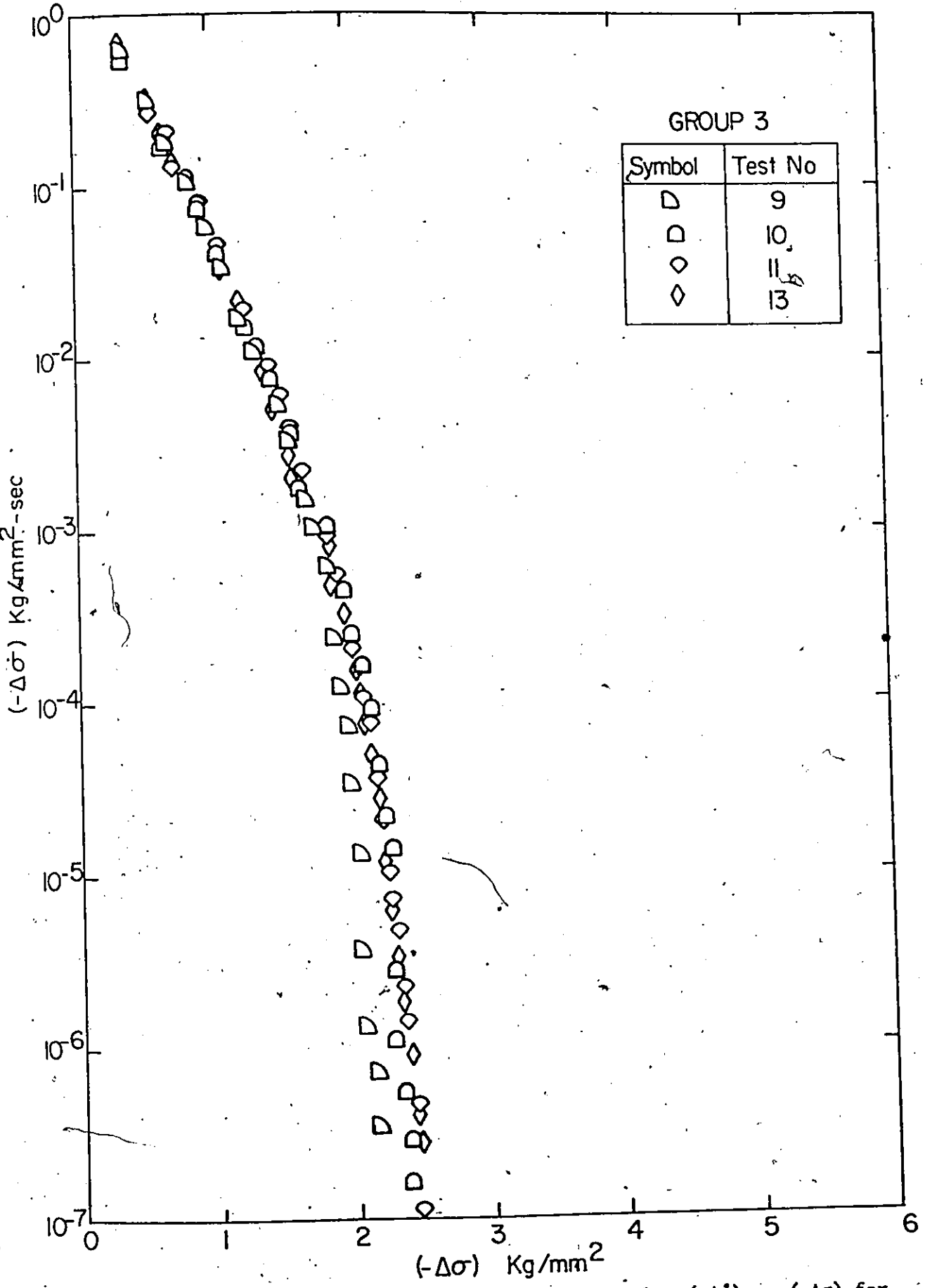

Figure 4.10 B The figure illustrates the dependence of log $(-\Delta\dot{\sigma})$ on $(-\Delta\sigma)$ for group 3 tests.

One term expression is physically justified as the backward movement of dislocations can be neglected at low stress change i.e. at high effective stress. At longer periods the relation between log $(-\Delta\dot{\sigma})$ and $(-\Delta\sigma)$ is nonlinear. Similar observations were made by other investigators (14, 22, 30, 38). The deviation from linearity may be due to the backward movement of dislocations. The rate of stress change in this region can be expressed by two term rate equation. Therefore, the rate of stress change will be

$$\Delta\dot{\sigma} = -A_f \exp(n_f \Delta\sigma) + A_b \exp(-n_b \Delta\sigma) \qquad (4.2)$$

As n_b can have only positive values, the limiting condition for the validity of equation 4.2 is

$$\Delta\sigma_2 - \Delta\sigma_1 > 0, \text{ and}$$

$$\Delta\dot{\sigma}_1 + A_f \exp(n_f \Delta\sigma_1) > \Delta\dot{\sigma}_2 + A_f \exp(n_f \Delta\sigma_2) \qquad (4.3)$$

where subscripts 1 and 2 correspond to the points shown in Fig. 4.11.

The parameters corresponding to backward movement were calculated by satisfying the conditions given in equation 4.3. The theoretical curve obtained by these parameters matches with the experimental curve within validity range of two term rate equation and then falls below the experimental curve. Finally, it loses the validity in low effective stress region. These observations support the possibility of second mechanism operating in parallel whose effect is negligible in initial part of relaxation process but takes over the process in low stress region as shown in Fig. 4.12. Parameters corresponding to for-

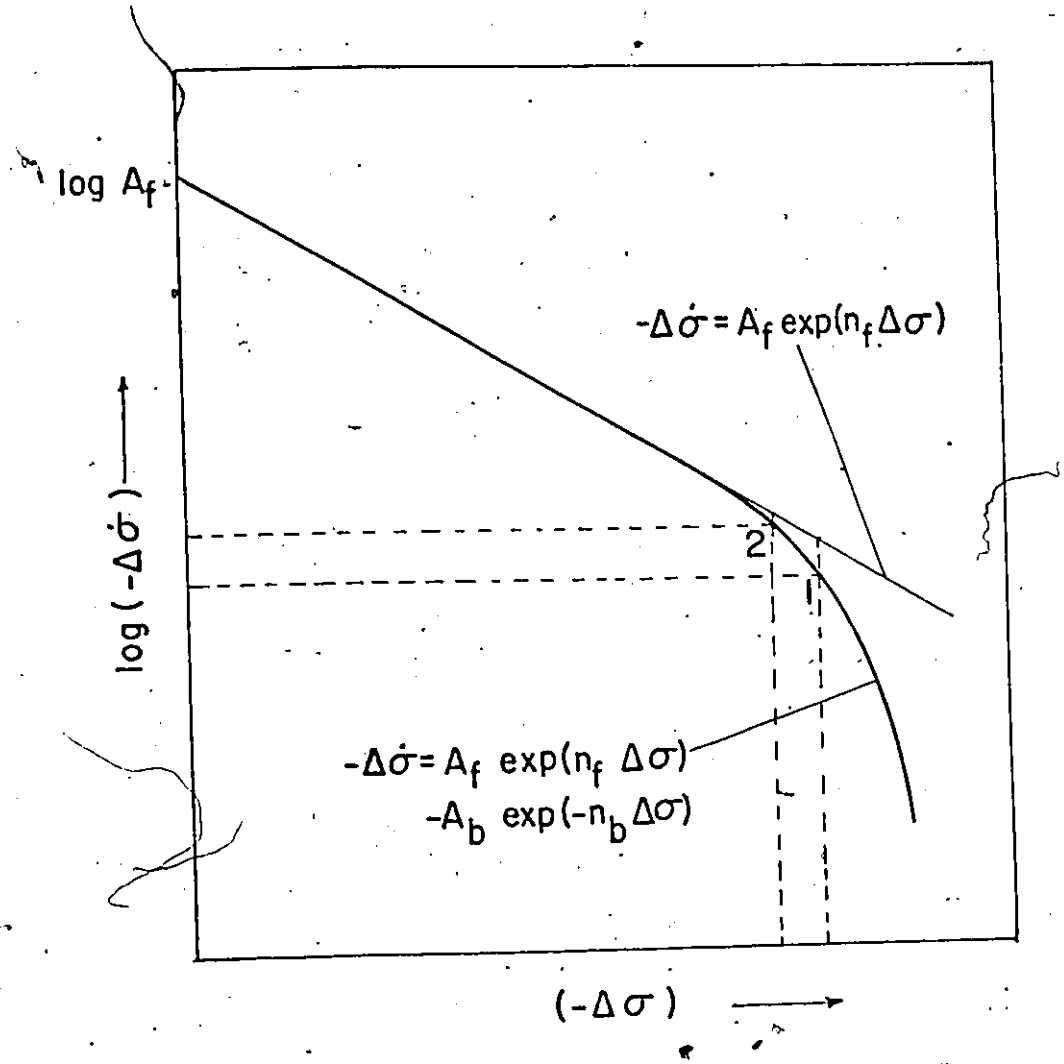

Figure 4.11 The figure illustrates the validity limit for two term rate equation

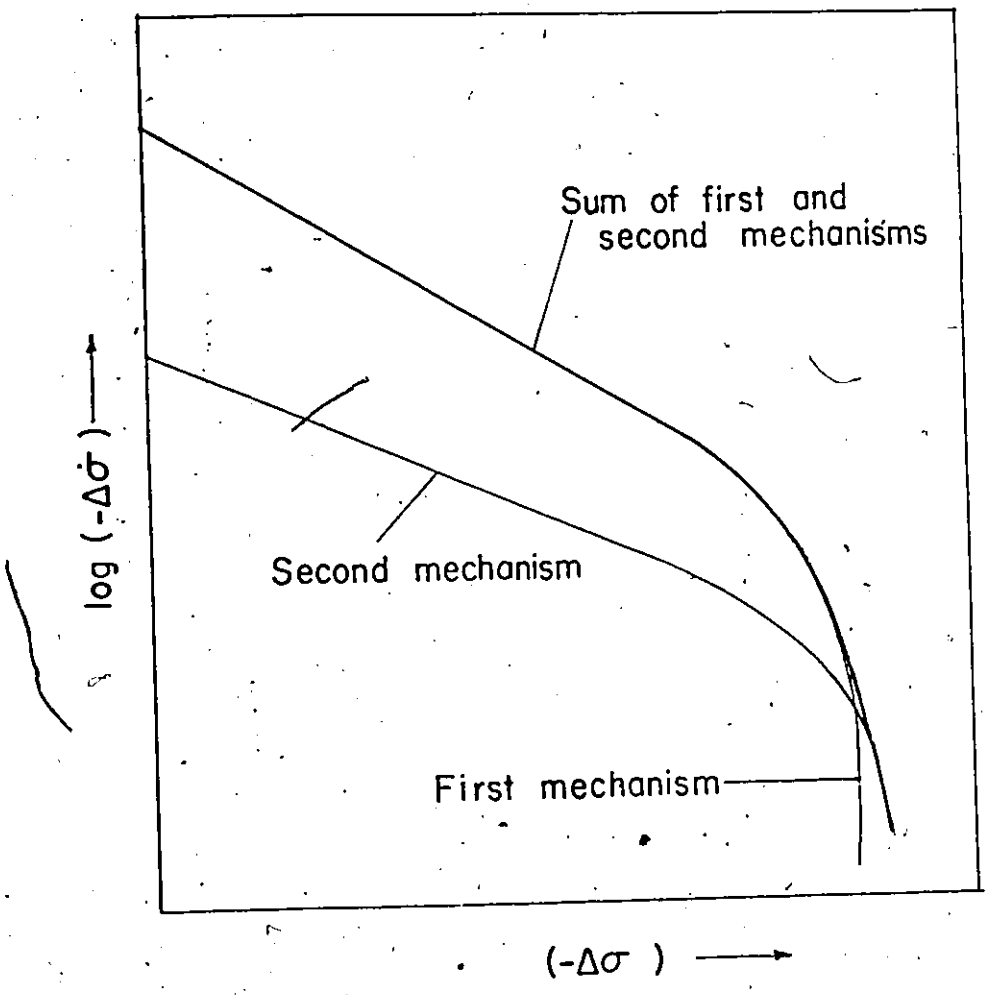

Figure 4.12 The figure illustrates two mechanisms working in parallel.

ward movement of second mechanism were calculated by satisfying the condition for the validity of second term. Remaining analysis was carried out as in case of first mechanism. The possibility of two mechanisms working in parallel was overruled as the theoretical curve could not be matched with the experimental curve.

A system of two barriers in series was considered next (Fig. 4.13). The number of dislocations crossing second barrier in unit time can be obtained by substituting n = 2 in equation 2.6. Therefore

$$\frac{d\rho_3}{dt} = \frac{\rho_1 - \rho_3 \exp\left[\frac{(\Delta E)_1}{kT}\right]}{\frac{1}{k_1} + \frac{1}{(k_2)_1}}$$

Substituting value of $\frac{d\rho_3}{dt}$ in equation 2.7, the rate of strain change will be

$$\dot{\gamma}_p = \alpha b \rho_m \bar{l} \left[\frac{\rho_1 - \rho_3 \exp\left[\frac{(\Delta E)_1}{kT}\right]}{\frac{1}{k_1} + \frac{1}{(k_2)_1}}\right]$$

During stress relaxation

$$-\Delta\dot{\sigma} = E' c \dot{\gamma}_p$$

Substituting for $\dot{\gamma}_p$ in the above equation and rearranging the terms, the rate of stress change during stress relaxation will be

$$\Delta\dot{\sigma} = -E' c \alpha b \rho_m \bar{l} \left[\frac{\rho_1 k_1 - \rho_3 k_1 \exp\left(\frac{(\Delta E)}{kT} 1\right)}{1 + \frac{k_1}{(k_2)_1}}\right] \qquad (4.5)$$

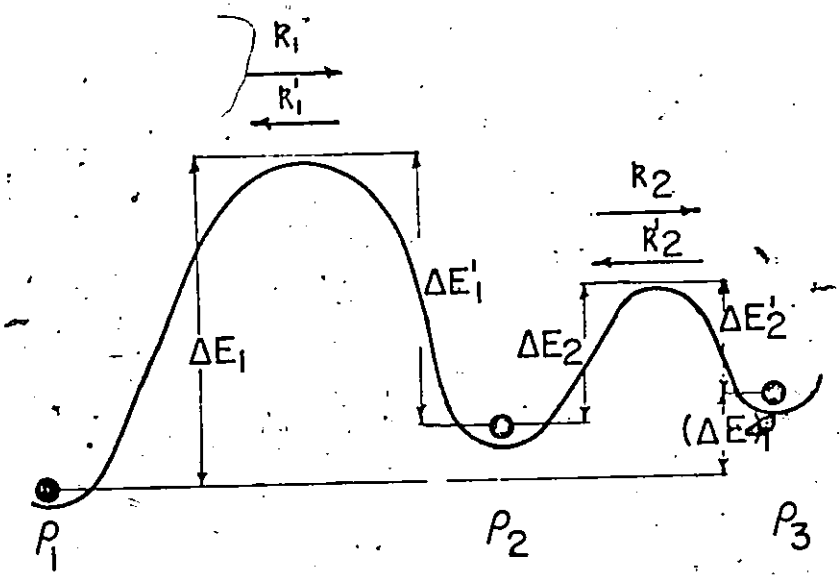

Figure 4.13 The figure illustrates two obstacles in series.

Substituting the values of R_1, $(\Delta E)_1$ and $(R_2)_1$ in equation 4.5, the rate of stress change will be

$$\dot{\Delta\sigma} = \frac{-A_f \exp(n_f \Delta\sigma) + A_2 \exp(-n_2 \Delta\sigma)}{1 + A_3 \exp(-n_3 \Delta\sigma)} \qquad (4.6)$$

where $A_2 = E' c a b \rho_m \bar{l} \rho_3 \frac{kT}{h} \cdot \exp\left(\frac{\Delta E_2^{\ddagger} - \Delta E_2^{\ddagger} - \Delta E_1^{\ddagger} - (V_{f_2}^* + V_{b_2}^* + V_{b_1}^*)(\tau_o - \tau_i)}{kT}\right)$

$$A_3 = \exp\frac{(\Delta E_2^{\ddagger} - \Delta E_1^{\ddagger} - (V_{f2}^* + V_{b1}^*)(\tau_o - \tau_i)}{kT}$$

$$n_2 = \frac{V_{b1}^* + V_{f2}^* + V_{b2}^*}{2kT}$$

$$n_3 = \frac{V_{f2}^* + V_{b1}^*}{2kT}$$

As discussed earlier the initial portion of the relaxation process can be described by equation (4.1). For simplicity of the remaining analysis, it was assumed that the effect of the backward movement over second barrier is negligible as compared to the forward movement. Values of A_3 and n_3 were calculated using this assumption. It was found that the experimental results could be described accurately by the equation

$$\dot{\Delta\sigma} = -\frac{A_f \exp(n_f \Delta\sigma)}{1 + A_3 \exp(-n_3 \Delta\sigma)}$$

A typical comparison of experimental and calculated results is given in Fig. 4.14. This justifies the earlier assumption that the effect of backward movement is negligible. It can be concluded that all the dislocations crossing second barrier move away.

Activation volume corresponding to forward flow over the first obstacles was obtained from equation 4.1. For the estimation of activation volume corresponding to forward flow over the second barrier, it is reasonable to assume that $V^*_{b1} < V^*_{f1}$. This assumption is justified as the net flow of dislocations is in forward direction. The results of the activation volume for forward flow over first and second barrier are tabulated in Table 4.2.

It can be concluded from these results that the most probable mechanism for the plastic deformation of pure iron could be the overcoming of Peierls-Nabarro stress field. This is in agreement with the results of other investigators (1, 3-9,11). Peierls-Nabarro stress field can be treated as two obstacles in series. First obstacle corresponds to the formation of double kink and second obstacle represents the spreading of the kink as shown in Figure 4.15. Because the activation volume for forward flow over the second barrier is large, the second barrier cannot be the overcoming of point defects.

Due to complexity of the problem it is not possible to separate activation energies and volumes. Therefore nothing can be concluded about the shape of the barrier.

Further analysis is therefore needed to determine the shape of barrier and the mechanism for overcoming the second barrier before any conclusive statement about the mechanism of plastic deformation in pure iron can be made.

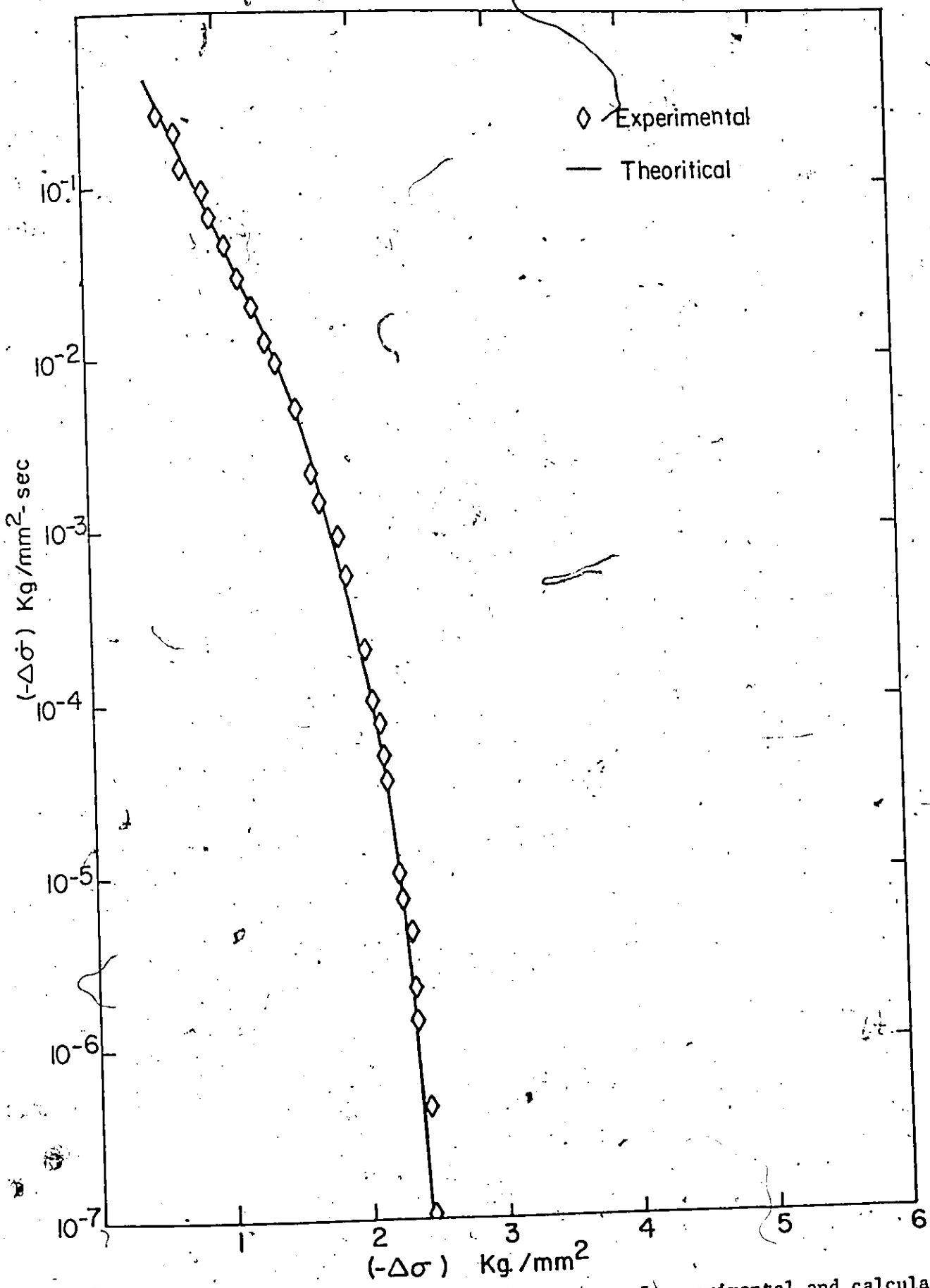

Figure 4.14 The figure illustrates a comparison of experimental and calculated results.

TABLE 4.2

ACTIVATION VOLUME FOR DIFFERENT STRESS LEVELS

Group No	Stress Level σ kg/mm^2	V^*_{f1} / b^3	V^*_{f2} > / b^3
00	5.00	1075-3800	500-1650
0	15.00	70-1050	710-1150
1	24.50	43-83	170-1170
3	27.50	228-442	280-970

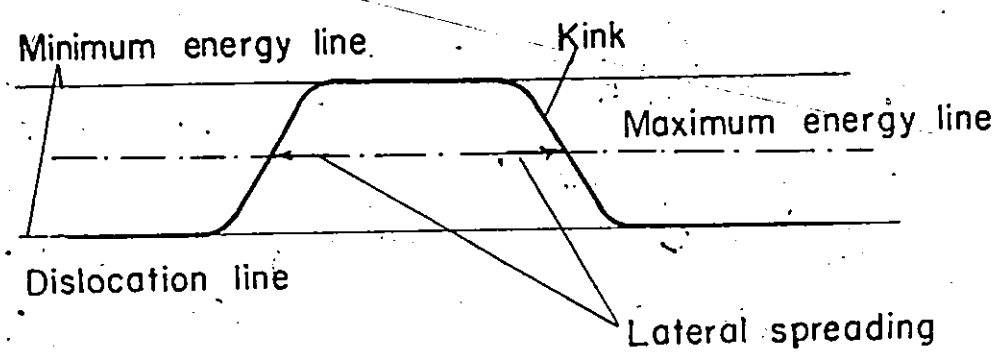

Figure 4.15 The figure illustrates a dislocation line containing a kink pair.

4.4 Determination of the Stress Exponent

Only few investigators have applied rate theory to plastic deformation process. Majority of the investigations are based on an empirical relationship between dislocation velocity and applied stress of the form

$$v = v_o \left(\frac{\tau_a}{\tau_o}\right)^m$$

Therefore, it is of interest to analyze the results of present investigations by the above equation. Substituting for dislocation velocity from above equation in Orowan's equation, the strain rate will be

$$\dot{\gamma}_p = \alpha b \rho_m v_o \left(\frac{\tau_a}{\tau_o}\right)^m$$

and the rate of stress change during relaxation can be described by the equation

$$\Delta\dot{\sigma} = - E' c \alpha b \rho_m v_o \left(\frac{\sigma_a}{\sigma_o}\right)^m$$

$$= - c_1 (\sigma_a)^m$$

where $c_1 = E' c \alpha b \rho_m v_o (\sigma_o)^{-m}$

Thus the slope of log $(-\Delta\dot{\sigma})$ vs log (σ_a) will give the value of stress exponent m. Figures 4.16 to 4.18 represent the relationship between log $(-\Delta\dot{\sigma})$ and log σ_a obtained in the present study.

The analysis showed that the value of m does not remain constant during stress relaxation of pure iron but changes with stress. It was observed that the relation between log $(-\Delta\dot{\sigma})$ and log σ_a is approximately

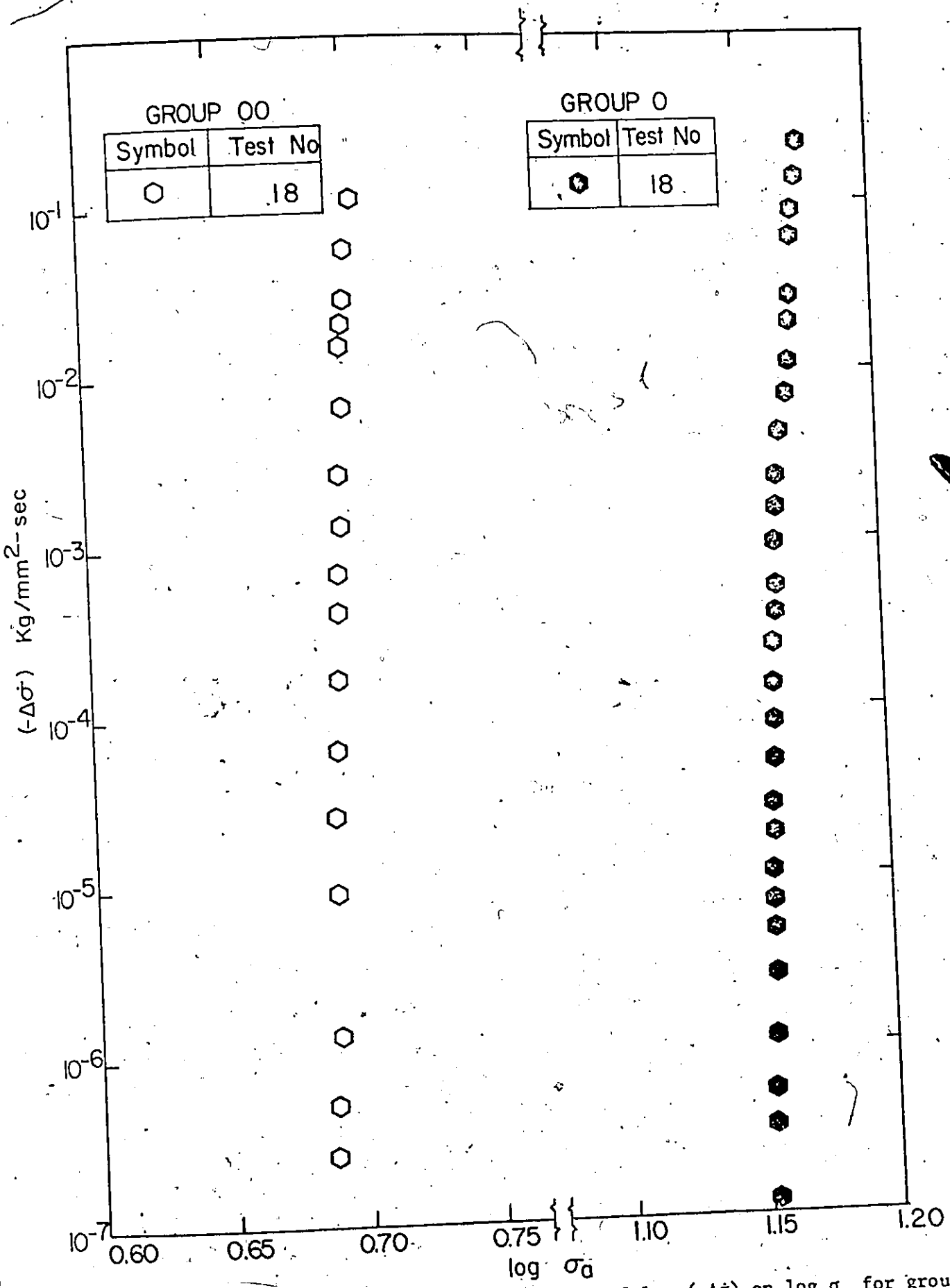

Figure 4.16 The figure illustrates the dependence of log $(-\Delta\dot{\sigma})$ on log σ_a for groups 00 and 0 tests.

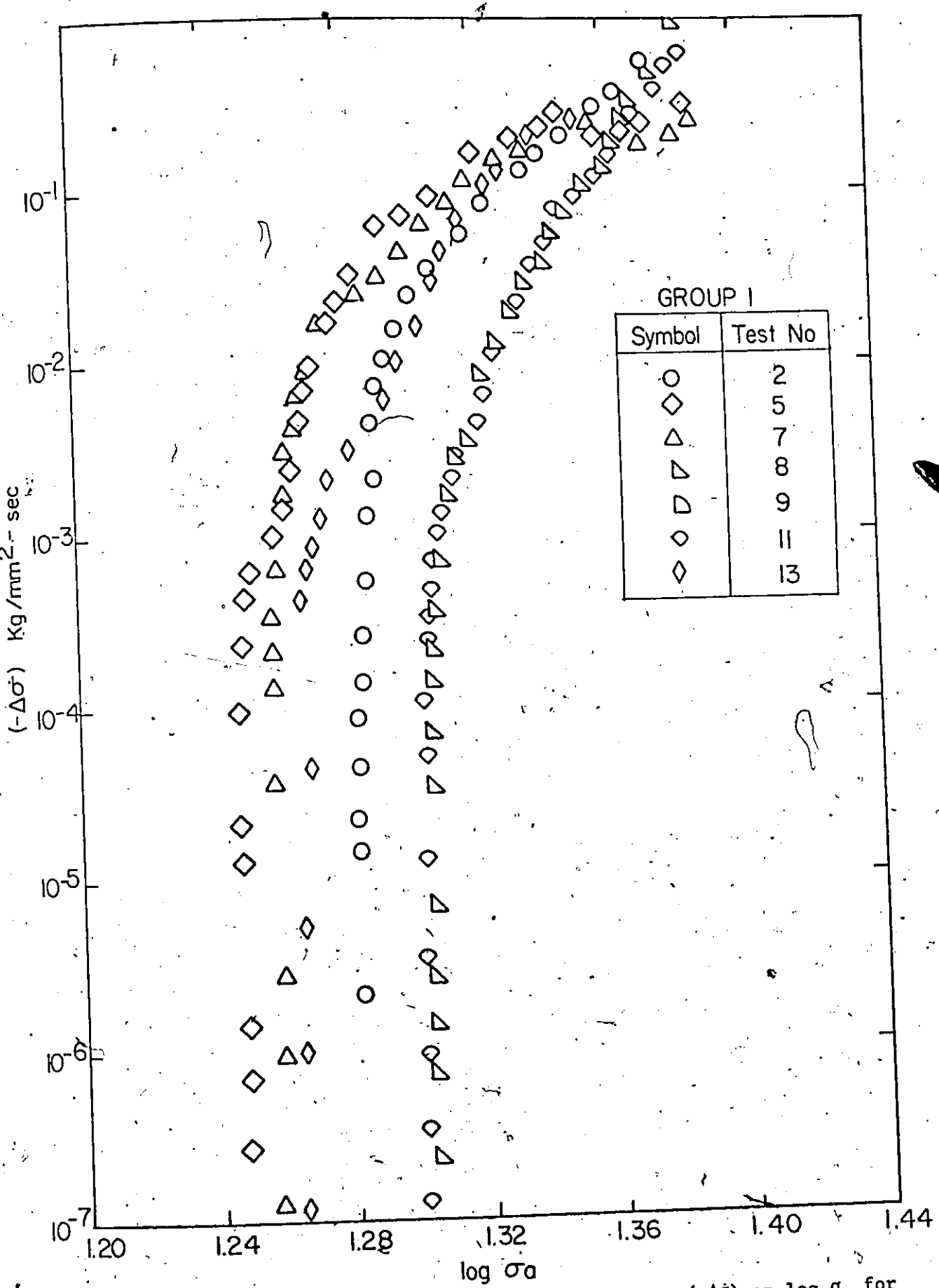

Figure 4.17 The figure illustrates the dependence of $\log_{10}(-\Delta\dot{\sigma})$ on $\log \sigma_a$ for group I tests.

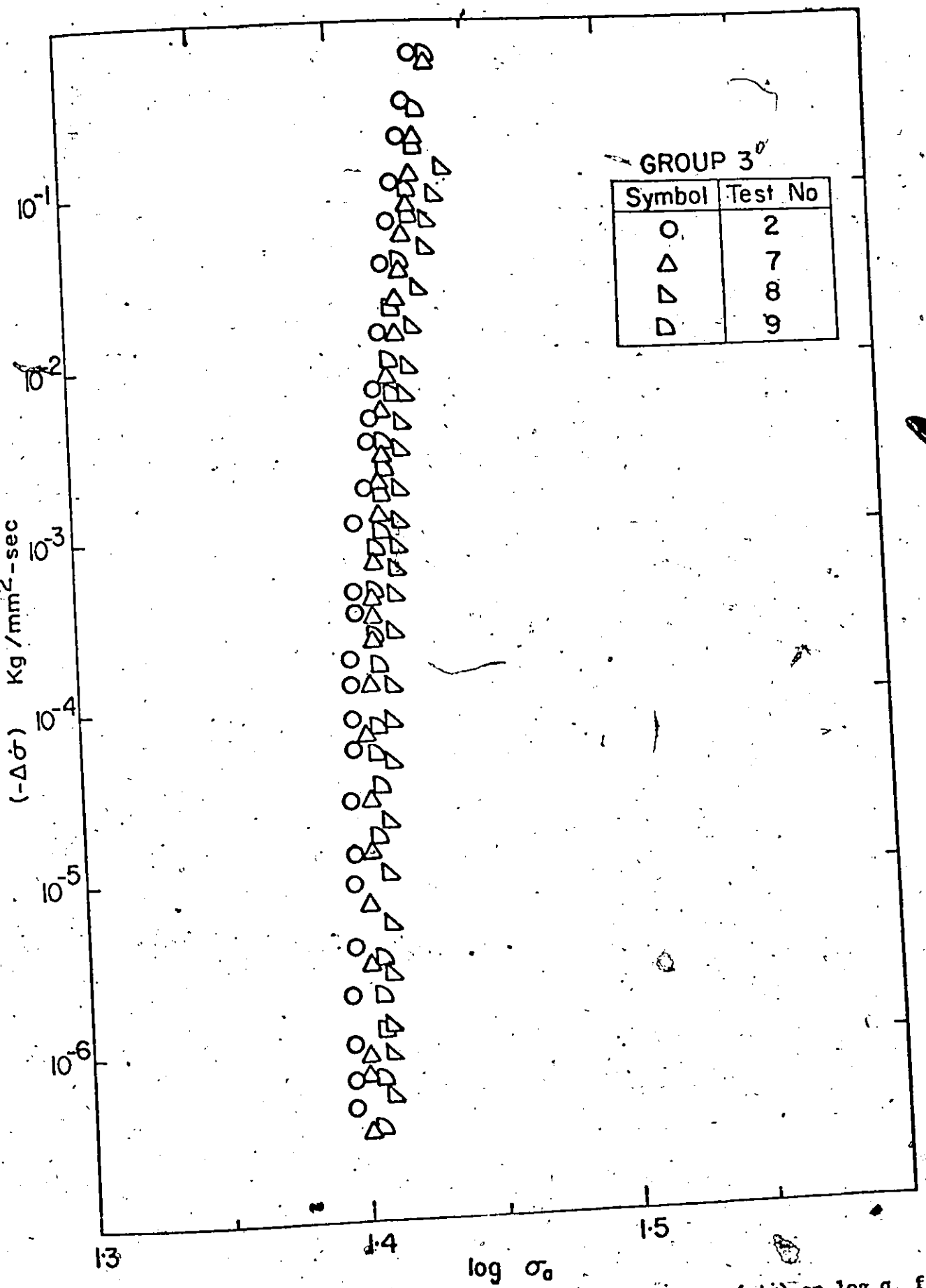

Figure 4.18 A The figure illustrates the dependence of log $(-\Delta\dot{\sigma})$ on log σ_a for group 3 tests.

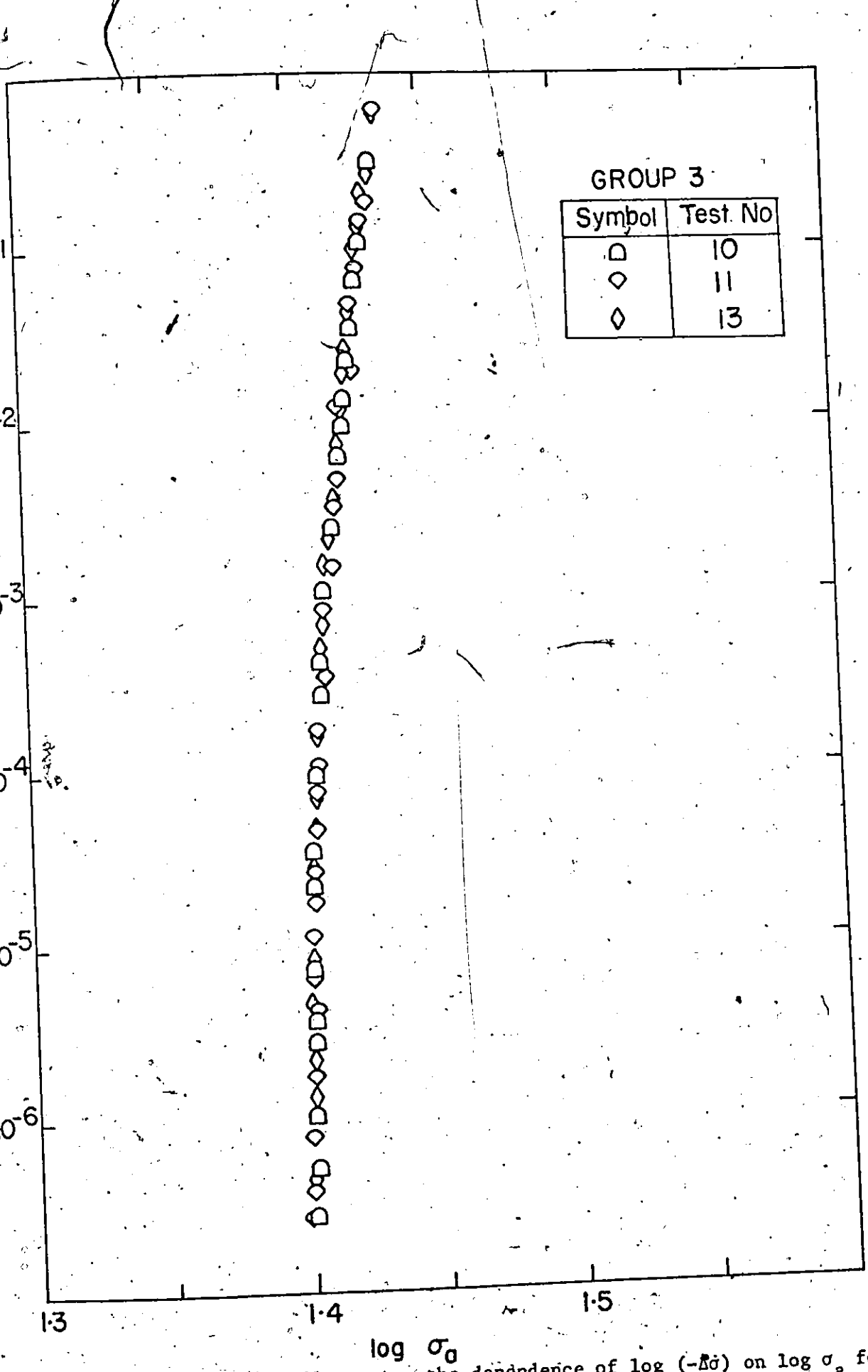

Figure 4.18 B The figure illustrates the dependence of log $(-\Delta\dot{\sigma})$ on log σ_a for group 3 tests.

linear in the initial and final region of the stress relaxation process. The stress exponent in initial and final region is designated by subscript 1 and 2 respectively. It was also observed that the value of m increases with initial stress. Similar observations were made by Noble and Hull (50). The variation of m with stress is given in Table 4.3.

As the movement of dislocation is caused by the effective stress, it is of interest to obtain the relationship between the rate of stress change and effective stress. Using effective stress instead of applied stress, the rate of stress change during stress relaxation process will be (Fig. 4.19).

$$\Delta\dot{\sigma} = -c_2(\sigma_{eff})^{m^*}$$

where $c_2 = E'\alpha b\rho_m v_o (\sigma_o)^{-m^*}$

The values of m* were calculated at different stress levels and the results are tabulated in Table 4.3. It was observed that the value of m* decreases with increasing σ_{eff}.

4.5 Dependence of Activation Volume on Effective Shear Stress

Fig. 4.20 represents the dependence of activation volume corresponding to forward movement over the first barrier on effective shear stress. It was observed that the results are much scattered at lower effective stresses than at higher stresses. The reason for this type of behaviour has been explained earlier in the discussion of stress relaxation test.

4.6 Comparison with the Results of Other Investigators

The majority of the investigations cover the region in which only one term of rate equation is applicable. Therefore, one term of this

TABLE 4.3

VARIATION OF m AND m* WITH STRESS

Group No.	Stress Level σ kg/mm^2	m_1	m_2	m_1^*	m_2^*
0	5.00	162	50	162	412.5
1	24.50	25-31	3500	4.6	35.7
3	27.00	100-150	300-400	8	17.65

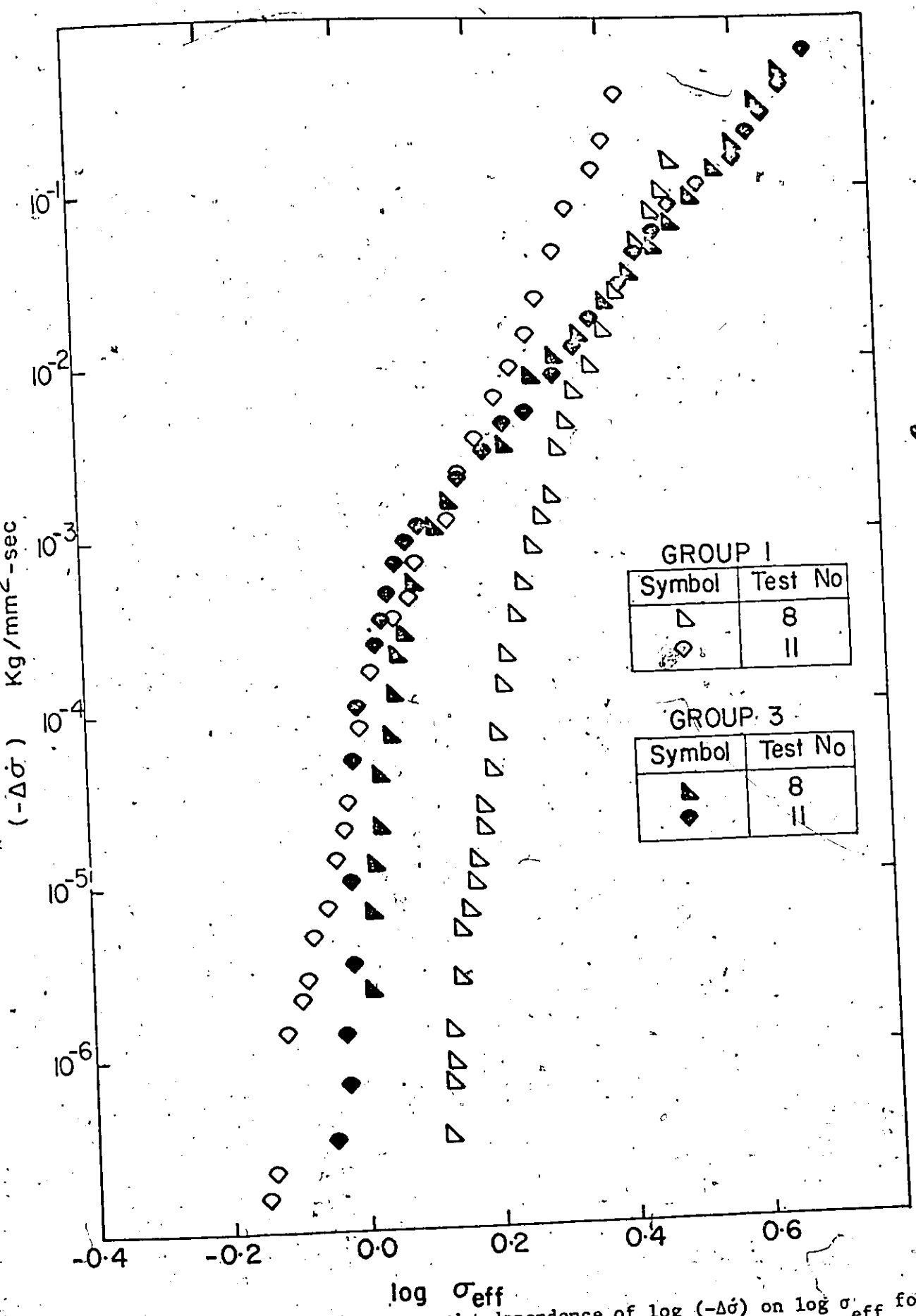

Figure 4.19 The figure illustrates the dependence of log $(-\Delta\dot{\sigma})$ on log σ_{eff} for tests of groups 1 and 3.

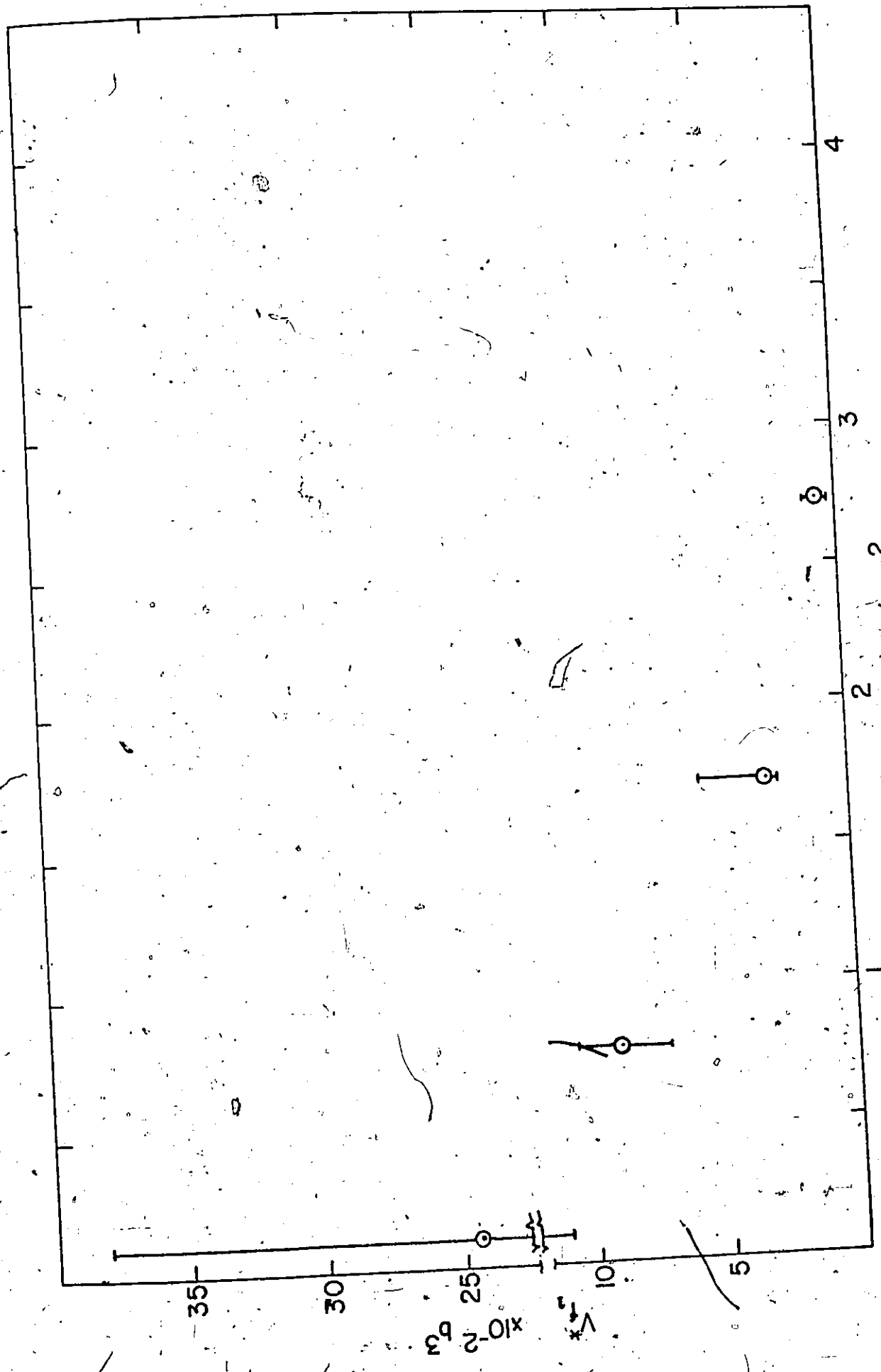

Figure 4.20 The figure illustrates the dependence of V_{f_1} on τ_{eff}

investigation can be compared with the work of other investigators under comparable testing conditions. This comparison is tabulated in Table 4.4.

TABLE 4.4

COMPARISON OF RESULTS

Reference	Material	Testing Method	T° C	m^*	V^*_{f1}	b^3
Smidt (8)	Zone Refined Iron	Stress Relaxation & Strain Rate Cycling	Room	3.2-18.9		
Wilson and Garofalo (10)	High Purity Iron	Stress Relaxation	25°		128	
Li (30)	High Purity Iron	Stress Relaxation	25°	3.5		
Altshuler & Christian (51)	High Purity Iron	Temperature Cycling	25°	2.75		
Mitchlak (52)	High Purity Iron	Strain Rate Cycling	27°	5.5		
MacRickard (53)	Ferrovac Iron	Stress Relaxation	25°		76.4	
Present Investigations	High Purity Iron	Stress Relaxation	27°	4.6-8.0	55-302	

CHAPTER 5

CONCLUSIONS

The following conclusions are drawn as a result of the present investigation:

1. Initial region of the stress relaxation process can be described by only one obstacle with negligible backward movement of dislocations while two obstacles in series seem to be working in latter region without significant backward movement of dislocations.

2. It is suggested that the plastic deformation in pure iron is controlled by overcoming of Peierls-Nabarro stress field. This operates as a system of two obstacles in series. The first obstacle corresponds to the formation of double kink and the second to the spreading of kink.

3. It is suggested that second obstacle cannot be a point defect.

4. All the dislocations crossing second obstacle move away.

5. The internal stresses increase with increasing strain.

APPENDIX 1

Determination of Probability of Acquiring the Activation Energy

Consider the ensemble of volume V_e, number of systems M and total energy E_t. Let T be the temperature of the ensemble and N be the number of atoms in each system. These systems can be assumed to be separated in such a manner that energy can flow from one system to another but the number of atoms, volume and temperature remain constant. If g_i systems are in ΔE_ith energy state, then corresponding to this distribution

$$\sum_{i=o}^{n} g_i = M \tag{1}$$

$$\sum_{i=o}^{n} g_i \, \Delta E_i = \Delta E_t \tag{2}$$

For this distribution, the number of possible states of the ensemble consistent with the given distribution (16)

$$G(g) = \frac{(g_o + g_1 + \ldots + g_n)!}{g_o! g_1! g_2! \ldots . g_n!}$$

as

$$g_o + g_1 + g_2 \ldots\ldots + g_n = M$$

Thus $$G(g) = \frac{M!}{\pi_i (g_i!)} \tag{3}$$

where

$$\pi_i \, g_i! = g_o! g_1! g_2! \ldots\ldots g_n!$$

As the energy levels within the ensemble can change, the possible states of the ensemble also change. Denoting these states by subscript μ, where $\mu = 1,2,\ldots$, the number of possible states of the μth distribution

$$G(g^{\mu}) = \frac{M!}{\prod_i (g_i^{\mu})} \qquad (4)$$

the average number of times the energy level $\Delta E_i^{\ddagger}$ is observed in distribution g^{μ} will be

$$G(g^{\mu}) \quad \frac{g_i^{\mu}}{\sum_i g_i^{\mu}}$$

The probability, P, of observing energy state $\Delta E_i^{\ddagger}$ in a large random sampling will be

$$P = \frac{\text{Number of times, condition i is observed}}{\text{Total number of observations}}$$

$$= \frac{\text{Number of systems in condition i}}{\text{Total number of systems}}$$

$$= \frac{1}{M}\left(\frac{\sum_{\mu=1} G(g^{\mu})\, g_i^{\mu}}{\sum_{\mu=1} G(g^{\mu})} \right) \qquad (6)$$

In equation (6), summation of all the terms except those corresponding to the most probable distribution i.e. activated state can be neglected.

For infinite number of systems, the distribution is represented by Dirac delta function (Fig. I-1). Thus

$$P = \frac{G(g^*)g_i^*}{\sum_{\mu=1}^{\infty} G(g^\mu)}$$

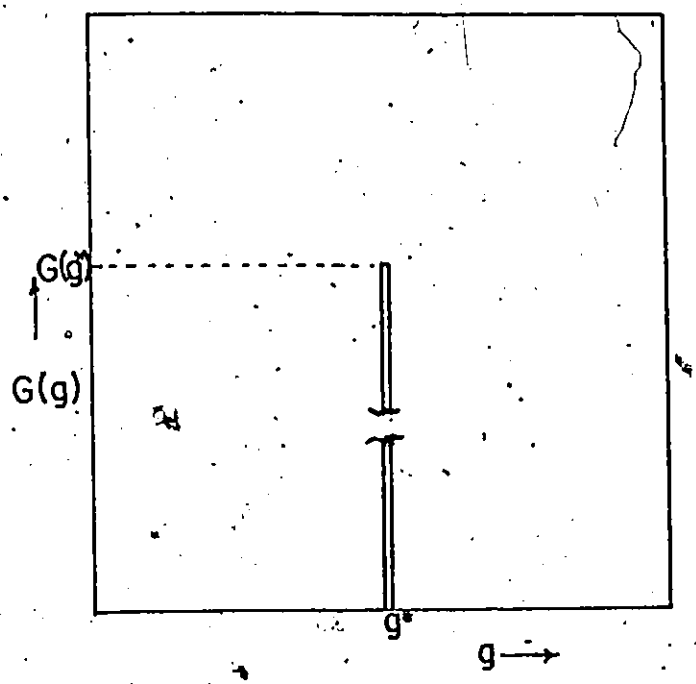

Fig. I-1 Dirac-Delta Function

The extreme value of $G(g^*)$ is determined by Lagrange's method of undetermined multipliers consistent with the conditions

$$\frac{\partial(\sum_i g_i \Delta E_i)}{\partial g_i} = 0 \qquad \text{as } \sum_i g_i \Delta E_i = \Delta E_t = \text{constant}$$

$$\frac{\partial(\sum_i g_i)}{\partial g_i} = 0 \qquad \text{as } \sum_i g_i = M = \text{constant}$$

Applying the Lagrange's method of undetermined multipliers,

$$\frac{\partial}{\partial g_i}[\ln G(g) - \alpha\sum g_i - \beta\sum g_i \Delta E_i] = 0 \qquad (8)$$

Taking log of both sides of equation (4)

$$\ln G(g) = \ln (M!) - \sum_i \ln (g_i!)$$

For large values of M, applying Stirling's approximation

$$\ln G(g) \simeq M \ln M - M - \Sigma (g_i \ln g_i - g_i)$$

$$\simeq \sum_i g_i \ln (\sum_i g_i) - \sum_i g_i \ln g_i$$

Substituting for ln G(g) in equation (8)

$$\frac{\partial}{\partial g_i} [(\sum_i g_i) \ln(\sum_i g_i) - \sum_i g_i \ln g_i - \alpha \sum_i g_i - \beta \Sigma g_i \Delta E_i] = 0$$

or $$\ln \sum_i g_i - \ln g_i - \alpha - \beta \Delta E_i = 0$$

as $$\sum_i g_i = M$$

$$g_i = M \exp (- \alpha - \beta \Delta E_i) \qquad (9)$$

or $$M = M \sum \exp (- \alpha - \beta \Delta E_i)$$

From this equation

$$\exp(\alpha) = \sum_i \exp(-\beta \Delta E_i)$$

Substituting in equation (9), the number of systems in ΔE_ith energy state for the most probable distribution will be

$$g_i^* = \frac{M \exp (-\beta \Delta E_i)}{\sum_i \exp (-\beta \Delta E_i)} \qquad (10)$$

In equation 10, β is unknown. To evaluate β consider a perfect gas in a box having a volume V, number of particles N and temperature T. Let the average velocity of particles in x direction be $\bar{v}_x$. The change in momentum in x direction will be $2m_a \bar{v}_x$ where m_a is the mass of atom. The pressure on the wall of the box will be due to the striking of atoms. The atoms at a distance of $\bar{v}_x$ will hit the wall in a unit time and the number of impacts on the wall per unit area in unit time will be $N/V\ \bar{v}_x$. If P is the force per unit area of the wall then, this will be equal to change in momentum per atom multiplied by the number of atoms striking the wall per unit area in unit time. Therefore

$$P = 2m_a \bar{v}_x \frac{N}{V} \cdot \bar{v}_x$$

$$= 2m_a \frac{N}{V} \bar{v}_x^2 \qquad (11)$$

For the calculation of mean velocity in x direction, consider translational kinetic energy of the atom. As the energy levels are so closely spaced, these can be considered to be continuous. The translational kinetic energy $= \frac{1}{2} m_a v_x^2$. By Boltzmann distribution, the fraction of atoms with velocity v_x in the range v_x and $v_x + dv_x$ is proportional to $\exp(-\frac{1}{2} m_a v_x^2) dv_x$ and the square of the average velocity in x direction will be

$$\bar{v}_x^2 = \frac{\int_0^\infty \exp(-\frac{1}{2} m_a v_x^2 \beta)\ v_x^2\ dv_x}{\int_{-\infty}^{\infty} \exp(-\frac{1}{2} m_a v_x^2 \beta)\ dv_x}$$

The limits of integration in numerator are taken from 0 to ∞ as only positive direction is of interest. Therefore

$$\bar{v}_x^2 = \frac{1}{2\beta m_a}$$

Substituting for $m_a \bar{v}_x^2$ in equation (11)

$$P = \frac{1}{\beta}\frac{N}{V}$$

From ideal gas law $P = \frac{RT}{V}$

Thus $\beta = \frac{N}{RT} = \frac{1}{kT}$

Substituting for β in equation (10), the number of systems in E_ith energy state for the most probable distribution is

$$g_i^* = \frac{M \exp(\frac{-\Delta E_i}{kT})}{\sum_i \exp(\frac{-\Delta E_i}{kT})}$$

Hence the probability of acquiring the activation energy $\Delta E_i^{\ddagger}$ will be given by

$$P_j = \frac{g_i^*}{M} = \frac{\exp(\frac{-\Delta E_i^{\ddagger}}{kT})}{\sum_i \exp(\frac{-\Delta E_i}{kT})}$$

APPENDIX II

CALCULATION OF REACTION RATE

The rate of reaction for the system shown in Fig. 2.2 will be

$$R = \frac{\bar{v}}{\delta} \cdot \rho^{\ddagger} \qquad (1)$$

where $\bar{v}$ = the average velocity of the activated complexes over the barrier

δ = the length of the barrier which separates the reactants from reacting molecules

$\rho^{\ddagger}$ = the number of activated complexes within distance δ.

For the calculation of number of complexes crossing the barrier in unit time, consider an infinitesimal velocity range v and v+dv over the top of the barrier. The corresponding energy for one degree of freedom is

$$K.E. = \frac{1}{2} mv^2$$

where m = the mass of the complex.

The probability that the activated complexes have the velocity in the range v and v+dv will be

$$P(v) = \text{constant } \exp\left(-\frac{mv^2}{2kT}\right)dv$$

The average velocity in forward direction is

$$\bar{v} = \frac{\int_0^{\infty} \exp\left(-\frac{mv^2}{2kT}\right)\, v.dv}{\int_{-\infty}^{\infty} \exp\left(-\frac{mv^2}{2kT}\right)\, dv}$$

The limits of integration in the numerator are taken from 0 to ∞ as the mean velocity in forward direction is required, while the limits in the denominator are from $-\infty$ to $+\infty$ to account for the movement in both directions. Thus

$$\bar{v} = \left(\frac{kT}{2\pi m}\right)^{1/2}$$

Substituting for $\bar{v}$ in equation (1), rate of reaction is:

$$R = \left(\frac{kT}{2\pi m}\right)^{1/2} \frac{1}{\delta} \cdot \rho^{\ddagger} \qquad (2)$$

If ρ_i are the initial complexes taking part in the process, the rate of process is defined as

$$R = k.\rho_i \qquad (3)$$

Where k is the rate constant for the process. From equation (2) and and (3), the rate constant will be

$$k = \left(\frac{kT}{2\pi m}\right)^{1/2} \cdot \frac{1}{\delta} \cdot \frac{\rho^{\ddagger}}{\rho_i} \qquad (4)$$

It has been assumed that the reactant complexes are in equilibrium with the activated complexes. For such a system the number of complexes are proportional to the total partition function of the system. Thus

$$\frac{\rho^{\ddagger}}{\rho_i} = \frac{q_{\ddagger}}{q_i}$$

where $q_{\ddagger}$ = the total partition function of activated complexes referred to ground level of initial state.

q_i = the total partition function of the initial complexes.

From definition of partition function, the ratio of partition functions for activated and initial complexes will be [Fig. II-1]

$$\frac{q^{\ddagger}}{q_i} = \frac{\sum_i g_{i\ddagger} \exp\left(\frac{-\Delta E_{i\ddagger}}{kT}\right)}{\sum_i g_i \exp\left(\frac{-\Delta E_i}{kT}\right)}$$

$$= \exp\left(\frac{-\Delta E_o^{\ddagger}}{kT}\right) \frac{\sum_i g_{i\ddagger} \exp\left(\frac{-\Delta E_i^{\ddagger}}{kT}\right)}{\sum_i g_i \exp\left(\frac{-\Delta E_i^{\ddagger}}{kT}\right)}$$

Thus $$\frac{\rho^{\ddagger}}{\rho_i} = \exp\left(\frac{-\Delta E_o^{\ddagger}}{kT}\right) \frac{\sum_i g_{i\ddagger} \exp\left(\frac{-\Delta E_i^{\ddagger}}{kT}\right)}{\sum_i g_i \exp\left(\frac{-\Delta E_i}{kT}\right)}$$

or $$\frac{\rho^{\ddagger}}{\rho_i} = \frac{q'^{\ddagger}}{q_i} \exp\left(\frac{-\Delta E_o^{\ddagger}}{kT}\right) \qquad (5)$$

where $q'^{\ddagger}$ = the partition function of activated complexes referred to ground level of activated state.

$\Delta E_i^{\ddagger}$ = the activation energy referred to ground level of activated state.

$\Delta E_o^{\ddagger}$ = the activation energy of activated complexes referred to ground level of initial state.

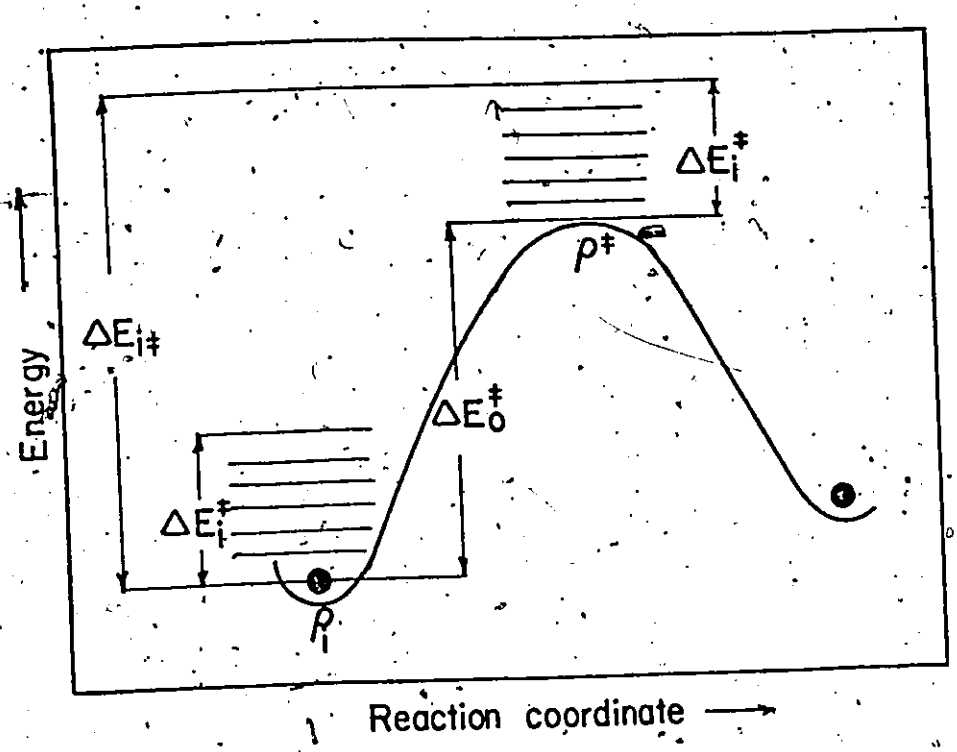

Fig. II-1 Energy curve for the determination of partition function.

The activated complexes behave in the same manner as the normal ones except in reaction coordinate. In reaction coordinate the energy falls off on both sides, thus the restoring force on the complex initially vibrating is reduced to zero. Hence the vibrational motion of the particle in reaction coordinate can be regarded as free translational. The partition function for the activated state referred to ground level of activated state is

$$q'^{\ddagger} = q_{trans} \cdot q_{rot} \cdot q_{ele} \cdot q_{vib} \cdot q'_{trans}$$

where q_{trans} = the translational partition function

q_{rot} = the rotational p.f.

q_{ele} = the electronic partition function

q'_{trans} = the translational p.f. in reaction coordinate

q_{vib} = the vibrational partition function except in reaction coordinate

Therefore $q'^{\ddagger} = q^{\ddagger} \cdot q'_{trans}$

in which $q^{\ddagger}$ is the total partition function with the exception of translational partition function in the reaction coordinate. The translational partition function in reaction coordinate is

$$q'_{trans} = \sum_i \exp\left(-\frac{\Delta E'_{trans}}{kT}\right) \qquad (6)$$

The translational energy corresponding to a motion of particle in one direction having mass m will be

$$\Delta E'_{trans} = \frac{n^2 h^2}{8\,\delta^2\, m}$$

where n = the quantum number

h = the Planck's constant

Substituting for $\Delta E'_{trans}$ in equation (6), the translational partition function in reaction coordinate

$$q'_{trans} = \sum_i \exp\left(-\frac{n_i^2\, h^2}{8\,\delta^2\, m\, kT}\right)$$

As all the energy levels are so closely packed, the distribution of energy may be regarded as continuous. Replacing the summation sign by integral and integrating from 0 to ∞

$$q'_{trans} = \int_0^\infty \exp\left(-\frac{n^2 h^2}{8 \delta^2 m kT}\right) dn$$

$$= \left(\frac{2\pi m kT}{h^2}\right)^{1/2} \cdot \delta$$

Thus $q'^{\ddagger} = q^{\ddagger} \left(\frac{2\pi m kT}{h^2}\right)^{1/2} \delta$

Substituting for $q'^{\ddagger}$ in equation (5)

$$\frac{\rho^{\ddagger}}{\rho_i} = \frac{q^{\ddagger}}{q'_i} \left(\frac{2\pi m kT}{h^2}\right)^{1/2} \delta \exp\left(-\frac{\Delta E_o^{\ddagger}}{kT}\right) \qquad (7)$$

Replacing $\frac{\rho^{\ddagger}}{\rho_i}$ from equation (4) by equation (7), the rate constant for the process will be

$$k = \left(\frac{kT}{h}\right) \cdot \frac{q^{\ddagger}}{q_i} \exp\left(-\frac{\Delta E_o^{\ddagger}}{kT}\right)$$

The above equation gives the rate constant from the rate theory of Eyring.

APPENDIX III

RATE CONSTANT FOR SYSTEM OF OBSTACLES IN SERIES

Consider a system of obstacles shown in Fig. (4.13). Let ρ_1 be the number of dislocations in front of 1st obstacle and ρ_2 and ρ_3 are the steady state concentrations at points 2 and 3. The rate constants in forward and reverse directions are denoted by the symbol k and k' respectively with an appropriate subscript corresponding to the number of the barrier.

For steady state concentration at points 2

$$\frac{d\rho_2}{dt} = 0 = \rho_2(k_2 + k_1') - \rho_3 k_2' - \rho_1 k_1$$

or
$$\rho_2 = \frac{\rho_3 k_2' - \rho_1 k_1}{(k_2 + k_1')} \qquad (1)$$

Similarly, for steady state concentration at point 3

$$\frac{d\rho_3}{dt} = 0 = \rho_3(k_3 + k_2') - \rho_4 k_3' - \rho_2 k_2$$

from which
$$\rho_3 = \frac{\rho_4 k_3' - \rho_2 k_2}{k_3 + k_2'}$$

Substituting for ρ_2 from equation (1) in the above equation

$$\rho_3 = \frac{\rho_1 k_1 k_2 + \rho_4(k_3' k_1 + k_3' k_2)}{k_1' k_2' + k_1' k_3 + k_2 k_3} \qquad (2)$$

The rate at which the dislocations are crossing the third barrier is:

$$\frac{d\rho_4}{dt} = k_3\rho_3 - k_3'\rho_4$$

Substituting for ρ_3 from equation (2) and dividing numerator and denominator by $k_1k_2k_3$

$$\frac{d\rho_4}{dt} = \frac{\rho_1 - \rho_4 \dfrac{k_1'k_2'k_3'}{k_1k_2k_3}}{\dfrac{1}{k_1} + \dfrac{k_1'}{k_1k_2} + \dfrac{k_1'k_2'}{k_1k_2k_3}} \qquad (3)$$

Assuming transmission coefficients to be unity. In this equation $(\Delta E)_1$ is the apparent activation energy between level 4 and 1. By taking reference point as ground level of state 1,

$$\frac{k_1'}{k_1k_2} = \exp\left(\frac{\Delta E_1 - \Delta E_1' + \Delta E_2}{kT}\right)$$

$$= \exp\left(\frac{(\Delta E_2)_1}{kT}\, 1\right)$$

$$= \left(\frac{1}{k_2}\right) 1$$

and $$\frac{k_1'k_2'}{k_1k_2k_3} = \frac{1}{(k_3)_1}$$

Substituting in equation (3), rate of crossing point 4 will be

$$\frac{d\rho_4}{dt} = \frac{\rho_1 - \rho_4 \exp\left(\dfrac{(\Delta E)_1}{kT}\right)}{\dfrac{1}{(k_1)_1} + \dfrac{1}{(k_2)_1} + \dfrac{1}{(k_3)_1}}$$

$$= \frac{\rho_1 - \rho_4 \exp\left(\frac{(\Delta E)_1}{kT}\right)}{\sum_{i=1}^{3} \left(\frac{1}{k_i}\right)_1}$$

Applying this to n barriers, the general form of this equation will be

$$\frac{d\rho_{n+1}}{dt} = \frac{\rho_1 - \rho_{n+1} \exp\left(\frac{(\Delta E)_1}{kT}\right)}{\sum_{i=1}^{n} \left(\frac{1}{k_i}\right)_1}$$

REFERENCES

1. Z. Basinski and J.W. Christian, Aust. J. Phys., 13. 299 (1960).
2. P. Feltham, Phil. Mag., 6, 847 (1961).
3. H. Conrad, J. Iron and Steel Inst., 198, 364 (1961).
4. H. Conrad and S. Frederick, Acta. Met., 10, 1013 (1962).
5. H. Conrad, National Physical Lab. London, Symposium 15 (1963).
6. J.W. Christian and B.C. Masters, Proc. of Royal Soc., 281, 240 (1964).
7. R.J. Arsenault, Acta. Met., 12, 547 (1964).
8. F.A. Smidt, Jr., Pacific Northwest Lab. Report, No. BNWL-184, December 1965.
9. P.J. Wray and G.T. Horne, Phil. Mag., 13, 899 (1966).
10. J.F. Wilson and G. Garofalo, Mat. Research and Standards, 6, 85 (1966).
11. F.A. Smidt, Jr., Acta Met., 17, 381 (1969).
12. R. Becker, Z. Physic, 26, 919 (1925).
13. A.S. Krausz and H. Eyring, J. App. Phys., 2, 2382 (1971).
14. R.W. Rohde and C.H. Pitt, J. Appl. Phys., 39, 3186 (1968).
15. T.L. Hill, Introduction to Statistical Thermodynamics, Addison-Wesley Pub. Co., Inc. (1960).
16. S. Glasstone, K.J. Laidler and H. Eyring. The Theory of Rate Processes, McGraw-Hill Book Co. Inc. (1941).
17. A.S. Krausz, Ph.D. Dissertation, University of Toronto, Ontario (1964).
18. O H. Wyatt, Proc. of Phys. Soc. London B, 66, 459 (1953).
19. A.H. Cottrell, J. Mech. and Phys. of Solids, 1, 53 (1952).

20. F. Guiu and P.L. Pratt, Phys. Stat. Sol., 6, 111 (1964).

21. P. Trouton and A.O. Rankine, Phil. Mag., 8, 538 (1904).

22. J. Boyd, A.S.T.M., 37, 218 (1937).

23. P. Feltham, Phil. Mag., 6, 259 (1961).

24. P. Feltham, J. Inst. Met., 89, 210 (1961).

25. P. Feltham, Phys. Stat. Sol., 3, 1340 (1963).

26. G.B. Gibbs, Phil. Mag., 13, 317 (1966).

27. G.A. Sargent, Acta. Met., 14, 663 (1965).

28. G.A. Sargent and B.J. Shaw, Acta Met., 14, 909 (1966).

29. A.S. Krausz and G.B. Craig, Acta Met., 14, 1809 (1966).

30. J.C.M. Li, Can. J. Phys., 45, 493 (1967).

31. S.M. Ohr, Progress Report U.S. Atomic Energy Commission, Jan. 1966.

32. P. Feltham, G. Lehman and R. Moisel, Acta. Met., 17, 1305 (1969).

33. A.S. Krausz, Mat. Sci. Eng., 4, 193 (1969).

34. P.M. Kelly and J.M. Round, Scripta Met., 3, 85 (1969).

35. I. Gupta and J.C.M. Li, Met. Trans., 1, 2323 (1970).

36. G.A. Sargent and H. Conrad, Scripta Met., 3, 43 (1969).

37. G.A. Sargent and H. Conrad, Scripta Met., 4, 129 (1970).

38. N. Krishna, M.A.Sc. Thesis, University of Ottawa, Ottawa (1971).

39. H. Conrad, J. Metals, 16, 582 (1964).

40. A.S. Krausz, Acta. Met., 16, 897 (1968).

41. A.A. Soloman, Rev. Sci. Instruments, 40, 1025 (1969).

42. S.R. MacEwan, O.A. Kupics and B. Ramaswami, Scripta Met., 3, 441 (1969).

43. C. Norman Ahlquist and W.D. Nix, Scripta Met., 3, 679 (1969).

44. J.J. Gilman and W.G. Johnston, J. Appl. Phys., 30, 129 (1959).

45. I. Gupta and J.C.M. Li, Mat. Sc. Eng., 6, 20 (1970).

46. R.A. Menezes and W.D. Nix, Acta Met., 19, 645 (1971).

47. C. Norman Ahlquist, Scripta Met., 5, 185 (1971).

48. H. Conrad, Mat. Sci. Eng., 6, 265 (1970).

49. A.S. Krausz, Can. J. Phys., 41, 167 (1963).

50. F.W. Noble and D. Hull, Acta. Met., 12 1089 (1964).

51. T.L. Alteshuler and J.W. Christian, Phil. Trans. Royal Soc., London Series A., No. 1121, 216, 253 (1967).

52. J.T. Mitchlak, Acta Met., 13, 213 (1968).

53. S.B. McRickard, Acta Met., 16, 969 (1968).